universität wien

MASTERARBEIT / MASTER'S THESIS

Titel der Masterarbeit / Title of the Master's Thesis

Separating Multiple Populations and Binaries in Globular Clusters

verfasst von / submitted by

Laura Posch, BSc

angestrebter akademischer Grad / in partial fulfilment of the requirements for the degree of

Master of Science (MSc)

Wien, 2021 / Vienna, 2021

Studienkennzahl lt. Studienblatt / degree programme code as it appears on the student record sheet:	UA 066 861
Studienrichtung lt. Studienblatt / degree programme as it appears on the student record sheet:	Masterstudium Astronomie
Betreut von / Supervisor:	Dr Prashin Jethwa, MSc MA

Acknowledgements

I wholeheartedly thank my supervisors Dr. Prashin Jethwa and Univ.-Prof. Dr. Glenn van de Ven for their guidance, support and helpful discussions, as well as the whole dynamics group at the Institute in Vienna for their questions and remarks. Especially, Alice Zocchi for her great ideas.

Abstract

This Master thesis is based in the research field of globular clusters (GCs) which host not only the oldest stellar populations in our galaxy but also a phenomenon called multiple stellar populations (MSPs). More specific these are star-to-star variations in light element abundances like N, Na, He, C and O among others. MSPs are mostly observed photometrically because it enables a large spatial coverage and their detection is possible in colour-magnitude diagrams (CMDs). In theses diagrams the stellar abundance variations are visible as a split in the main sequence (MS) of the populations. The incidence of binary stars in MSPs biases the estimation of population and binary fractions in clusters because they are partially among the single population stars in CMDs. They are therefore often not recognised as binaries. However, the numbers and characteristics of binary stars are of great interest as they can shed light on the formation mechanisms and environments of MSPs and GCs. Effectively, the formation of GCs and their MSPs is yet unknown and a highly discussed topic.

Therefore, in this thesis I investigate the question of the influence of binary stars on the photometric detection of MSPs and the possibility of separating the binary from single stars in the CMD. This is achieved by recreating observed MSPs in mock CMDs with simple stellar populations (SSPs). In the analysis, I vary several parameters controlling the cluster stellar populations – binary fraction, population ratio, abundance variation and number of data points – and look for dependencies among them. I created several algorithms for the analysis examining the detection of MSPs dependent on the fraction of blue binary stars and the abundance variation by fitting Gaussian mixture models (GMMs) to the colour distribution. Furthermore, they allow me to estimate the population fractions and compare the actual mock distributions with the Gaussian fits to see if they match each component.

I find that the fraction of blue binary stars does indeed influence the detection of MSPs such that higher binary fractions disguise the split MS which leads to fewer detections. Further, I find that the method applied to estimate the population fractions is insensitive to reasonable binary fractions producing fair population fraction estimates. However, the algorithm is not sophisticated enough to deal with large binary fractions and which leads to inaccurate estimates. Comparing the results to observations, 700 stars per cluster and binary fractions of up to 0.15 provide successful detection of MSPs and good estimation of population fractions. In the effort to separate the binaries from the single stars I find that the colour difference between single and binary stars is a narrow range, which could be used to set a prior for binary separation in subsequent works.

Abstract (german)

Diese Masterarbeit basiert auf dem Forschungsgebiet der Kugelsternhaufen, die sich nicht nur aus den ältesten Sternen in unserer Galaxie zusammensetzen, sondern auch ein Phänomen aufweisen, das als multiple Sternpopulationen (MSPs) bezeichnet wird. Diese MSPs weisen Unterschiede in der Häufigkeit von leichten Elementen wie unter anderem N, Na, He, C und O in der Sternatmosphäre auf. MSPs werden meist photometrisch beobachtet, wo die Schwankungen der Elementhäufigkeiten in Farb-Helligkeitsdiagrammen die Hauptreihe der Sternpopulation sichtbar in zwei oder mehr Spalten (blauer und röter) teilen. Zusätzlich fügen Doppelsterne (zwei unaufgelöste Sterne, die als ein heller Stern erscheinen) ein weiteres Level an Komplexität hinzu, da sie photometrisch nicht eindeutig erkennbar sind und so Abschätzungen der Masse, Helligkeit und des Energiehaushalts beeinflussen. Die korrekte Einschätzung von Doppelsternen ist jedoch von großem Interesse, da ihre Charakteristiken Aufschluss über die Bildungsmechanismen und -umgebungen von MSPs geben können. Tatsächlich wird die Entstehung von Kugelsternhaufen und MSPs noch nicht verstanden und ist seit Jahren ein viel diskutiertes Thema.

Daher untersuche ich in dieser Arbeit den Einfluss von Doppelsternen auf die photometrische Detektion von MSPs und inwiefern es möglich ist, Doppelsterne vom Rest der Population zu trennen. Dazu werden observierte Farb-Helligkeitsdiagramme mithilfe von "simple stellar populations" (SSPs) nachgeahmt. Folgend werden in der Analyse diverse Parameter der Kugelsternhaufen, die in die Diagramme eingehen (Anteil der Binärsterne, Verhältnis der Populationen zueinander, Ausmaß der Variation in Elementhäufigkeiten und Anzahl der beobachteten Sterne), variiert und nach Abhängigkeiten untersucht. Ich habe mehrere Algorithmen für die Analyse erstellt, die einerseits den Nachweis von MSPs und weiters deren Populationsverhältnisse untersuchen. Es werden Gaußsches Mischverteilungsmodelle (Gaussian Mixture Model, GMM) an die Farbverteilung gefittet und eine Metrik für die Ausprägung der bimodalen Verteilung eingeführt. Außerdem werden die tatsächlichen Subverteilungen mit den Gaußschen Wahrscheinlichkeitsverteilungen verglichen, um eine Übereinstimmung mit einzelnen Komponenten zu überprüfen.

Es wird festgestellt, dass der Anteil der Doppelsterne insofern einen großen Einfluss auf die Detektion von MSPs hat, als mit wachsender Anzahl weniger MSPs erkannt werden, da sie den Spalt zwischen den Hauptreihen teilweise füllen. Außerdem wird ermittelt, dass ein moderates Ausmaß an Binärsternen wenig Einfluss auf die Abschätzung des Populationsverhältnisses hat, das die Methode mit GMMs in dieser Ausführung nicht sensibel genug auf deren Anteil reagiert. Für Diagramme mit großem blauen Anteil der Sterne und deren Doppelsterne ist der Code nicht anspruchsvoll genug und es entstehen unzuverlässige Abschätzungen. Verglichen mit Beobachtungsdaten, ermöglichen 700 Sterne pro Kugelsternhaufen und einem Gesamt-Doppelsternanteil von bis zu 15%, eine zuverlässige MSPs Detektionsrate und eine gute Abschätzung von Populationsverhältnissen. Abschließend wird gefunden, dass der Abstand zwischen Binärsternen und ihrer Mutterpopulation im Farb-Diagramm stabil ist und so der GMM Fit mit "a priori Annahmen" erstellt werden kann, was möglicherweise eine Selektion von Doppelsternen ermöglicht.

Contents

Chapter 1

Multiple Stellar Populations in Globular Clusters

The topic of this thesis is a phenomenon called Multiple Stellar Populations (MSPs) that occur in Globular Clusters (GCs), and specifically, the interplay of binary stars in the detectability of the MSPs phenomenon. In this first chapter the topic is introduced and the main components, the GCs, the MSP phenomenon and the binary stars, are presented in detail.

Starting with GCs in Section 1.1 and their properties, I continue with MSPs, what they are, how they are detectable, their possible formation scenarios and further open question in Section 1.2. Next, Section 1.3 gives an introduction to binary stars and explains their participation in the topic of the thesis. The first chapter is concluded in Section 1.4 with a summary about the topic, putting binaries and MSPs into context and present the science questions the thesis is based on.

1.1 Globular Clusters

GCs are very old, very metal poor stellar systems, that are found in the halos of galaxies. These systems are very dense and have spherical or globular shape, hence the name. In Weigert 2012, a textbook for basic astronomy, mainly focuses on their density and especially on their old stellar population but not mentioning anything special about them. However, when they are observed in the blue and ultra-violet (UV) they show remarkable features, called MSPs (Section 1.2) in photometric diagrams (Section 1.2.4).

The fact that they have no recent star formation makes these clusters relics of the Early Universe through which it is now possible to investigate star formation conditions from a dozen billion years ago. They are perfect laboratories for star formation, dynamics and stellar evolution. Because of their density they and their cores survive encounters with greater systems such as galaxies and gather in the halos for us to observe.

Figure 1.1: This image of the globular cluster NGC 6121 (M4) was made with Wide Field Imager on the 2.2-meter telescope at the La Silla Observatory in Chile and taken from the ESO Archive[1]. The cluster hosts MSPs and has a measured binary fraction of 0.148 ± 0.0014 (Milone et al. 2012). Image Credit: ESO

1.1.1 Globular cluster properties

The age of GCs is inferred from isochrone[2] fittings (e.g. Martocchia et al. 2017, Milone et al. 2017b Figure 10). From Figure 12 in Martocchia et al. 2017 (later also adapted in Bastian and Lardo 2018 Figure 5a) it is possible to read that most GCs host stars with ages between 10 Gyr to 13.7 Gyr. This makes them stellar populations that are born very early in the Universe, probably under different circumstances. GCs are ancient systems that enable a view into past conditions regarding gas and dynamics. However, it has to be noted that objects with similar properties are existing today and still forming stars (Bastian and Lardo 2018 e.g. Section 7). Age is one factor deciding if MSPs are found in a GC (Section 1.2.2).

Furthermore, these spheroidal stellar systems have extreme masses of sometimes more than $1 \times 10^6\,M_\odot$ (Martocchia et al. 2017, Bastian and Lardo 2018) compared to the most massive open clusters of $1 \times 10^4\,M_\odot$ (Janes 2000)[3]. Although there are also less massive GCs (ranging from $1 \times 10^{4.5}\,M_\odot$ to $1 \times 10^6\,M_\odot$) the cluster mass is another factor for the pronunciation of MSPs in these cluster (Section 1.2.2).

The stellar density of GCs is very extreme as the high masses are confined to rather small spatial scales. In fact, contrary to other systems in the universe, the centres of GCs are considered collisional, meaning they regularly have star-star interaction. The stellar density is as high as several 1000 stars per pc^3 in the centres and less than 0.1 stars per pc^3 in the outskirts

[1] ESO Archive (M4) https://cdn.eso.org/images/screen/eso1235a.jpg (retrieved on February, 28 2021)

[2] Isochrones are stellar populations where all stars (of all different masses) have the same age and metallicity. See Section 1.2.3 for details.

[3] found when searching for: 'Star Clusters Encyclopedia of Astronomy and Astrophysics', retrieved March 5, 2021

(see Figure 6 from de Boer et al. 2019 for reference). This extreme number density in the centres make it very hard to resolve single stars. However, there are studies on individual GCs that aim to resolve their centres (Milone et al. 2014, Giesers et al. 2019).

GCs are also known to have very low metallicity ([Fe/ H]) from their formation in the Early Universe. In Figure 5b from Bastian and Lardo 2018 most of the GCs are in a metallicity range between -1.0 and -2.5 [Fe/ H] where solar metallicity is $[Fe/H]_{\odot} = 0.0$.

1.1.2 Occurrence

GCs are found in galactic halos of dwarf galaxies as well as major galaxies which is found for example by Forbes et al. 2018 who finds that the number of GCs and the GC-system mass increases for increasing galaxy halo mass. There is also evidence that some GCs are disrupted by the galactic gravitational potential during their orbit forming tidal tails and resulting in tidal streams (Ibata et al. 2019, Sollima 2020). Their formation is a yet unanswered question but there are studies, that look at the possibility of accretion or in-situ formation via simulations (Keller et al. 2020) and observations (Leaman et al. 2020). As the formation of MSPs is tightly linked to that of their GCs this topic is discussed in more detail in Section 1.2.6.

There are also several younger very massive clusters in our galaxy, called young massive clusters (YMCs) that even succeed GC masses and densities. They are the ideal places to study star formation scenarios in similar conditions as GCs even more so as they feature complex CMDs as well. The YMCs in our galaxy are mostly hidden behind molecular clouds but the Magellanic Clouds host some as well for us to study. (Bastian and Lardo 2018 Section 7)

1.2 Multiple Stellar Populations in Globular Clusters

Following the brief introduction to GCs I also give an overview of their most exciting feature: the Multiple Stellar Populations (MSPs). MSPs are a variation in star-to-star light element abundances which can not only be measured spectrocopically but also seen in photometrically generated Colour-Magnitude diagrams (CMDs). Their formation is a frequently discussed topic that I will briefly touch upon in Section 1.2.6. There are many mysteries yet to be uncovered such as the mass-budget problem researchers are faced to solve (Section 1.2.5).

Contrary to reference literature I do not imply that the populations are divided in generations and are neither older nor younger. In this chapter I mainly refrain from putting the P1 and P2 name on the said sequence as they are repeatedly confused in the literature and so is their relative position in the CMD not yet clearly defined (e.g. conflicting conventions in Nardiello et al. 2015 and Martocchia et al. 2017 also in connection to Figures 1 and 3 in Bastian and Lardo 2018) . Therefore, I named the populations from left to right as seen in the CMDs. The left sequence is called P1 and the right one, P2. Their binary stars are accordingly called b1 and b2.

1.2.1 Light element abundances

MSPs in GCs often consist of two populations that do not vary in age or metallicity but they do vary in light-element abundances (Bastian and Lardo 2018 Section 2.1.1)[4]. Whereas the one population has the same light element abundance pattern as field stars of the same metallicity the stars of the other population(s) have a difference abundance pattern. Specifically, they are mainly overabundant in helium (He), nitrogen (N) and sodium (Na) while they are depleted in carbon (C) and oxygen (O). The abundance patterns of N-C and Na-O are anticorrelated whereas N-Na is correlated in most clusters. (Bastian and Lardo 2018 Section 2.1.1) For example populations with low Na abundance are enriched in O and the population that is enriched in Na is also enriched in N but depleted in O (cf. Figure 1 a and b in Bastian and Lardo 2018).

Without going into detail of the creation of said light elements most of them are created during the CNO-cycle in giant stars from later evolutionary stages. Therefore the question remains how these abundance patters can be found in MS stars as well since they can not have been produced yet which leads to assume a previous generation produced them. (Bastian and Lardo 2018 Section 2.1.1) However, as already mentioned the populations in GCs have the same age, thus creating a puzzle with many pieces that is not easily solved. Another peculiarity is that these enriched stars have lithium (Li) in their shells which should be destroyed by the same processes that create the N and Na abundances. Some proposed scenarios are presented in Section 1.2.6 later in this chapter.

1.2.2 Dependency on cluster mass and age

The above mentioned star-to-star variations in light element abundance is in fact found to be linked to their GC's properties. Specifically, MSPs only appear in old clusters and the amount of light element and He variations increases with cluster mass.

Concerning the dependency on cluster mass Figure 4 in Bastian and Lardo 2018 illustrates this topic well. Studies with a larger amount of data found that the Na-O anticorrelation does depend on cluster mass in the sense that higher mass clusters exhibit more extended Na-O anticorrelations. This is not explained yet since there is no apparent connection between the extend of processed stellar material and the cluster properties. (Bastian and Lardo 2018 Section 2.5.1) The He spread between the two populations increases with increasing cluster mass and so does the number of enriched stars as well. Specifically, the fraction of chemically enriched stars stars is larger for higher mass clusters ranging from 40 % to 80 % for clusters of masses between $1 \times 10^5\,M_\odot$ to $1 \times 10^6\,M_\odot$. (Bastian and Lardo 2018 Section 2.5.1)

Martocchia et al. 2017 found that MSPs are exclusively found in GCs that are older than $\approx 2\,\mathrm{Gyr}$ (Figure 12). None of the clusters that are younger host MSPs. On the other hand, almost all massive GCs that are older than $\approx 6\,\mathrm{Gyr}$ do have these star-to-star variations. The questions if MSPs stopped to form around 2 Gyr ago is not answered as no study has yet

[4]Bastian and Lardo 2018 is an Annual Review Article, thus giving a good overview of the topic. I mention the section specifically to make the source and references they use in their review easily detectable. I mainly cite the review except for papers I read myself.

found any trace of abundance spreads in younger clusters. (Bastian and Lardo 2018 Section 2.5.2)

A further characteristic of most GCs seems to be a radial distribution of the population ratios. Here, in a large fraction of GCs the enriched population is more centrally located than the primordial population. (Bastian and Lardo 2018 Section 2.4.1)

1.2.3 Isochrones and simple stellar populations

An isochrone is a curve on the Herzsprung-Russel diagram that describes a population of stars that have the same age and metallicity. It is possible to create a simple stellar population (SSP) with a given age and metallicity by populating the isochrone with stars of different masses. The stellar masses are taken from an initial mass function (IMF) that describes how many stars for each stellar mass there are in a population. The SSP includes stars of many evolutionary stages (main sequence (MS), red giant branch (RGB), horizontal branch (HB) etc.) because stars with higher masses in the SSP evolve more quickly. For older populations, like the ones found in GCs, only the less massive stars ($< 1\,M_{\odot}$) remain in the population because the more massive ones already died. This SSP is not the same as a stellar population in a GC but as this thesis aims to recreate the CMDs of MSPs it is a good approximation. The main difference is in using metallicity variations to mimic actual light-element abundance variations. Whereas metallicity includes all elements heavier than hydrogen (H), I am varying the sum of all elements and not the abundance variation of the specific elements. The effect of both, metallicity and light-element variation, in the CMD is similar for MS stars and we take advantage of that.

1.2.4 MSPs in Colour-Magnitude diagrams

Ideally, we could have wide field spectroscopic observations to positively determine the light element variations in MSPs. However, as spectroscopic observations are limited, photometric analysis are commonly used and the base of most studies investigating MSPs. They enable to include a large numbers of stars over a spatially broader region in the sky which improves statistics. Also, most of the time only two to three filters are needed to detect MSPs (partly based on Milone et al. 2012 page 2 and Bastian and Lardo 2018 Section 2.2).

In CMDs GCs are found to host MSPs due to their split MS, one to the redder and one to the bluer side of the diagram. This is done by using specific colours on the abscissa and also combinations of colours (so called 'chromosome maps' (Milone et al. 2017a)) to reveal MSPs. Where variations in N, C and O are mostly detected by blue and UV filters (3000 Å $<$ $\lambda <$ 4000 Å), He variations are mostly seen in optical (B - I and V - I, (Nardiello et al. 2015) and references therein). Because the light element variations between the two populations differ most near the UV spectrum it is the most sensitive to the split sequences of the MS, RGB and the HB. (Bastian and Lardo 2018 Section 2.2.1)

Apart from usual CMDs Milone et al. 2017a introduced chromosome maps (pseudo colour-

colour diagrams) which are sensitive to the abundance spreads in populations. It was later found that these diagrams show N spreads on the ordinate and He variations on the abscissa. The diagram is so sensitive as to make the division into several subpopulations possible. (Bastian and Lardo 2018 Section 2.2.1)

1.2.5 Mass-budget problem

It has been found that a typical GC is made of $\approx 33\%$ P1 stars and $\approx 67\%$ P2 stars (Bastian and Lardo 2018 Section 5.4). So if the polluted material comes from a prior generation of stars (see Section 1.2.6 below), which now only makes up a third of the cluster, their polluted material could never explain the overabundance of light elements found in the ensuing generation of stars. Studies suggested that the prior generation must have been much larger and the cluster lost almost all of them due to internal and external forces. This argument is, however, shown to be unlikely based on observations and simulations that find such huge losses can not be expected. For instance the fact that the fraction of enriched stars grows for increasing cluster mass suggests that even greater numbers of primordial stars must have been lost to more massive clusters. This, however, is unlikely as higher mass clusters are less affected by mass loss. (Bastian and Lardo 2018 Section 5.4.1)

Further, there is a mass-budget problem when comparing the number of primordial stars in the cluster to those in the galactic halo. After counting the low metallicity stars in a dwarf galaxy and in all of its GCs, it was found that about a quarter of all primordial stars reside in the dwarf galaxy's halo. So if all of the stars in the field origin in GCs this would only explain a small fraction of the actually needed stars for this prior/ ensuing generation scenario. (Bastian and Lardo 2018 Section 5.4.2)

The mass-budget problem remains yet to be solved. Some formation scenarios are build around this conflict and try to explain MSPs regarding the observed mass budget (Bastian and Lardo 2018 Sections 4.5 and 4.7).

1.2.6 Formation Scenarios

Several formation scenarios of MSPs and GCs have been proposed and investigated, some being slightly exotic. I will briefly present two scenarios. The inconsistencies that need to be explained are the enhancement of MS stars in the enriched populations that could not have happened within their cores. Further the problem that Li is still found in some stars where the presence of light element abundances would otherwise suggest all Li should be burned already by the hot temperatures. One more major aspect of MSPs is that the primordial populations consists of too few stars to sustain the enhancement in light element abundances of the enriched populations. (Bastian and Lardo 2018)

The most commonly considered and/ or investigated scenario is the asymptotic giant branch (AGB) scenario (mentioned in Bastian and Lardo 2018 Section 4.1, D'Ercole et al. 2008). It starts with one SSP of primordial stars referred to as the first generation (1G). Their massive stars will pollute the interstellar medium (ISM) during their AGB phases and after the processed material mixes with primordial gas (dilution) a second generation (2G) is born with a range of primordial O abundances and enriched in Na. However, the models shortcoming lie for one in (i) the mass-budget problem, also that (ii) too little Na is produced, (iii) the unexplained Li abundance and (iv) that cooling rates are not likely achieved to so rapidly form the 2G stars. 1G AGB stars produce too little processed material to enrich the number of 2G stars to such an extent without loosing almost all 1G stars. The rapid cooling needed to quickly produce a second enriched population is unlikely because of radiation produced by several components (e.g. x-ray binary stars) in the cluster. (Bastian and Lardo 2018 Section 4.1.1)

Other scenarios include fast-rotating massive stars (FRMSs) as the polluters for the enriched population. The fast rotation is needed in order to transport processed material from the star's core to its surface and to be subsequently lost through stellar winds. One method includes generations as well, with the 1G FRMSs providing the polluted material for the 2G. Here, thy naturally produce large He spreads and an Na-O anticorrelation (including dilution with primordial gas) in the 2G stars. Another way of releasing the processed material of a star is by binary interactions. However, the mass budget problem and observed abundance variations that can not be reproduced are the main limitations again. It is also very difficult to explain the not existing spreads in metallicity. (Bastian and Lardo 2018 Section 4.2)

There are several more methods, some making use of FRMSs in combination with other events, trying to solve one problem but not able to explain some others. Several methods not only base their theories on GC observation but also on YMCs as present GC analogues. For a general and more detailed overview see Section 4 in Bastian and Lardo 2018. The above mentioned scenarios (and some others) use binary interactions to explain various outcomes. It is therefor of interest to estimate binary fractions in GC MSPs.

1.3 Binaries in Globular Clusters

Binary stars are two stars that are gravitationally bound to one another rotating around the common centre of gravity. Although they are separate stars, given resolution limits they often appear as a single point-source in photometric observations. There are several methods to detect binaries, one of them being photometrically in CMDs (Section 1.3.2) as they reside in diagram areas of higher magnitude. Independent on the method understanding binaries is of great interest because they have a large influence on the evolution and understanding of MSPs and their formation in GC.

1.3.1 Binary stars and MSPs in GCs

Binary systems are not only interesting because of their impact on the cluster but also they give insight into the birth environment of the cluster itself. As found by Dalessandro et al. 2018 the two populations, primordial and enriched, vary in velocity dispersion in their analysed cluster NGC 6362. They showed that the higher binary fraction of the primordial population could be responsible for the energy difference. Similar results were found by Hong et al. 2019 in their simulations. This implies the influence binaries have on the energy budget.

The information of binaries are further used to investigate the formation environment of clusters. It has generally been found that the fraction of primordial binary stars is higher than the fraction in the enriched population (Lucatello et al. 2015) (Dalessandro et al. 2018) while at the same time the fraction of binaries increase towards the cluster centre (Milone et al. 2012) (Giesers et al. 2019). Additionally, Milone et al. 2020 found that the fractions of binary star per population are similar. This would support the formation scenarios where the enriched populations is born in the centre of the cluster in very dense environments destroying all loose binaries (Lucatello et al. 2015). Also that mass segregation pulls binary systems to the centre (Hong et al. 2019) suggesting that if enriched stars are centrally concentrated but the binary fractions are similar most primordial stars in the centre are in multi-star systems.

As mentioned in Milone et al. 2012 in binary systems stellar evolution happens differently. In the second version of the FRMS formation scenario it is proposed that massive binary stars are able to quickly mix their produced material from their cores to their shells. This enables quick stellar evolution and pollution of the ISM. (Bastian and Lardo 2018 Section 4.2)

Generally, in the field the majority of stars are actually binary systems (Milone et al. 2012) whereas in GC the binary fractions are mostly smaller than 10%, some between 10% and 20% and few have binary fraction larger than 30% (from Table 2 in Milone et al. 2012).

The binary stars in the GC are found to have a flat mass ratio distribution for mass ratios ≥ 0.5 (Milone et al. 2012). This means, that on average there is the same number of equal mass binaries as binary systems where one star is only half as massive ($q = 0.5$, see Chapter 2 Section 2.2.3 for details). Further, the binary fraction in a GC shows a significant anticorrelation with cluster luminosity and hence with cluster mass as well (from the mass-luminosity correlation e.g. Weigert 2012 Section 11.1) (Milone et al. 2012). So the more massive a clusters the smaller the binary fraction. This paper also mentions that binary stars influence the mass estimate and luminosity functions of GC making it necessary to know the binary fractions and spatial distribution.

All these discoveries and simulations support the fact that binary stars play a major role in GC evolution and therefor we need more data to improve statistics and get better estimates on how they are distributed.

1.3.2 Binary stars and MSPs in Colour-Magnitude diagrams

This thesis only works on a photometric representation of GC populations and also includes binary stars in the CMDs as most studies are done photometrically as well (see Section 1.2.4). Since they are two unresolved stars they are brighter than their single star neighbours. The excess in brightness depends on the mass ratio of the binary system. The maximal increase in brightness is given for a binary pair of two equal mass stars. For a clear illustration of this topic see Figure 1 in Milone et al. 2012. The equal mass binary sequence runs parallel to the single star MS of the population.

This already foreshadows what the implied complexity between binary stars and MSPs in a CMD. Taking the blue MS and adding binary stars will have them to the redder side of the CMD some magnitude-fraction above the blue MS. Now a second red MS is added to the CMD which also brings binaries that are even to the redder and brighter still. Now the question is where the blue binary stars are positioned in the CMD relative to the second red population. Milone et al. 2020 show an example of two populations with binary stars and this thesis also investigates this aspect of binary sequences and how they photometrically interact with the MSPs.

1.3.3 Mixed binaries

Maybe missing in this analysis is the mixed binary population that Hong et al. 2015 and Milone et al. 2020 discuss and find in their studies. Mixed binaries is the name for a binary system where one star is from the enriched and one from the primordial population. Hong et al. 2015 find that when they increase the binding energy of binary systems for both populations they end up with more mixed binaries at the end. Meanwhile in Milone et al. 2020 it is shown that fitting the binary distribution of two populations is achieved more accurately when they include a third sequence to their fit. In the CMD their mixed binaries lie between the blue and red binary sequence as would be expected. This topic is taken up again and discussed further in Chapter 4 Section 4.1.5.

1.4 Brief summary and outlook

Finally, I will summarise the introduction to GCs, MSPs and binary stars and connect them in order to have a foundation to build the following chapter on.

GCs are the oldest stellar systems around the galaxy and for a bit more than a decade now it is know that they are very interesting subjects indeed, due to the phenomenon of MSPs. This phenomenon is where there are star-to-star variations in light element abundances within one population of stars. These abundance variations can be observed in the optical and near UV in colour magnitude diagrams where they feature in split sequences of the MS, the RGB and occupy different colour-magnitude positions in the HB. Their origin and/ or formation is yet unsolved as there are several complexities and seeming contradictions to our observations. One element that can shed light on some formation constraints are the binary stars in these clusters. They influence the energy budget and might even leave fingerprints of initial conditions.

The objective of this thesis is now to investigate the interplay between binary stars and their parent single-stars populations. Where do the blue binaries lie relative to the red main population and (how) do they influence the detection of MSPs? Another topic is to probe a method to separate the populations and eventually also investigate the possibility to select the binary stars from the total distribution of cluster stars.

Chapter 2

Methods

In this chapter the methods are described that I developed to identify Multiple Stellar Populations (MSPs) in Globular Clusters (GCs). It is structured mostly in chronological order. It starts with the acquisition of the data in Section 2.1 (page 11) which is followed by the description of building the photometric mock cluster data in Section 2.2 on page 13. I conclude the methods chapter by explaining how the mock data is verticalised and analysed regarding several different parameters. Section 2.3 (starting on page 21) also contains the creation of a metric to ascertain the existence of MSPs in the mock clusters.

All cluster creation, data analysis and figures are created with the programming language *Python*[5]. I use *matplotlib*[6] (Hunter 2007) for every figure and *numpy*[7] in every script. More specific Python packages are mentioned in the sections where they are used.

2.1 Stellar Populations Models

The main aim was to create photometric mock data of a GC hosting MSPs. This data then needs to show two separate sequences of the two populations when visualised in a colour-magnitude diagram (CMD). An easy way to achieve this mock cluster representation is to create simple stellar populations (SSPs). As mentioned in Chapter 1 Section 1.2.3 it is a fair assumption to represent a stellar population by an SSP as stars in one population are born at roughly the same time. As indicated, SSPs are not an accurate representation of MSPs, however it serves as a reasonable approach. Thus, the first step is to create a populated isochrone with a metallicity and age that is usual for a GC. To create the isochrone I chose to use PADOVA[8] (Bressan et al. 2012) isochrone data which is downloadable from the CMD web interface site[9]. Leaving all other parameters on default I made sure to use the Kroupa (two-part power law and binary corrected) initial mass function (IMF) and download absolute magnitudes for the 'UBVRIJHK (cf. Maiz-Apellaniz 2006 + Bessel 1990)' filter system.

[5]Python Software Foundation https://www.python.org/
[6]Matplotlib https://matplotlib.org/
[7]NumPy https://numpy.org/
[8]PARSEC STELLAR EVOLUTION CODE https://people.sissa.it/~sbressan/parsec.html
[9]CMD 3.4 input form http://stev.oapd.inaf.it/cgi-bin/cmd

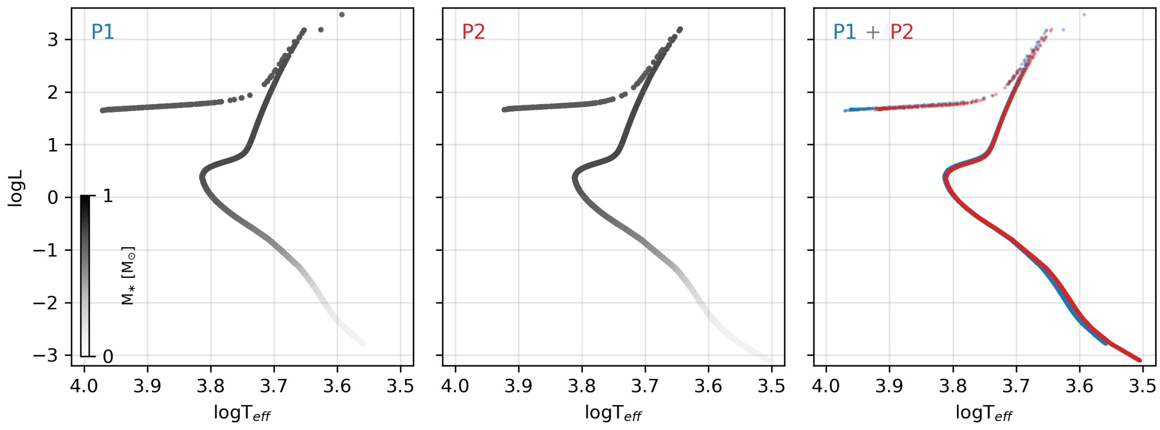

Figure 2.1: From left to right: the isochrone of the population one stars (P1) plotted in an Hertzsprung-Russel diagram (HRD), the isochrone of the population two stars (P2), both isochrones in one HRD to visualise the shift in metallicity which mimics the variation in light element abundances of the two populations. The isochrones are coloured in blue (P1) and red (P2), respectively.

Considering the latest addition[10] to the stellar population tables, which is the Long Period Variability (LPV), I need to mention I only used the fundamental mode and first overtone periods, as I did not make use of LPV in my thesis. With the help of Figure 12 in Martocchia et al. 2017 I decided on an age of 13 Gyr. For the first population metallicity (Z_{P1}) I chose 0.0001 in absolute metallicity ($[Fe/H]_{P1} = -2.09$) by looking at Figure 5b in Bastian and Lardo 2018.

I downloaded three sets of populated isochrones, all with the properties that are mentioned above and each SSP having a mass of $1 \times 10^5\,M_\odot$. Because the sum of the stellar mass of one SSP table as computed after downloading is only about $3.5 \times 10^4\,M_\odot$, three sets of SSP tables are needed. $1 \times 10^5\,M_\odot$ per populated isochrone is enough data to allow for variation in the contribution of each population (P1 and P2) later on.

The result of three sets of SSP tables is plotted in the left panel of Figure 2.1 labelled P1 in the upper left corner. The plot is a Herzsprung-Russel diagram which shows the effective temperature against the luminosity of stars. The population has a main sequence (MS) on which stars evolve from the bottom right corner and move up- and leftwards. There is also a sub-giant (SGB) and red giant branch (RGB) where stars evolve towards the upper right again after which they turn down and left again into the asymptotic giant branch (AGB). Most stars are along the main sequence in this SSP and they are lower mass stars as the colour-scale shows.

This populated isochrone now represents one population in a GC. In order to investigate the phenomenon of Multiple Populations it is necessary to add a further population that differs in light element (LE) abundances. However, as a variation in LE abundances is not implemented in any stellar population code I approached this problem by creating a second set of three populated isochrone tables with different metallicity. If the second isochrone has

[10] noted on March 11, 2021

higher metallicity or age it will be shifted to the right.

Because I am focusing on the MS of isochrones in my thesis I use the CMD that Nardiello et al. 2015 presents and which proves to be efficient in photometrically detecting the existence of MSPs in the MS. Because MSPs in the MS are especially well detectable in the ultra-violet (UV) and blue light (Nardiello et al. 2015) it shows the colour of the U-band minus the B-band plotted against the B-band magnitude. This leaves stars with redder colours to the right bluer colours to the left. The brighter a star the smaller the magnitude and thus the higher it is found in the CMD. Depending on this diagram, the metallicity of the second population was chosen to show a colour difference (in U-B) of close to 0.1 mag. This resulted in a metallicity for P2 (Z_{P2}) of 0.000 17 or $[Fe/H]_{P2} = -1.86$. The result of this second population is shown in the second panel of Figure 2.1.

Comparing the first (P1) and second population (P2) HRDs in Figure 2.1 and looking closely at the grid, a slight shift is noticeable. Putting them together in one HRD (right plot labelled P1+P2) directly compares the two populations in blue and red for P1 and P2, respectively.

2.2 Creating a model cluster CMD

After having sampled a broad data set of stars the cluster can be built. To start with, the cluster is created making the first and then the second population separately. So all steps are done first for P1 and then for P2 and are subsequently combined to one file which I call a cluster. The parameters that define the clusters are cluster mass, distance to the cluster, the mass share of P1 and P2 stars, the percentage of binary stars per population and which method to use for creating the binary stars.

The general method is to take stars from each population until a given mass is reached. Then, binary stars are created from stars in the cluster and added to the population. Finally, a realistic error is added to the data points to create CMDs that are similar to observed ones (for example in Nardiello et al. 2015 or Milone et al. 2019).

2.2.1 Adding an error to the data

Before building the cluster I created the photometric error that is added to each data point. As a first attempt, I added a random error to the data that is drawn from a normal distribution with constant standard deviation (σ) of 0.04 (as taken from Stetson et al. 2014) and mean as 0.0. However, a constant standard deviation failed to capture noise as observed in real data sets. Consequently, in order to make it more realistic the standard deviation of the magnitude error needed to increase with decreasing brightness. To achieve that Dr. Prashin Jethwa used observed data of 5 GC (NGC104 (blue), NGC188 (orange), NGC1851 (green), NGC2682 (red), NGC2818 (purple)) in 5 different bands (U, B, V, R, I). He calculated the median error for several magnitude bins and then used those to fit the curve to the median of the magnitude errors across all bands and clusters. See Figure 2.2 for a visualisation. As an example, all

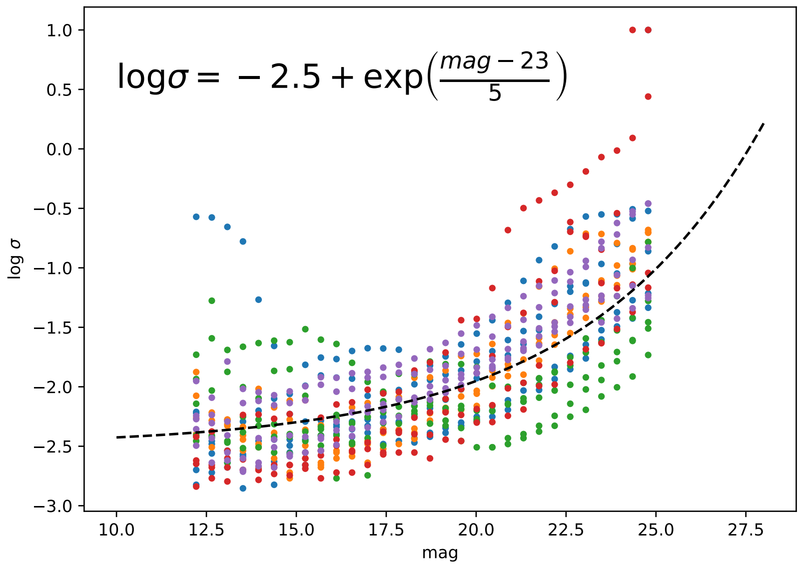

Figure 2.2: This figure has been created by Dr. Prashin Jethwa. It shows observed magnitudes of GC on abscissa and the corresponding magnitude error ($\log\sigma$) on the ordinate. Each coloured dot shows the measured error from the same cluster for different bands. On top is the fitted curve to the data which is then used to create the error.

blue dots are from cluster NGC104. For each magnitude bin there are 5 different error values resulting from the 5 pass bands. The curve is fitted to all magnitude error values of all pass bands and all clusters. For clusters NGC188 (orange) and NGC2682 (red) the U and R band errors, respectively, are missing. This is the fitted function:

$$\log\sigma = -2.5 + \exp\left(\frac{mag - 23}{5}\right) \tag{2.1}$$

The resulting σ gives a standard deviation dependent on the apparent magnitude mag. With the standard deviation the magnitude error is drawn from a random normal distribution with the above standard deviation and a mean at 0.0. This is then added to the apparent magnitude mag of a star.

The apparent magnitude (mag) is calculated with the distance modulus for each star from its absolute magnitude (M) which comes with the SSP tables. The distance modulus is specified below in a version where absorption is not taken into account. d is the distance.

$$mag = \mathrm{M} + 5mag \cdot log10\left(\frac{d}{10\mathrm{pc}}\right) \tag{2.2}$$

Figure 2.3 shows how the implemented error behaves depending on magnitude for the first and second populations separately in the left and middle panel, respectively. The right panel shows how they look in one plot overlapping with each other. It is clearly visible how the magnitude error increases with decreasing apparent magnitude.

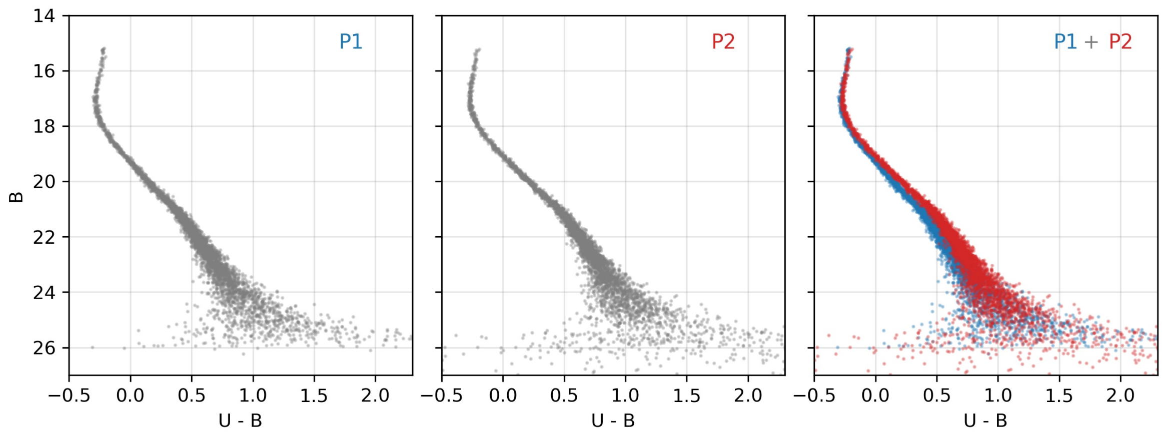

Figure 2.3: From left to right: colour-magnitude diagram (CMD) picturing a fraction of the P1 stars on the MS, the same for the P2 stars in the middle panel, both populations shown in one CMD coloured in blue and red for P1 and P2 respectively. The ordinate is in units of apparent magnitude.

2.2.2 The population ratios

The cluster mass of all mock GC created in this thesis is $1 \times 10^5\,\mathrm{M}_\odot$ regarding Figure 12 in Martocchia et al. 2017. This is on the lower mass end, however, it is represented often in observations and allows for a reasonable data size to manage computationally. The standard cluster which represented if not mentioned otherwise has a population ratio of 33 to 67 for P1 and P2, respectively. This is in accordance with literature, e.g. Bastian and Lardo 2018. However, the population ratio will be diversified to analyse their effects on CMDs and detection of MSPs.

When given the cluster mass, the mass of each population is calculated from the given ratio. After randomly adding stars to P1 until the mass is reached, all stars above a log-luminosity (logL) value of 0.72 and a log-effective temperature (log$\mathrm{T_e}$) above 3.84 are removed because I focus on the main sequence of GCs. This affects few stars, however, it is done while building the cluster to avoid having to do it every time when analysing the final clusters and thus saving time.

2.2.3 Creating binary stars

The number of binaries (N_{b_k}) created depends on the binary fraction (f_{b_k}) or as mentioned above, the percentage of binaries per population. This fraction refers to the number of stars in the population (N_{P_k}) like in the equation below. The number of binaries is then added to the population stars.

$$N_{b_k} = N_{P_k} \cdot f_{b_k} \tag{2.3}$$

f_{b_k} can be altered freely.

$$N_{P_{k,tot}} = N_{P_k} + N_{b_k} \tag{2.4}$$

For the standard cluster described above (Section 2.2.2) the first population (P1) has 30 % binaries added to them. The P2 has only 5 % binary stars added to it. This shifts the population ratios slightly. However, that does not make a difference as long as I track the correct population ratio. Similar to the population ratios the binary percentages will also be varied to inspect the effects they have on CMDs and MSPs detection.

For this work two algorithms are investigated to select which stars will be matched to become binaries. Binaries are two unresolved stars that consequently appear as one star with above average brightness in a CMD. With either method to join stars the aim is to recreate observed binary mass ratio distributions (e.g. Milone et al. 2012 in Figures 23 and 24). The algorithms differ such that the first method matches stars randomly and the second method pairs stars in a more sophisticated way. Both algorithms are explained in more detail below. In the end I picked the first method because it is effective and much faster than the second method.

The first algorithm randomly adds up one star with the star next to it. For that the number of binaries is calculated based on their percentage of stars from P1 and P2 (see Equation 2.3). Then twice the amount of single stars are randomly chosen and paired. This method works well because the stars are not listed in any order and the majority of stars have similar mass (Kroupa IMF). The corresponding mass ratio distribution is shown in Figure 2.4. The purple triangles represent the randomly created binaries.

The olive green dots correspond to the second method to create binaries. For this method I created uniformly distributed random values between 0.2 and 1.0. These values represent the mass ratios for the binaries that are to be created. The number of mass ratio values and single stars depends on the number of binaries to be created. Taking one star and mass ratio value after the other I search for a second star. This second star is selected when it has the mass to complement the first star in order to create a pair with the chosen mass ratio value.

$$M_{\star_2} = M_{\star_1} \cdot R_{\text{mass}} \tag{2.5}$$

Here, $M_{\star_k}$ are the star masses and R_{mass} is the randomly chosen mass ratio from a uniform distribution. For example, if the first star has a mass of $0.5\,\mathrm{M}_\odot$ and the mass ratio value is a) 1.0 or b) 0.5 the second star needs to have a mass close to either a) $0.5\,\mathrm{M}_\odot$ or b) $0.25\,\mathrm{M}_\odot$.

Independent of the chosen method the actual creation process is the same. To mimic a binary star in the CMD I needed to add up the luminosities of two stars. Therefore, the absolute magnitudes of the original data sets are converted to luminosities. This uses the following equation.

$$\mathrm{M}_\star - \mathrm{M}_\odot = -2.5 \cdot log_{10}\left(\frac{\mathrm{L}_\star}{\mathrm{L}_\odot}\right) \tag{2.6}$$

And in order to get the luminosity where the absolute magnitude of the Sun ($\mathrm{M}_\odot$) is equal

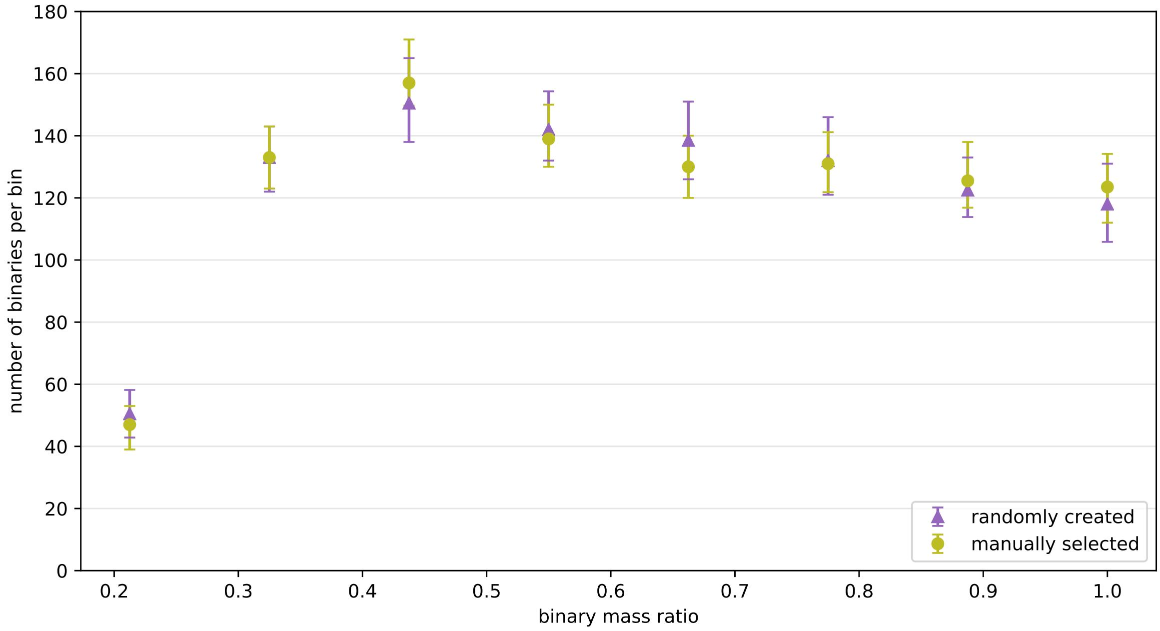

Figure 2.4: This shows the mass-ratio distribution of the binary stars for two methods. Randomly created binaries are plotted in purple triangles and manually matched binaries are shown in olive dots. In both cases the distribution is nearly flat beyond mass ratios of 0.5 which agrees with observational constraints. As the random matching is computationally much more efficient I chose this method to work with.

to 4.74 the equation is rearranged as so.

$$\frac{\mathrm{L}_\star}{\mathrm{L}_\odot} = 10^{\,0.4\,\cdot\,(\mathrm{M}_\odot - \mathrm{M}_\star)} \tag{2.7}$$

After calculating the luminosity for two stars they are added up and the sum is converted back to absolute magnitudes and further to apparent magnitudes (see Equation 2.2).

Meanwhile, both masses are added up and the mass ratio of the two stars is calculated in order to check the binary mass ratio distribution.

$$M_{\text{bin}} = M_{\star_1} + M_{\star_2}$$

$$R_{\text{mass}} = \frac{M_{\star_j}}{M_{\star_k}}$$

for j and k being 1 or 2 and 2 or 1, respectively, depending on which version results is the ratio being smaller than 1.0. According to Milone et al. 2012 MS binary mass ratio distribution for ratios that are larger than 0.5 is mostly flat and below 0.5 constraints are not available. Both methods achieve such a mass ratio distribution.

As can be seen in Figure 2.4 there is almost no difference in the outcome of the two methods of randomly or 'manually' pairing stars to binaries. Both distributions show a nearly flat or uniform distribution for mass ratios greater than 0.5. This is the range that compares to Milone

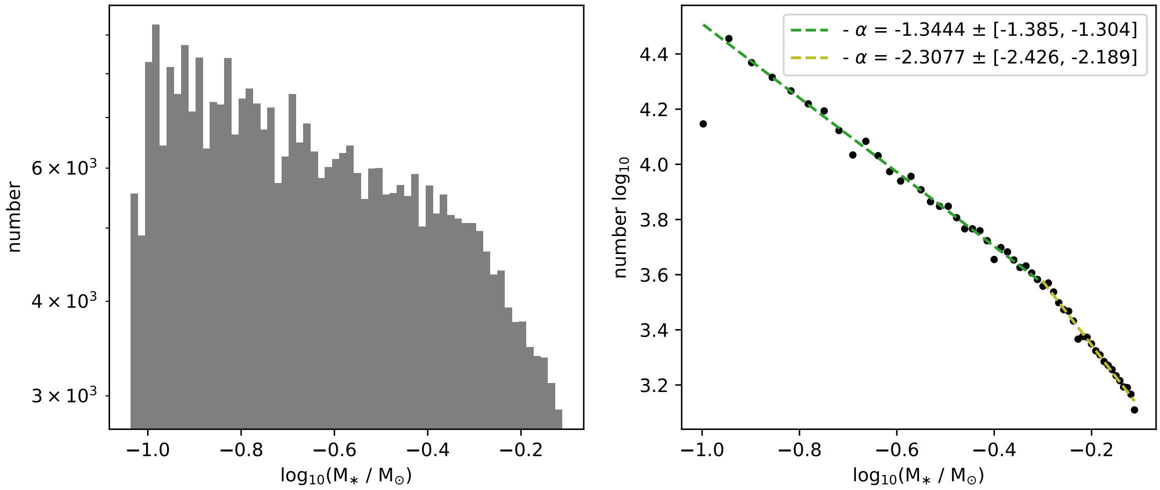

Figure 2.5: This figure shows that the artificial cluster data sets approximately matches the original mass function slopes when the binary stars are not included. The legend plots the fitted gradients and the 95% confidence interval.

et al. 2012. The slight increase in number of binaries towards lower mass ratios has also been found by Cohen et al. 2020 for MS binary populations. Although it is possible to choose which method to use when creating a cluster the random method was used to create all the clusters investigated for this thesis. The reason is that the distribution is so similar for either method and the randomly pairing is much faster.

There are no binaries created from the first and second population mixed together. According to Milone et al. 2020 mixed (population) binaries can make a fair amount of binary stars in GCs. However, this thesis only regards binaries that consists of two stars from the same population. For a discussion of this constraint see Chapter 4 Section 4.1.5 (page 54.

2.2.4 The final cluster

After binaries are created and added to the populations the error (as describes in Section 2.2.1) is applied and all stars are saved in a data file. This is now called a cluster. For further mentions of 'the cluster', it refers to the standard cluster with a [P1, P2] percentage of [33, 67] and a binary [b1, b2] percentage of [30, 5].

Subsequently, it is necessary to check if the mass distribution of the cluster still follows the chosen initial Kroupa mass function. This is done without the binaries since the IMF was also corrected for binaries. The comparison is done by fitting the cluster mass distribution and checking its gradients. The result is shown in Figure 2.5. The gradients are very close to the initial mass function and the 95% confidence intervals are reasonably narrow.

Finally, CMDs of the cluster are plotted to examine how the mock Globular Cluster compares to observational data. The Colour–Magnitude diagrams are visualised in Figures 2.6 and 2.7.

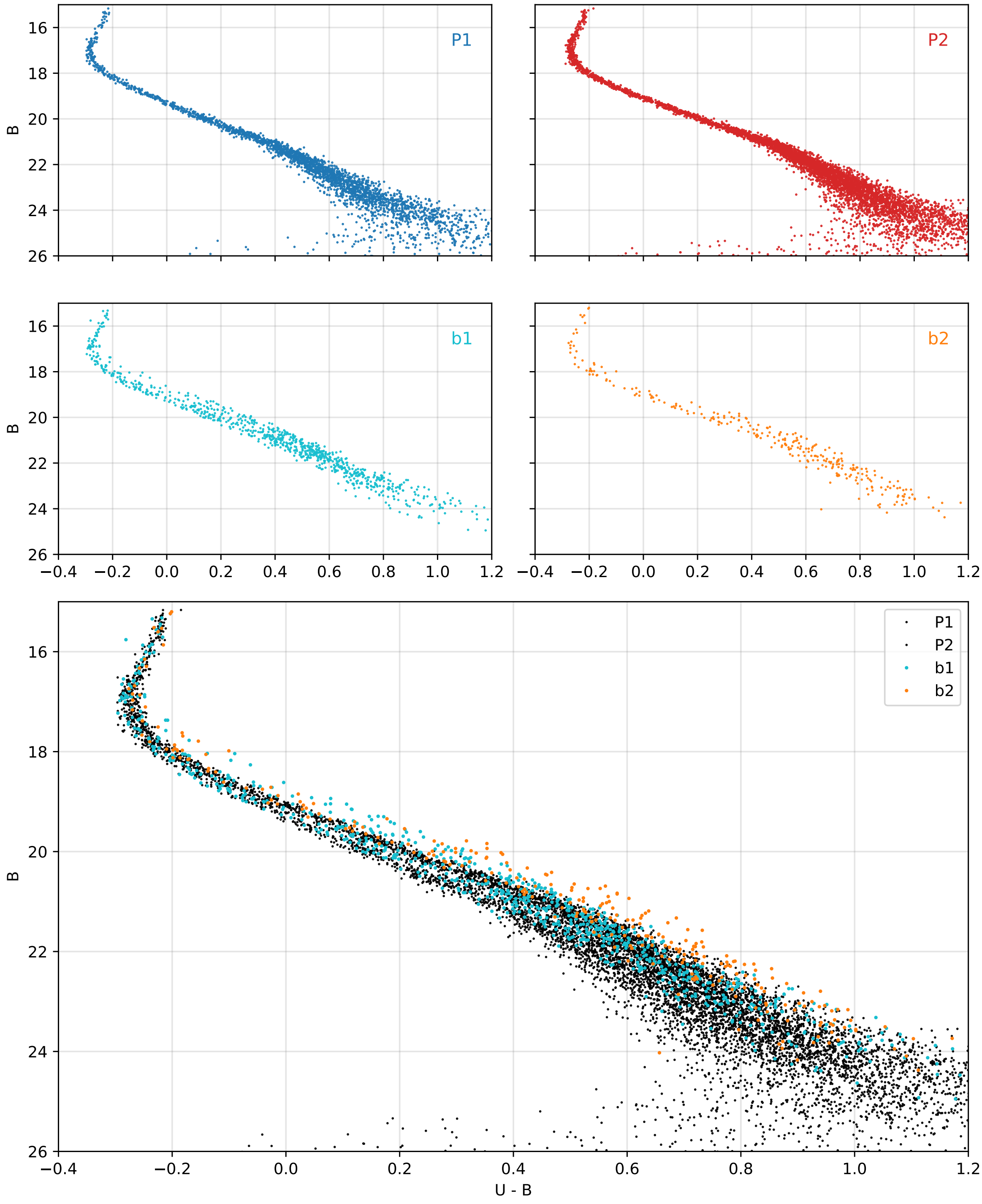

Figure 2.6: This figure shows the final result of the cluster build, plotting each component separately on top and combined at the bottom. The total number of stars is 10000 of which are 33% P1 stars plus 30% P1 binaries (b1), 67% are P2 stars plus 5% P2 binaries (b2). At the bottom panel, the single stars are black dots and the binary stars are plotted in their respective colours on top. It is apparent that the binaries significantly overlap with the single stars along the main sequence of both populations.

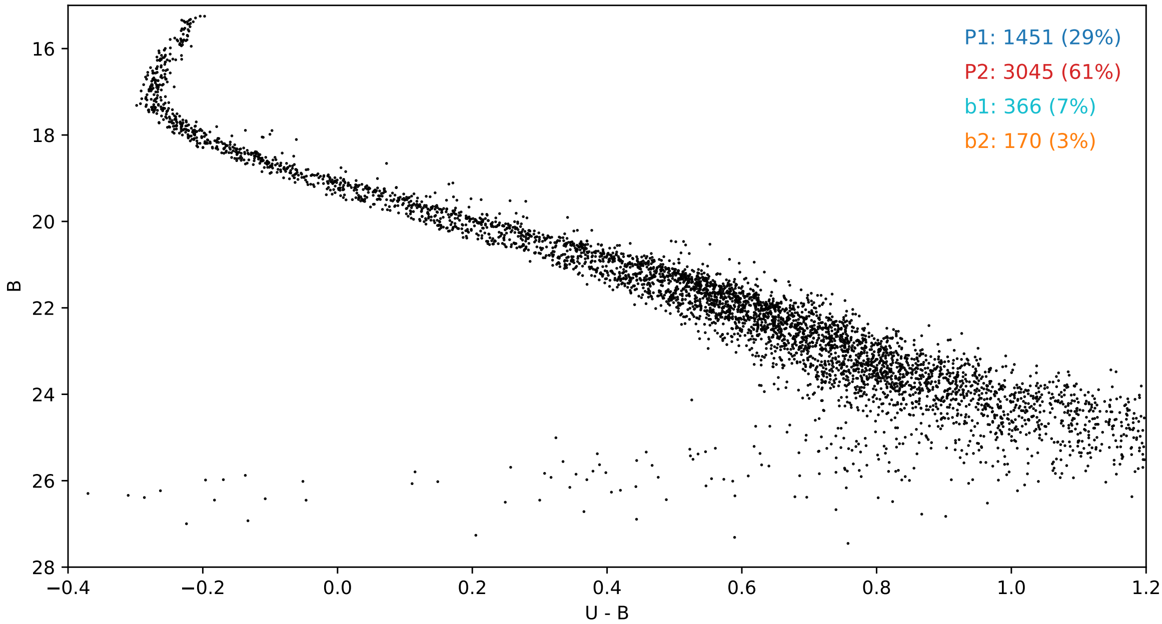

Figure 2.7: This CMD shows 5000 data points of a cluster that accommodates MSPs and binaries, all printed in black to make it look as it were observed. At the top right corner are printed the total number of stars (and the relative number) per component (P1, P2, b1 and b2).

First, in Figure 2.6 each component is plotted separately to illustrate their positions and trends. The first population single stars (P1) are in the upper left in blue, the second population single stars (P2) in red in the top right corner, the P1 binaries (b1) in cyan in the centre left and the P2 binaries (b2) in orange in the centre right. Exact separation of four populations can only be done with certainty in simulations and is interesting to be aware of.

The bottom panel shows all 4 components in one CMD. However, P1 and P2 stars are black dots and can not be distinguished so easily but the focus lies on the two binary populations (b1 and b2) and their relative positions to the main populations. They are plotted in their respective colours again (cyan and orange). Interestingly, the binary stars are spread over the entirety of the cluster in the CMD. There seems to be no definite space where b1 and b2 lie in the CMD. b2 stars range from P1's isochrone to beyond the isochrone of P2 and b1 occupy the same areas but are shifted slightly to the bottom left as expected. This CMD also demonstrates a very well visible gap between the MSPs.

Figure 2.7 shows how the observed CMD of the MS of this cluster would really look if having 5000 data points available. There are 29 % P1 stars, 61 % P2 stars and 10 % binary stars. Of those belong 7 % to the b1 and 3 % to the b2 component.

Content with the result, several other clusters were created. All have a cluster mass of $1 \times 10^5\,M_\odot$ and are located at a distance of 2 kpc. The metallicities of the first and second populations are $[Fe/H]_{P1} = -2.09$ and $[Fe/H]_{P1} = -1.86$, respectively. The contribution of the populations [P1, P2] varies as follows:

$$[25, 75]\,, \quad [33, 67]\,, \quad [40, 60]\,, \quad [50, 50]\,, \quad [60, 40]\,, \quad [67, 33]\,, \quad [75, 25].$$

However, when adding the binary stars to the populations they still change minimally. Further, the binary contribution of each population [b1, b2] is also varied using the following values:

$$[5, 5]\,,\quad [10, 5]\,,\quad [15, 5]\,,\quad [20, 5]\,,\quad [30, 5]\,,\quad [40, 5]\,,\quad [50, 5].$$

b2 is fixed to b2 = 5 while only I only vary b1 as I want to investigate whether b1 stars fill the gap between the P1 and P2 stars in the CMD. Equipped with these clusters the Analysis could begin.

2.3 Analysis of the model data

To us the main interest was how binary stars photometrically influence the detection and or classification of MSPs. Further, can we also distinguish between binary sequences and MSPs? To investigate GC fractions and their influence in a CMD, it is necessary to split the 'observed' mock data into single components. Approaching this topic with mock clusters makes it easy to compare 'true' with computationally estimated compositions. One way to separate MSPs is creating hard cuts by visually deciding in a CMD which colours and magnitudes segment the cluster into P1 and P2. However, it is statistically much more trustworthy to do it by fitting several distribution functions to recreate the shape of the probability density distribution (PDF). In order to create this PDF we chose the method to 'verticalise' the CMDs so that the cluster's MS is vertically orientated. This is covered in detail in Section 2.3.1. In Section 2.3.2 the method of fitting Gaussian Mixture Models to the data is explained. Subsequently, I investigate metrics to differentiate binary stars and MSPs in Section 2.3.3 and finally the metric's dependence on several parameters is investigated in Section 2.3.4.

2.3.1 Verticalisation of the CMD

We chose to verticalise the data because this makes it possible to compare the results to previous work (e.g. Milone et al. 2014, Nardiello et al. 2015, Martocchia et al. 2017). It also simplifies the distribution problem to one dimension (colour-difference) instead of two dimension (colour and magnitude of the stars). Specifically, the data is manipulated in order to achieve a vertically oriented MS. This way, it possible to investigate the distribution of the differential colour of the GC's MS in the CMDs. The process is the following.

I first take two bands from a cluster and calculate the colour by subtracting one band from the other. In my thesis I again used the U and B bands as described in Section 2.1 (Nardiello et al. 2015) because this combination displays MSPs on the MS well. As can be seen in Figure 2.7 most of the colour values from stars are between -0.4 and 1.2 for the Main Sequence of the GC. Because there are some errant colour values beyond values of ± 100 only colour values between -1 and 1.5 were used for the verticalisation. With these values sorted by one magnitude band (U-band magnitude in this case) the mean is calculated for every 30 stars. So every 30 stars have the same mean value similar to calculating the mean in bins of 30 data points.

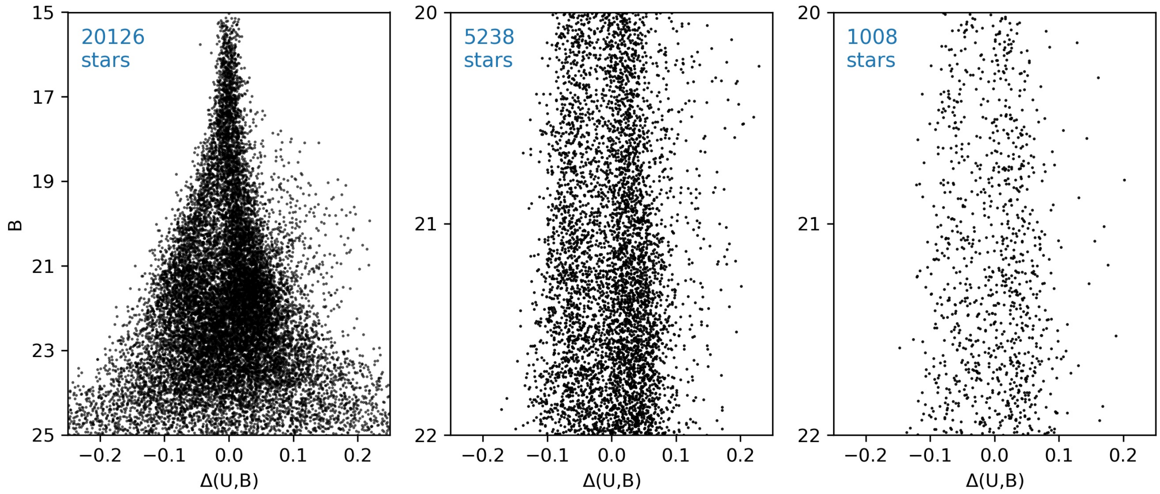

Figure 2.8: This figure shows a verticalised standard cluster. **Left:** about 20000 stars in a magnitude interval which shows the whole MS. **Middle:** 5000 stars to clearly depict the two sequences in the interval used for analysis. **Right:** 1000 stars between 20 and 22 magnitudes, which is the fiducial setup.

Subsequently, the colour value of each star is subtracted from its mean value and saved as 'vertical' [colour] to be accessed later.

Concerning the values beyond the included colour range mentioned above but which are within the used magnitude range (22 mag to 20 mag), their mean value is interpolated. For those outside both ranges, the mean value is extrapolated. However, almost all of the values beyond the colour-difference range have magnitudes larger than 24 mag and are thus not included in the subsequent investigation. Setting their mean to an interpolated value is a manipulation which I would desist from in future work. Possible general effects are discussed in Chapter 4 Section 4.1.3. However, as almost none of these values are included in the thesis there is little to no influence on this analysis.

An example for a verticalised mock CMD is shown in Figure 2.8. In all three panels of the MSPs phenomenon looks convincingly real. The full main sequence is shown in the left panel which shows about 20 000 stars between 15 mag to 25 mag. The middle and right panels show the magnitude range that is used henceforth. The middle panel shows about 5000 stars and the right panel has close to 1000 stars which is the amount that is used as default. This means effectively that all further data analysis is done with 1000 stars (if not otherwise stated) between the magnitude range of 20 mag to 22 mag.

It was tested in the range between 19 mag to 22 mag as well, however, there is an apparent cone-shape in the distribution if the magnitude range is to large (see Figure 2.8. Because of the influence of the photometric error the cone-shape also becomes more apparent the brighter the stars. The range between 20 mag to 22 mag seems to be a good choice as it is fairly straight from top to bottom.

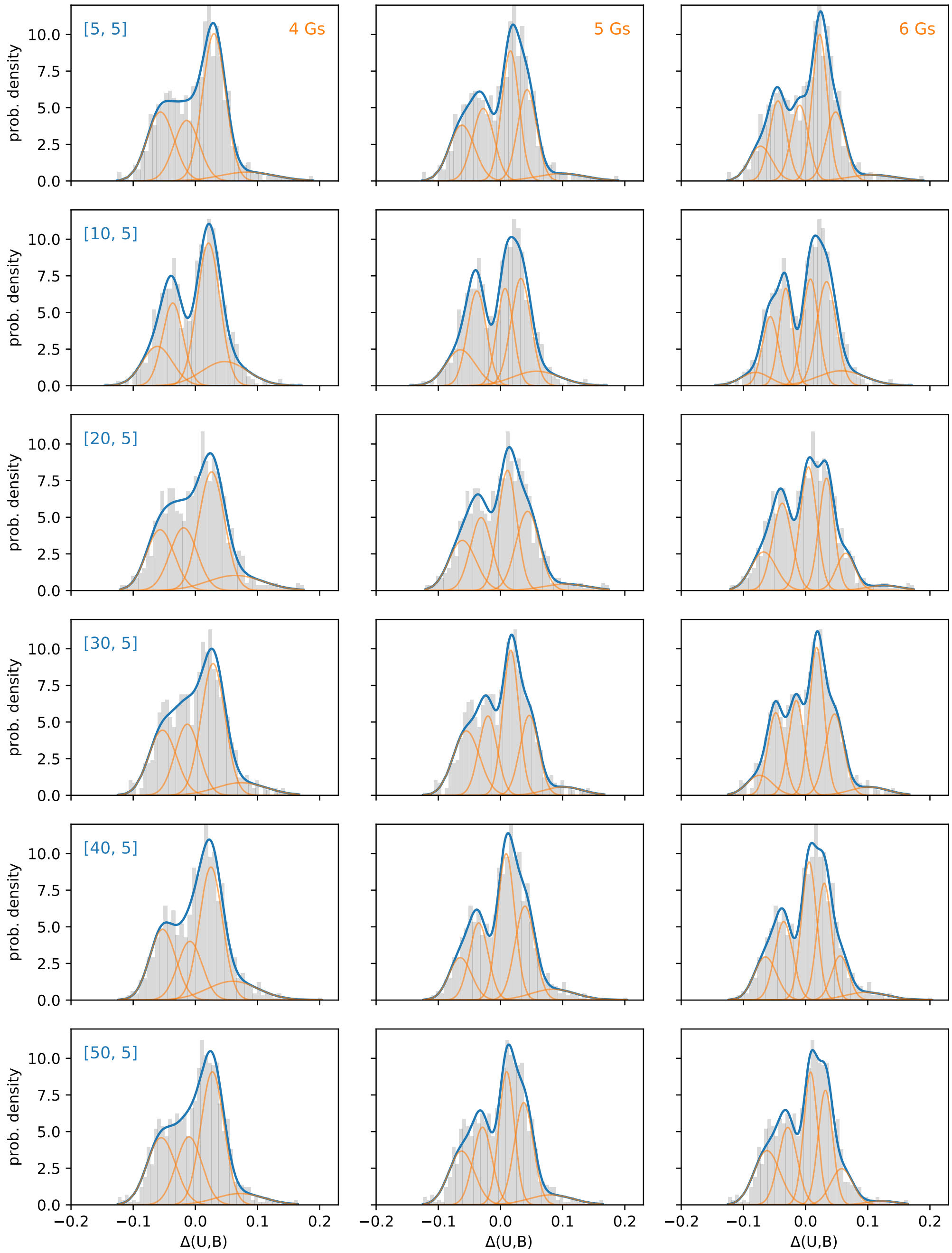

Figure 2.9: Such a figure was used to determine how many Gaussians are to be used for fitting the GMM to the colour distribution (grey histogram). The blue curve shows the final PDF. From top to bottom the binary fraction of P1 increases (5% to 50%, while fb2 is constant) and from left to right the number of Gaussians changes ((orange curves) 4, 5 and 6, respectively). Looking at some of these figures, shows that 4 components do not fit the gap as well as 5 components. 6 components do also very well with the middle dip, however they often overfit details that are unnecessary (eg. right plot in the third row: right double peak).

2.3.2 Fitting Gaussian Mixture Models

Now, that the colour distributions is reduced to a one dimension on the abscissa it is possible to fit distribution functions to it. This is to recognise patterns that are visually not noticed but computationally found. For the metallicity difference that is used so far ($[Fe/H]_{P1} = -2.09$ and $[Fe/H]_{P2} = -1.86$) visually there is two components detectable. Also, some of the P2 binary population (b2) is also visible to the right of the split sequence (see Figure 2.8). However, there might be more to be detected computationally.

Gaussian distributions have been used previously (e.g. Nardiello et al. 2015, Martocchia et al. 2017, Milone et al. 2017a) to look for bimodality within a verticalised CMD. I will use code to combine several normal distributions to fit data in a Gaussian Mixture Model (GMM). For this purpose a *Python* module called scikit-learn[11] (Pedregosa et al. 2011) is applied which has efficient code for Machine Learning purposes in *Python*. Using the *Gaussian Mixture* function this code will fit as many Gaussian distribution functions to some data as specified by the user. In my GMM fitting script the code returns the probability distribution function (PDF) and the logarithmic Likelihood function (*log* L) for all data points. Every data point now has a ΔC position on the abscissa and the corresponding PDF and *log* L values.

Figure 2.9 on page 23 shows how the data fit depends on the number of Gaussians that were forced by the user. Each row shows the PDF of the same cluster for all three columns where the percentage of P1 binaries increases from top to bottom. Meanwhile, every column shows the fit with 4, 5 and 6 Gaussian components on the left, middle and right, respectively. Comparing the columns with each other shows that while the left column with 4 GMM components does not fit the gap between the populations as closely as a fit with 5 Gaussians does for the same cluster. However, using 6 GMM components 'over-fits' some peaks and gaps (e.g. for b1: 20% and 30%).

As this thesis investigates the effect of the binary sequences on the detection of MSPs, it is our aim to detect bimodality in the ΔC distribution. Thus, it is not helpful to fit all details such as in the right column. Also, since it is known here that there are 4 components contributing to the ΔC distribution I did not want to use many more than that, just enough to get consistently good fits for the distribution. This is why the main analysis focuses on 5 component Gaussians Mixture Models from here on. Comparisons to fits with 4 and 6 Gaussians are still included in the thesis in the Appendix Sections A.2 and A.3.

2.3.3 Creation of a Metric

In order to be able to measure the degree of bimodality in the cluster we needed to introduce a metric. The aim of the metric is to give a value to the size of the gap and how pronounced the gap is. I looked into two different metrics (ΔArea and ΔlogL) which are explained in detail below.

[11] Scikit-learn `https://scikit-learn.org/stable/`

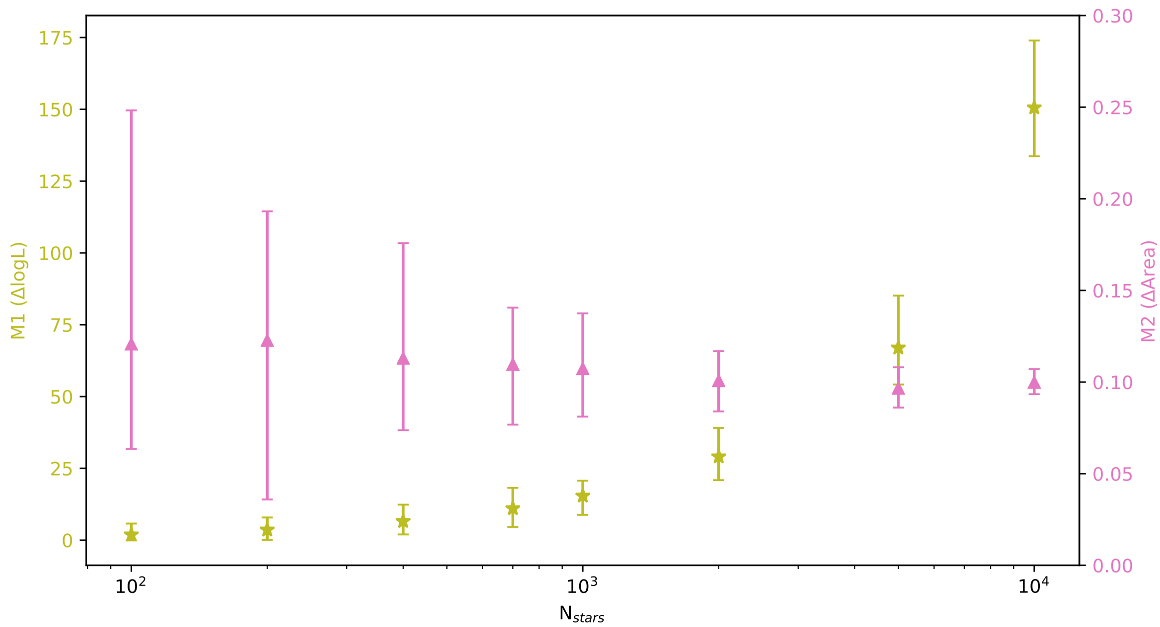

Figure 2.10: Here the log-likelihood (M1, green stars) and area (M2, pink triangles) difference is plotted against an increasing number of data points. The M2 value actually stays constant over the number of stars within the error bars. The trend of the M1 values seems counter intuitive at first. It increases, seemingly meaning the gap increases between the flattened and fitted log-likelihood, but it is rather because more data points means greater likelihood. But because I want a metric to be sensitive to the number of data points the M1 metric is appropriate here and I chose to use 1000 data points for future analyses because it is the first value significantly offset from 0 while still being the most realistic.

As mentioned already before, the GMM fit returns two functions: the PDF and the log-likelihood (logL) function. The first idea was to measure the size of the gap by using the PDF. The process is to create a second function from the original, that connects the two peaks of the PDF. This version of the PDF is called the flattened function (f_{flat}) in this thesis. It is no PDF as it is not normalised to 1.0. Figures 2.13 (on page 29) and 2.14 (on page 30) help visualisation of the method described below.

The code for creating the f_{flat} first looks at how many peaks the PDF has. If there are none, then the f_{flat} is exactly the same as the PDF and ΔArea equals 0.0 after subtraction. If there are two peaks, then the peaks are connected by a straight line and ΔArea equals the difference in the area under the original PDF and flattened function. However, sometimes there are more than two gaps as well. If there are three peaks in the PDF then I want to exclude the possibility that a peak caused by P2 binary stars is taken into account. Therefore, it is checked if the third peak (peak at the highest ΔC value) is larger than the second. Since b2 stars in my clusters will not result in a larger peak than P2 stars this condition will only hold if the third peak does not result from b2 stars. Otherwise the third peak is ignored and the first to peaks are connected. However, when the above condition is the case the f_{flat} connects all three peaks and includes two gaps.

In order to visualise it, is best to take a look at Figure 2.9 and its third panels (6 components) in the third and forth rows. Both PDFs have three peaks, however the third peak of the one in the third row has a probability density below the the second peak. On the other hand, in the forth row, the third peak is larger than the second one. Now, for the case in the third row, the third peak is ignored and the first and second are connected. But in the forth row, the f_{flat} connects all three peaks and has two gaps.

In the very rare case of having four or five peaks the algorithms draws a straight line between the two highest peaks. This sometimes does not result in the correct gap to be measured, however, as it occurs very rarely when using 5 Gaussians and as we decided on a statistical approach, it will not be significant. The last case is more than 5 peaks which has never been observed, I set the f_{flat} to be the original PDF.

Now for the M2 metric (ΔArea) a function from the *Python scipy*[12] module is used that integrates with Simpson's rule. Integrating over each version (PDF and the flattened curve f_{flat}) and subtracting the original from the flattened PDF returns a value for the area of the gap or gaps. I integrate over all the data points in sorted order from minimum to maximum and this results in the value of the area beneath the data points.

$$\Delta\text{Area} = \int_{min}^{max} f_{\text{flat}}(x)\,dx \quad - \quad \int_{min}^{max} \text{PDF}(x)\,dx$$

where the x are the verticalised colour values (ΔC or Δ(U, B) in the figures) and *min* and *max* refer to their minimum and maximum for both functions. How ΔArea depends on the number of data points, the number of binary stars from P1 and the population fraction are shown as pink triangles on the right axis in Figures 2.10, 2.11, 2.12, respectively.

The ΔArea metric does not depend on the number of data points used to fit the GMM (see Figure 2.10) within its error. However, more data points should in some way influence the metric, that shows the certainty of bimodality, significantly. Even though the error bars of M2 decrease a lot, the actual median value does not vary meaningfully.

A way to include the number of data points is by evaluating the Likelihood of the observed data under two models: the GMM and the flattened version. Therefore, I took the created flattened function (f_{flat}) of the distribution and normalised it so the area equals 1.0 again. This is now the flattened PDF (fPDF). Then the logarithm of the fPDF is taken so it compares to the original log-Likelihood function from the GMM fit. Finally, to calculate the M1 metric (ΔlogL) the difference in log-Likelihood is the subtraction of the sums of each log-Likelihood (flattened and original) of the GMM fitted distribution.

$$\text{fL} = \frac{1}{A} \cdot f_{\text{flat}}(x_i) \tag{2.8}$$

x_i are all data points and the A is the area beneath the f_{flat} determined by using Simpson-integration.

[12]SciPy https://www.scipy.org/

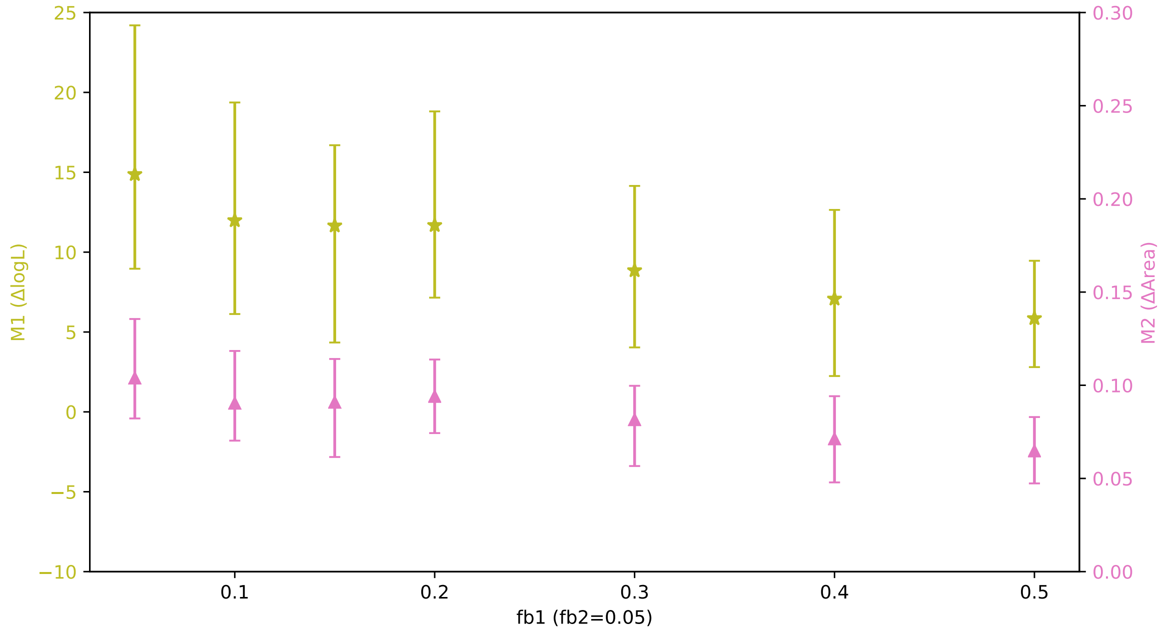

Figure 2.11: This plot shows both the M1 log-likelihood (green stars) difference and the M2 area (pink triangles) difference for a changing fraction of P1 binaries while the fraction of P2 binaries is constant. As the fb1 increases both the M1 and M2 values decrease, meaning the binary sequence of the first population is filling up the gap between the two MSPs. As the M1 metric is also affected more by the increase of binaries I again chose to take M1 as an indicator of bimodality.

$$\Delta\mathrm{logL} = \sum_{i=1}^{N} log\,\mathrm{PDF}(x_i) \quad - \quad \sum_{i=1}^{N} log\,\mathrm{fPDF}(x_i) \tag{2.9}$$

This M1 metric is represented as olive stars on the left axis in Figures 2.10, 2.11, 2.12. It is a great result that the ΔlogL increases for the number of data points. This suggests M1 has higher values for more data which is what we needed.

2.3.4 Metric dependencies on Parameters

Subsequently, it is necessary to investigate how the metrics (ΔlogL (M1) and ΔArea (M2)) that I created depend on the number of data points, b1 and the population ratios.

Briefly, it has to be noted how the M1 and M2 values in the figures are created and the errors are treated. This is mentioned in more detail in Chapter 3 Section 3.1. For every combination of parameters (number of stars, fraction of binary stars and populations) 50 random data sets are created from the clusters. Of these 50 repetitions, the median values are plotted as olive green star or pink triangle in the Figures 2.10 to 2.12. The error bars are the 16th and 84th percentile of the distribution the 50 data sets.

Starting with the dependency on the number of stars (Figure 2.10 on page 25). As already discussed briefly the metrics behaves differently on the increasing number of data points.

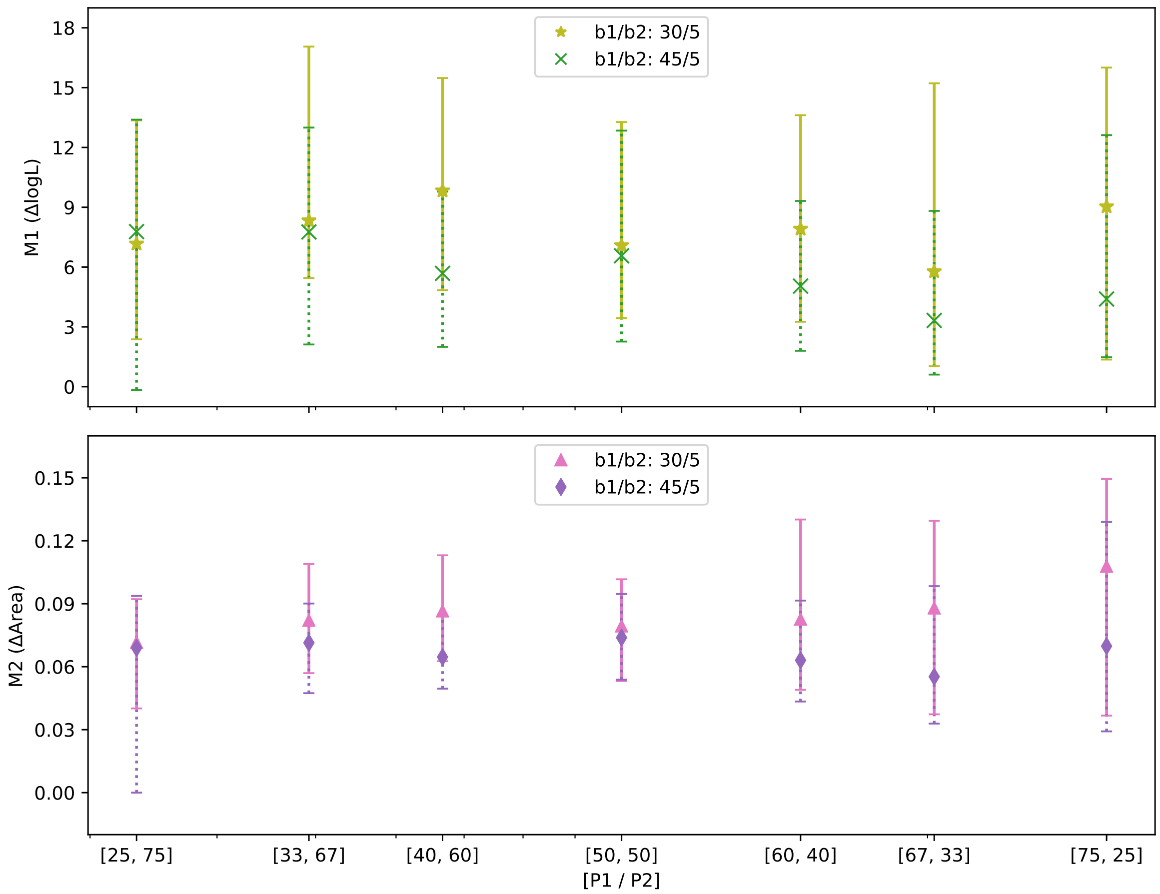

Figure 2.12: Here again it is the same plot showing the metric values but now the fraction of P1 binary stars changes. The log-likelihood difference (ΔlogL) in the top panel shows clusters with 30% and 45% binary stars added to P1 in light green stars and dark green crosses, respectively. In the bottom panel, where M2 (ΔArea) is depicted, the lower P1 binary fraction corresponds to the pink triangles and the higher fraction to the purple diamonds. What is really interesting is that irrespective of the population ratios the clusters with a higher fraction of P1 binaries seem to 'fill the gap' between the two populations in the colour distribution.

Where ΔArea on the one hand is nearly constant within the error bars or gently declines, ΔlogL on the other hand strongly increases with the increasing amount of data. The size of the error bars decrease for M2 but increases for M1. This is because for M1 the effect of variation in the sum of 10 000 stars is severe and results in largely different values even though the distribution does not vary greatly. This in turn increases the error. M2's errors decrease because the ΔArea value does not vary greatly anyway and so 10 000 different stars of the same cluster seem to qualify the area very well.

Where the metrics behave differently for the amount of data, they agree on the relation to an increase in b1 observed in Figure 2.11 on page 27. Both metrics decrease where b1 increases. This suggests again that b1 does play in important role in the detection of binaries. Although both metrics behave the same the decrease of ΔArea is more subtle ($\approx$0.13 to $\approx$0.08) and ΔlogL magnifies the effect ($\approx$25 to $\approx$10). This is another reason for choosing M1 as the

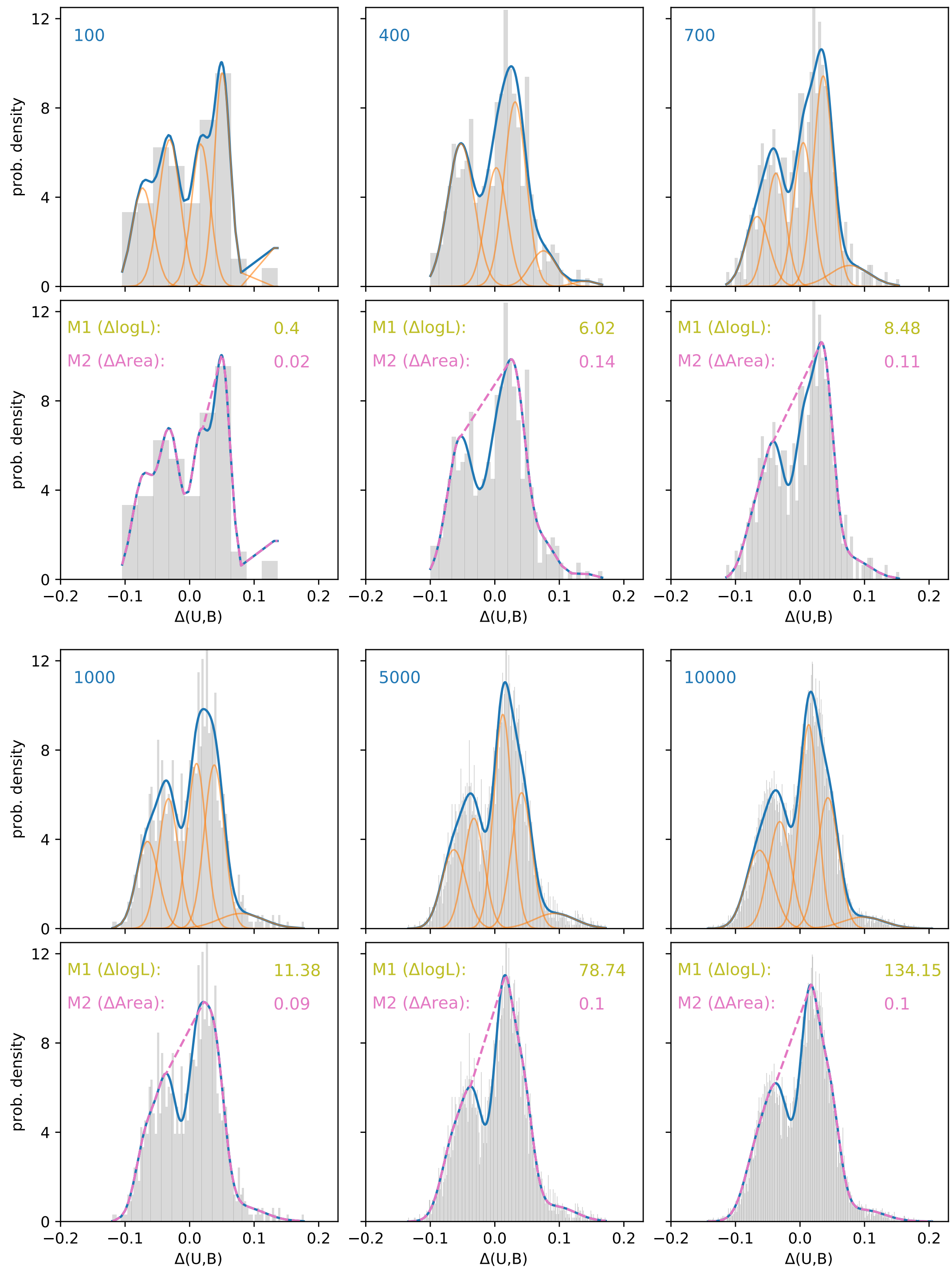

Figure 2.13: From left to right and top to bottom the number of data points increases (upper left blue value). The plots in the top rows show how the GMM fitted the colour distribution (overall PDF is the blue line and single Gaussians are orange). The second and fourth row plots show the flattened fit (pink dashed line). The corresponding M1 and M2 value for each cluster is printed on the top in olive green and pink, respectively. (See Section 2.3.4 for a detailed explanation.)

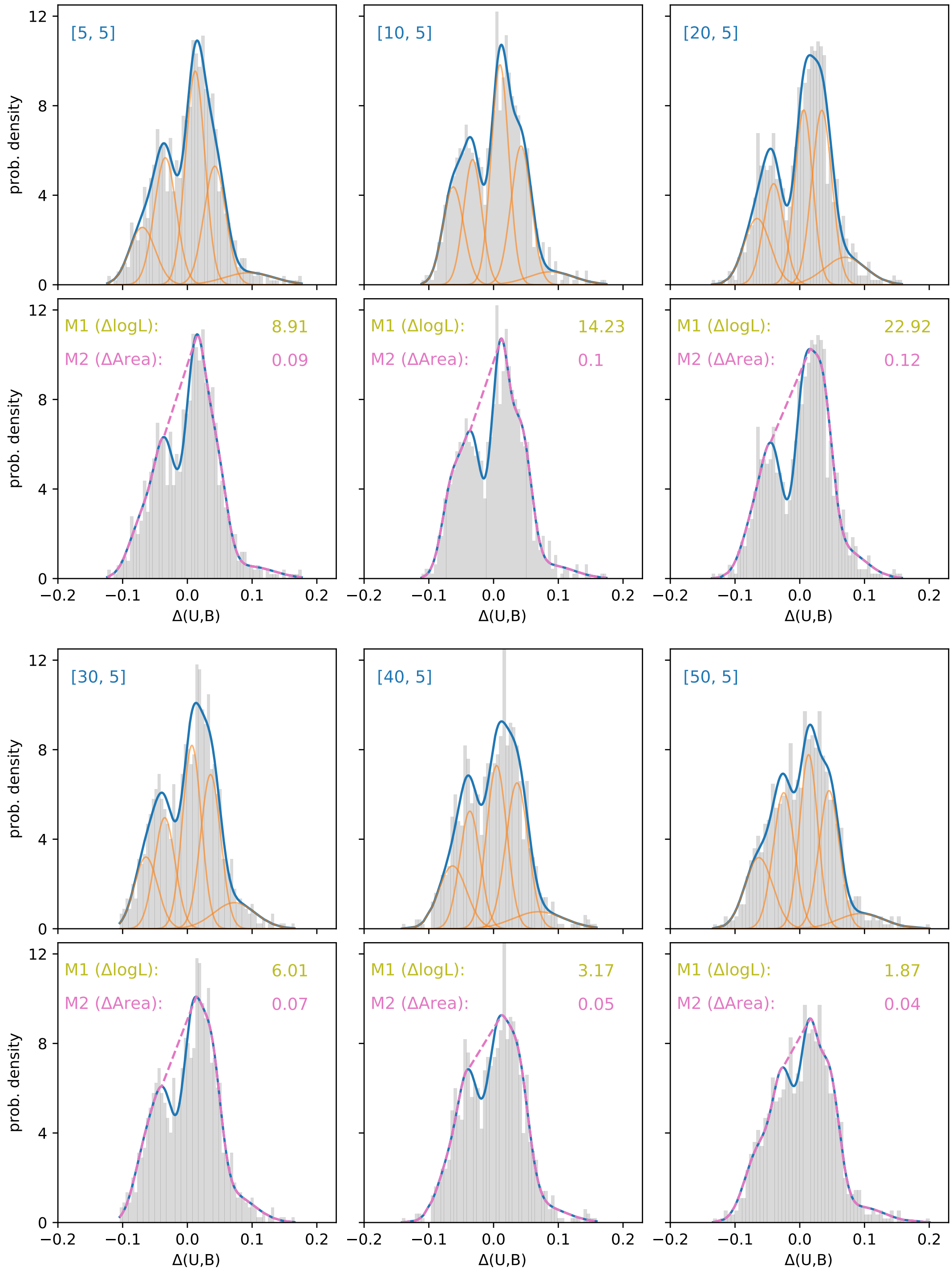

Figure 2.14: This is the same plot as Figure 2.13 except that here all clusters are represented with 1000 data points and the binary fraction of P1 is increasing from left to right and top to bottom, whereas fb2 stays constant at 0.05. It is already hinted how the middle gap is disappearing as the number of b1 stars increases and the metric values decrease.

metric to make sure MSPs are detected.

The effect of population ratios is also investigated (Figure 2.12 on page 28), however, no dependency can be found. As I included two different values b1 in the plots, it can be seen clearly again, how the number of P1 binary stars reduces the gap between the two populations which are the peaks of the PDF. The higher b1 number is dark green crosses and purple diamonds for the M1 and M2, respectively. In both panels the median values of the metrics for the higher b1 number (45%) is smaller than if b1 were 30%. The effect also increases with increasing fraction of P1 stars. This is because 30% of 25% of P1 stars compared to 45% of 25% of P1 stars is a smaller difference than 30% of 75% of P1 stars compared to 45% of 75% of P1 stars.

Regarding the Figures 2.13, 2.14 and 2.15, they are more qualitative visualisations of the effects that are described above. Similar figures were used to decide which metric is more suited to qualify the extend of the gap between the two population sequences. In the next section, ΔlogL thresholds are used to assess the significance of bimodality.

In Figure 2.13 the colour-difference distributions and according PDFs (and single Gaussians (orange)) are plotted for an increasing number of stars (100, 400, 700, 1000, 5000, 10 000). The number of stars is the blue number in the upper left corner of the panels in the first and third rows. The panels in the second and fourth rows show the PDF and the fPDF. At their top the metric values are written. Here, it is very interesting that as M1 is monotonically increasing, M2 is not affected by the number of data point. Also as this is the same cluster ([P1/P2] = [33, 67] and [b1/b2] = [30, 5]) the visual difference between 5000 and 10 000 data points is very little which is shown in the same M2 value. The first data set with 100 stars shows an example of a wrongly created fPDF. This effect is neutralised by those 50 repetitions that are explained at the beginning of this subsection and by using the median of all 50 M1/ M2 values.

Figure 2.14 qualitatively demonstrates how P1 binaries fill the the gap between the two populations with stars. This results in a decrease of both metric values which is already known from Figure 2.11.

After looking at several figures, similar to those above, filled with panels of randomly created clusters we decided that M1 is more efficient in rating the extent of the gap and with it the likelihood of the cluster hosting MSPs. Although all clusters host MSPs at this stage, the cluster with the highest fraction of b1 (bottom right) in Figure 2.14 visually would be rated as 'very unlikely to host MSPs'. Using ΔlogL , it will now give a value to the certainty of MSPs inhabiting a GC.

Figure 2.15 shows clusters that have M1 values close to the four ΔlogL threshold values we decided upon and which are used in the next section to assess the significance of bimodality. The thresholds values equal M1 = 5.0 (yellow), 7.0 (orange), 10.0 (light red) and 15.0 (burgundy). The thresholds of the clusters increase from left to right over all rows and their actual M1 values are printed in the top right corners of the panels. The clusters are selected such that their M1 value is greater than ($\geq$) the threshold in question but smaller than ($<$) the next integer. At the same time the amount of data increases from the first to the second row and

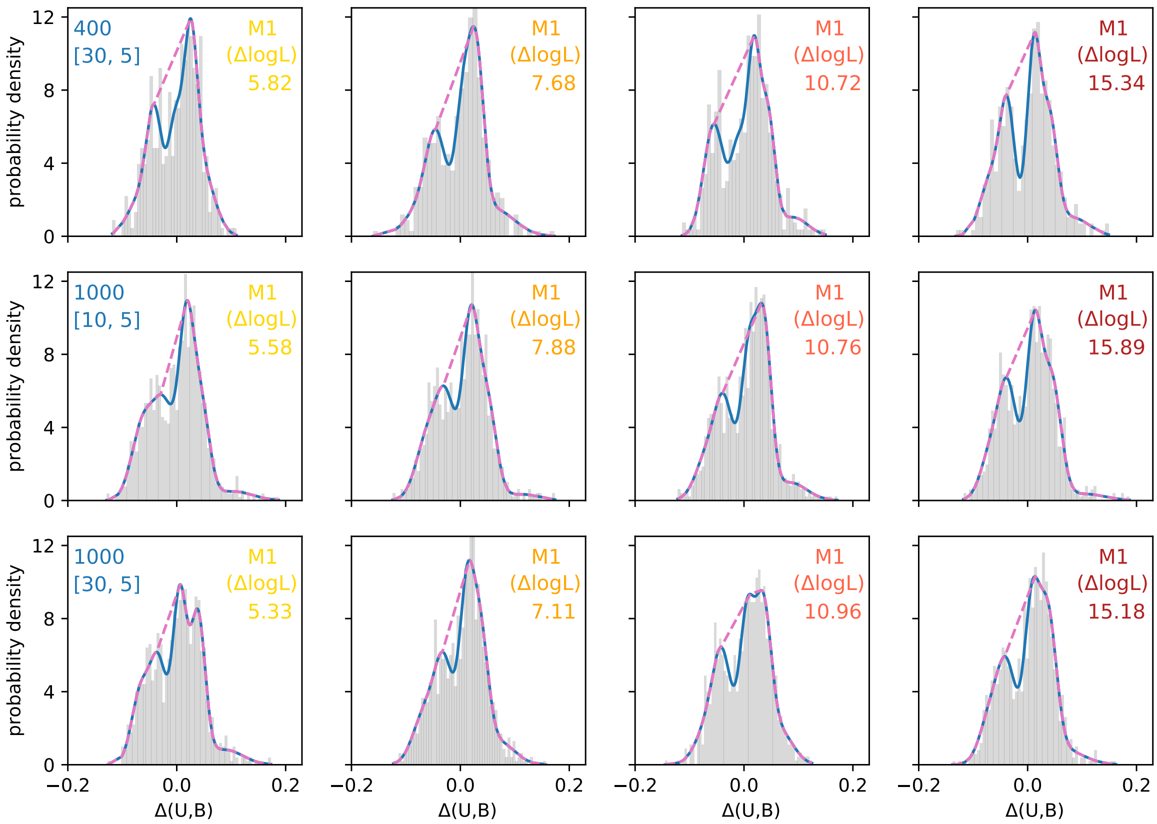

Figure 2.15: Again, this is a similar plot showing how clusters with different M1 (ΔlogL) thresholds (5, 7, 10 and 15 from left to right from bright yellow to dark red, respectively) look depending on the number of data points and the fraction of P1 binaries (top to bottom). This plot shows that with an increasing number of data points the gap does not need to be as pronounced in order for a MS to be accepted as being bimodal.

the number of P1 binaries increase from the second to the third row. The composition shows that for a larger number of stars the gap does not need to be as pronounced to be considered bimodal with certainty. There seems to be no systematic influence on the cluster shape or M1 values for the increase in b1. Also, clusters with $\Delta\log L \approx 5.0$ are not reliably bimodal.

For this reason we chose M1 = 7.0 to be the primary threshold at which it can be said that MSPs are detected in the cluster.

Chapter 3

Results

In this chapter the created data and metric $\Delta \log L$ are used to find answers to the questions I pose in this thesis. How do binary stars influence the detection of MSPs in GCs? Can we estimate the population fractions from CMDs? What role do binaries play in the estimation? Can we estimate the weight that each component contributes to the full distribution? Is it possible to separate binary stars from single stars based on their colour-difference distribution?

To answer these questions, I first investigate the impact P1 binaries have on the CMD in Section 3.1. Subsequently, Section 3.2 shows that it is possible to estimate the number fraction of each population from the fitted PDF. Section 3.3 deals with the separation of and into each component. Subsequently, in Section 3.4 follows an inspection of varying the metallicity difference between the first and second population and its impact. This chapter is concluded in Section 3.5 with a reflection on the robustness of the code and the result of using the code on a single population with binary stars.

3.1 Lost bimodality cluster fraction

The question here is how binary stars from the first population influence the CMD and our detection of MSPs. Therefore, I investigated what fraction of clusters is detected as having bimodal colour distributions for each increasing number of binary stars. I also investigate how these fractions depend on the threshold used to select whether a bimodality exists.

Figure 3.1 shows the result. There are seven clusters in this plot, each having a different fraction of b1 stars. For each of these clusters and each threshold value 50 data sets with 1000 data points are created randomly. The thresholds are $\Delta \log L = 5.0, 7.0, 10.0$ or 15.0 and correspond to the yellow diamonds, orange squares, bright red dots and burgundy triangles in the figure, respectively. For each threshold the algorithm counts how many data sets have an M1 value that is equal to or greater than the threshold value and returns one value. This process is repeated 10 times. Thus, I end up with 10 bimodality fraction values per cluster and threshold. The bimodality fractions tell how many data sets of the cluster have M1 values above the threshold. Of these 10 numbers I calculate the median and the 16th and 84th percentiles which are plotted in the figure (as briefly mentioned in Chapter 2 Section 2.3.4).

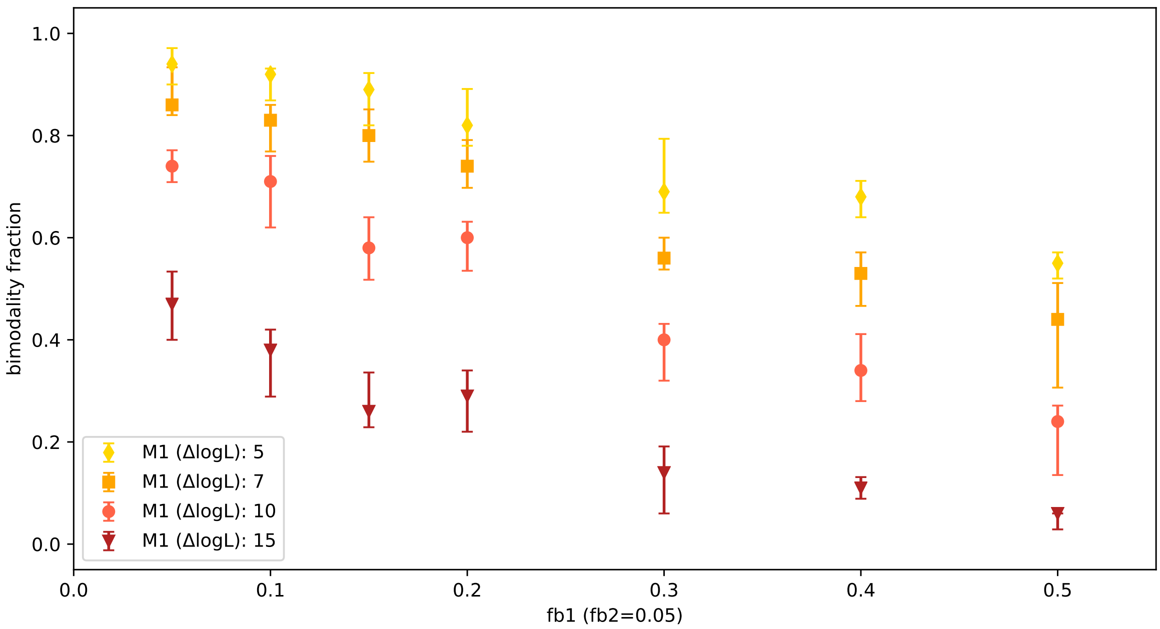

Figure 3.1: The figure shows the fraction of clusters that are recognised as being bimodal depending on the fraction of P1 binary stars. The M1 selection thresholds 5, 7, 10 and 15 are plotted in yellow diamonds, orange squares, red, circles and burgundy triangles, respectively (see Fig. 2.15 for comparison). It shows that with an increasing fraction of P1 binaries, less clusters are recognised as being bimodal. This fraction also decreases with an increase in detection limits (M1).

Figure A.2 in the Appendix is a pseudo-code version of this section in the algorithm which aims to simplify the above description and helps clarification.

The plot clearly shows the dependency on P1 binary stars across all thresholds. As the abscissa increases in the fraction of b1 less and less clusters are recognised as having a bimodal MS. For a stricter threshold this effect is greater. In this case all the clusters host MSPs and should be bimodal. When using a threshold of 7.0 at a b1 percentage of 30% about 60% of data sets show bimodality. However, using a threshold of 15 which only counts the most distinct split sequences, the fraction of detected bimodal distributions is reduced to only about 20%. Overall, it is very interesting that with a third of P1 being binary stars[13], the lost bimodality is as high as 50% for M1 $\geq$ 7.0 and 90% for M1 $\geq$ 15.0.

As previously mentioned we defined that detection of a split MS happens when ΔlogL is equal to or greater than 7.0. This is when most distributions are consistently and very clearly bimodal (Figure 2.15 on page 32). Now, how does the amount of data improve the detection? Therefore, instead of counting recognised MSPs for different thresholds, I now count for various numbers of stars. The different data sets include 200, 700, 1000 and 5000 stars that are represented, respectively, as yellow diamonds, orange squares, red dots and burgundy triangles in Figure 3.2. Again the median and the (16th and 84th) percentiles are

[13] Adding 50% binary stars to the 100% P1 single stars approximately results in b1 being a third of the whole P1.

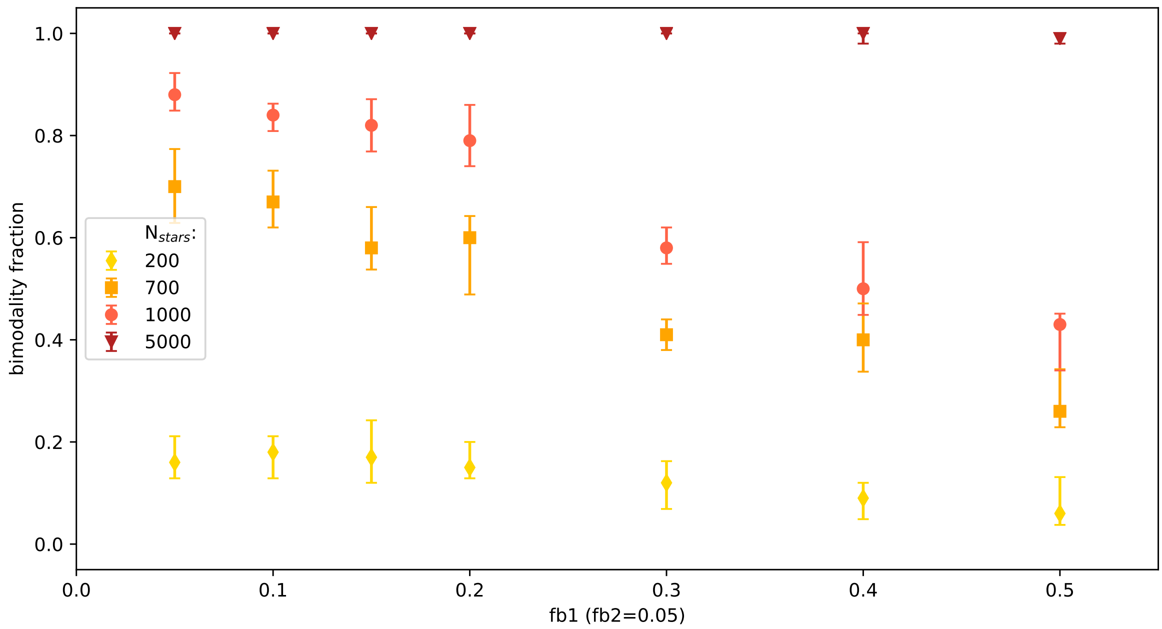

Figure 3.2: The bimodality fraction also decreases when fewer data points are available. The number of data points increases from 200, 700, 1000 to 5000 which are plotted as yellow diamonds, orange squares, red, circles and burgundy triangles, respectively. It can be seen that when enough data is available, no bimodal cluster remains undetected. Although there is already a major improvement between 200 and 700 stars.

calculated from 10 repetitions of 50 data sets per cluster and number of stars.

Figure 3.2 shows very well how the amount of data improves the detection of MSPs. Where 200 stars show an overall very low bimodality fraction 5000 stars detect bimodality in every data set of all clusters except the one with the highest fb1. The bimodality fraction in the version with 700 and 1000 stars significantly decline towards higher numbers of b1 stars. In this figure the red dots nearly show the same results as the orange squares in Figure 3.1 as they represent the same cluster with the same number of data points.

These results clearly show that P1 binary stars strongly populate the split between the MSP sequences. The more b1 stars are in a cluster the more difficult it becomes to detect the MSPs therein. This can be countered by working with larger data sets.

3.2 Estimating the Population Fractions

The second question that needs answers is if we can estimate the population size from the verticalised colour distribution. This would be a powerful tool to investigate GCs with. The idea is to split the distribution and look at the number fraction each population has. The method with which this is realised is described in detail below.

I am using GMM fits in this thesis to fit the overall PDF to the model data sets that are

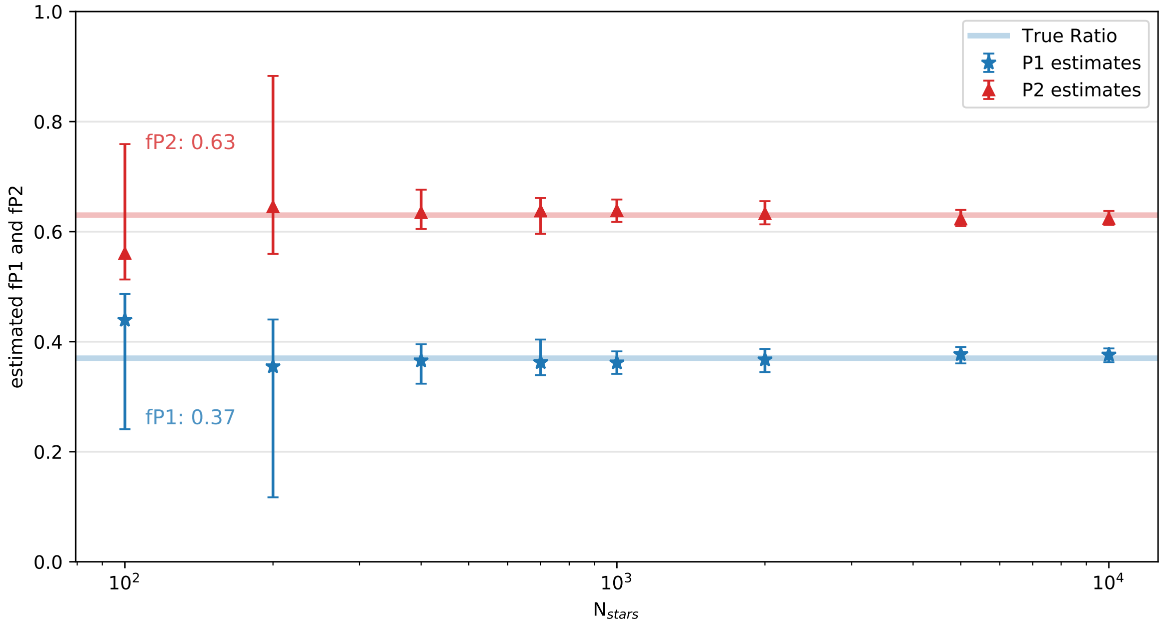

Figure 3.3: True population fractions are plotted as horizontal lines and their values below and above, in blue and red for P1 and P2, respectively. The median estimated fraction values are plotted in blue stars and red triangles, respectively. The error bars are the 16 and 84 percentiles. The number of data points (N_{stars}) increases along the abscissa and with it the error-bars shrink and the estimated fraction value gets more accurate.

created. The scikit-learn library[14] (Pedregosa et al. 2011) makes it possible to get the mean, standard variation and weights of each individually fitted Gaussian along with the overall PDF. The code first looks for minima in the PDF. If there is just one, the Gaussians are divided into belonging to P1 and P2 by looking at the mean values. All the Gaussians with means smaller than the colour value of the minimum are counted as P1, the rest as P2. Then, the weights of all Gaussians per population are added up. These values are the estimated population fractions.

Figure 3.6 (page 23) illustrates this procedure. The right panel shows a PDF (black line) and four Gaussians divided in blue and red groups. This is because there is one minimum found here and it is at $\Delta C < 0.07$. Therefore the Gaussian's mean values are divided at this minimum into belonging to P1 (blue) and P2 (red). Their weights are summed up which gives the estimated number fraction (upper left corner with 'True - Estimated').

However, if there is no minimum found or more than one minima found the the procedure varies slightly. Figure A.5 in the Appendix describes the details of this procedure. Most of the time, I set the minima to 0.0 colour difference. Because the data is verticalised 0.0 ΔC is the mean value of the colour distribution in the CMD and thus an appropriate choice for a separation. So if no minimum is found the Gaussians are divided into means greater and smaller than 0.0 ΔC. Also if there is one minimum found, but its corresponding colour

[14]Scikit-learn `https://scikit-learn.org/stable/`

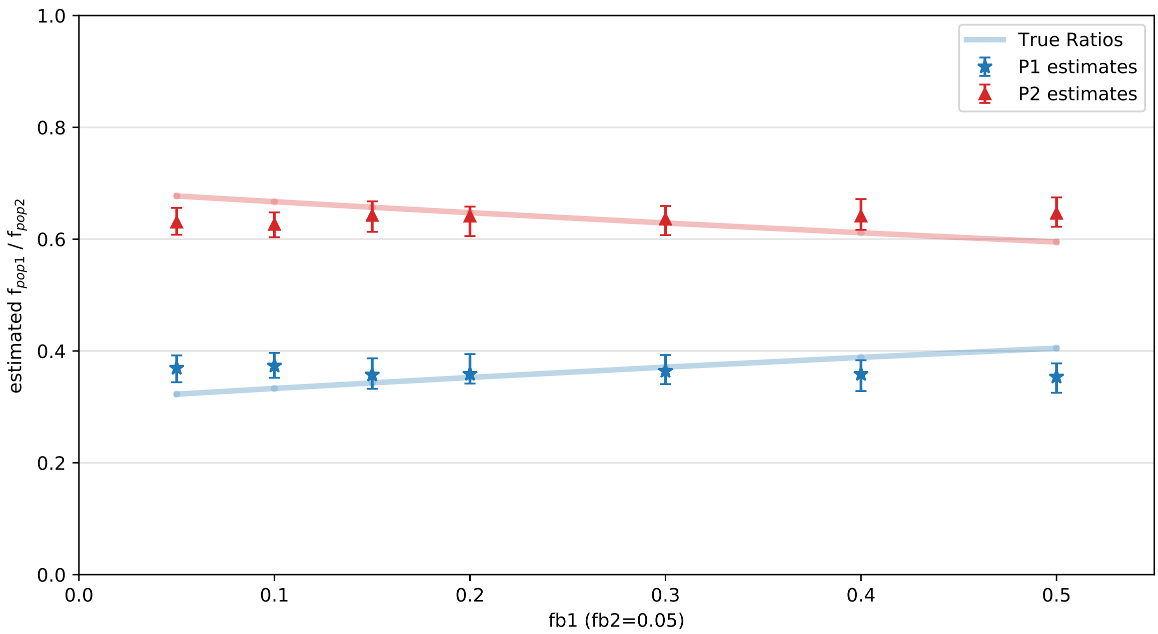

Figure 3.4: This figure is constructed similar to Figure 3.3, however along the abscissa the fraction of P1 binaries increases. The population fractions vary because of the increase in binaries, however the estimation does not notice the variation. It stays constant over each P1 binary fraction.

difference value is ≥ 0.07 (suggesting the minima is between P2 and b2) the separator is set to 0.0. For more than one minima and two maxima I look for the minima that is between the two maxima. If there are more than one minima and three maxima either the one minima that is between two maxima is chosen, otherwise the first enclosed minima is taken as separator. If there are more than one minimum and more than three maxima the separator is set to 0.0 ΔC again. All these cases have occurred while testing and the code is written so that all outcomes are covered.

After creating the algorithm I applied it to multiple data sets of the standard cluster with varying numbers of data points. The errors are treated as previously explained (Section 3.1 on page 33) using median values of 50 repetitions per data set an the 16% to 84% percentiles thereof. The result is shown in Figure 3.3. Clearly, the errors decline as the number of stars increases, but even the roughest estimate (symbols) at 100 data points does come closely to the true fraction (solid line).

The same is now adapted to see how the estimation process depends on the fraction of b1 stars. There are seven different clusters each with a different fraction of b1 stars. The estimated population fractions are the median for 50 repetitions per cluster and the errors are the 16% to 84% percentiles. Figure 3.4 shows the result. The true fractions show a slope because the increase in b1 stars lead to a shift in the overall population fractions. The estimates however, stay fairly constant over the different number of binary stars. This suggests that this estimation method is not sensible enough to detect their increase. But on the other hand this

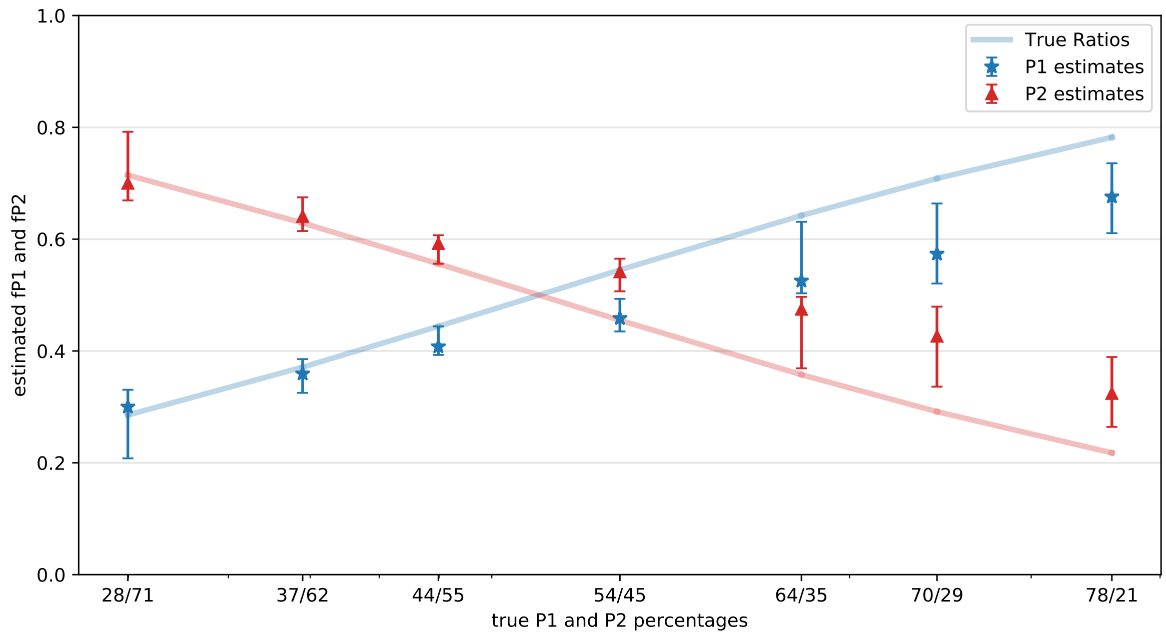

Figure 3.5: This figure shows how the estimation succeeds when the fraction of P1 binaries stays the same, but the ratio between P1 and P2 stars varies. It is constructed as Figures 3.3 and 3.4. With an decrease of P2 stars, this population gets overestimated, due to the P1 binary stars which increase along with the P1 and mostly share the colour-space with P2 stars.

means that it is not influenced by the different reasonable numbers of binary stars as well.

Now it remains to investigate the method's dependency on a variation of population fractions. Here I use seven different clusters with varying ratio of P1 and P2 stars. The binary percentage stays the same as [b1, b2] = [30, 5], However, this implies more binaries for higher population fractions as the binary percentage grows with population stars. Again the median values result from 50 repetitions/ data sets per cluster and the errors are the 16% to 84% percentiles. The colours and format is the same as before.

The estimates clearly detect the trend of the true fractions, even though it under- or overestimates the true values towards higher share of P1 stars in the cluster. This again shows the code's ignorance of the binary percentage. As more and more b1 stars are included due to the increase of P1 stars, an increasing amount is counted among the P2 fraction. This explains not only the larger error bars towards higher P1 numbers but also why P2 is over- and P1 underestimated. A more detailed analysis of this situation is discussed in Chapter 4 Section 4.2.2.

To conclude this section, I can say that the estimation method works well and its dependencies on the previously discussed properties are understood and not unexpected. When increasing the data size the estimation on the standard cluster gets more accurate. Overall, the population fractions are recognised well by the estimation method (see Figure 3.5), especially for the population fractions of our fiducial cluster (e.g. Figure 3.3). The code does not detect the increase of the b1 fraction and the standard cluster's population ratio is (by chance)

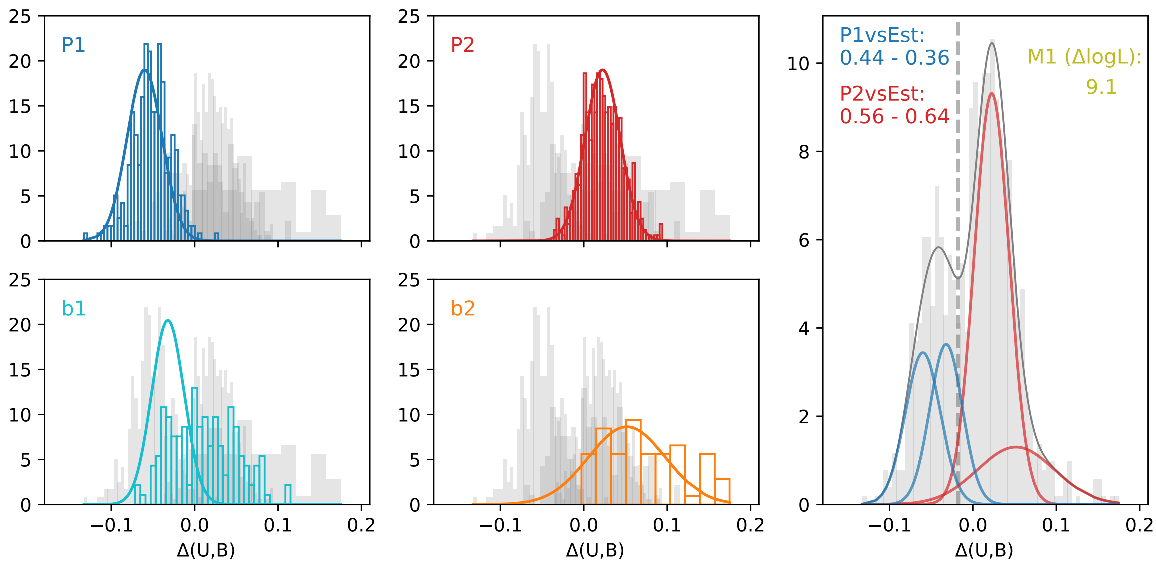

Figure 3.6: The four plots on the left show each component (P1, P2, b1, b2 in blue, red, cyan and orange, respectively). In all four panels the weights of each component or Gaussian is 1. They are not weighted relatively, compared to the plot on the right. The faint histograms of the other components are plotted for orientation. This figure shows a surprisingly good fit of the P2 and b2 stars. The b1 stars are the only component which is not 'fitted' almost correctly. On the right plot is the distribution with relative weights and Gaussians are split between P1 and P2 and coloured (blue, red) respectively of their classification. The upper left corner shows the true vs the estimated fraction of each population. On the right side I printed the ΔlogL value of this distribution.

estimated perfectly. This is also visible in the dependency on population ratio (Figure 3.5).

3.3 Comparing the GMM with real distributions

As we found that population fraction estimation works well we went on to investigate some follow-up questions. Can be separate the distribution into each component? What fractions do they have? Can we separate the binary sequences from their corresponding populations? This section investigates the first two questions in depth, whereas the third is connected to Section 3.5 as well.

For this I first looked at how GMM with four Gaussians compares to the true distribution. It might be that the model finds all elements and can fit them. In Figure 3.6 I plot the coloured histogram of each component (P1, P2, b1 and b2 are blue, red, cyan and orange, respectively) as the true distribution. The Gaussian from the fit, their means sorted by colour-difference, are plotted in the corresponding colour as a solid line on top. The ratio between each component is not correct as all are normalised to 1.0 in order for each histogram to be comparable to its PDF. The correct ratio is plotted in the leftmost panel, where the separation of the Gaussians is shown as well.

The figure shows that the single star populations (P1 and P2) are found and fitted reason-

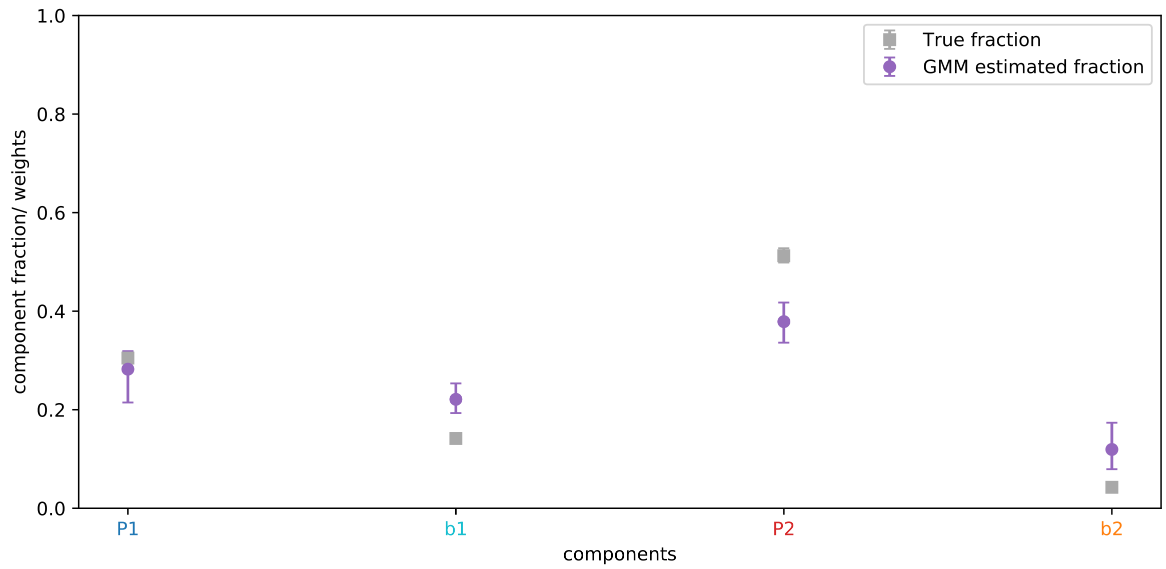

Figure 3.7: The true fractions of each component (grey squares) are compared to the weights of each Gaussian from a cluster GMM fit (purple dots) for a [33, 67] P-ratio and [30, 5] b-ratio cluster. The symbol is the median of multiple repetitions and the error bars are the 16-th and 84-th percentiles thereof. This only compares weights and neither shape nor mean of the colour distribution versus the Gaussians of the GMM fit.

ably well by the GMM. This is no surprise as their numbers are the greatest. The b2 fits is slightly shifted towards b1 and P2 stars and thus does not completely overlap with the histogram. The b1 stars are fitted the most imprecisely. The Gaussian fits is taking some of the P1 stars into account while the true distribution is included partly in the P2 and b2 stars, both. Because b1 stars are distributed almost over the entire colour difference distribution they are fitted by all four Gaussians.

These shifts between fits and true distributions neither change for higher number of data points nor for a broader metallicity gap between P1 and P2.

3.3.1 Comparing the GMM weights with their true fractions

In order to investigate this subject more quantitatively, I do 100 repetitions of standard cluster fits with 4 Gaussians and compare the weights of each Gaussian to the true fraction of the population. The Gaussians are sorted by their mean value from left to right in ΔC. Then they are paired from first to fourth with the components P1, b1, P2 and b2. The Gaussian's weights are compared to the true number fractions in each of the 100 data sets. The median values are chosen as symbols (grey squares and purple dots for the true and estimated fractions, respectively) and the errors are again the 16% to 84% percentiles. Figure 3.7 shows the result. The colour scheme at the bottom is the same as before.

It can be seen that for 100 different data sets and fits the P1 stars are fitted well by the first Gaussian. The other components are not fitted as closely. Where b1 and b2 are overestimated,

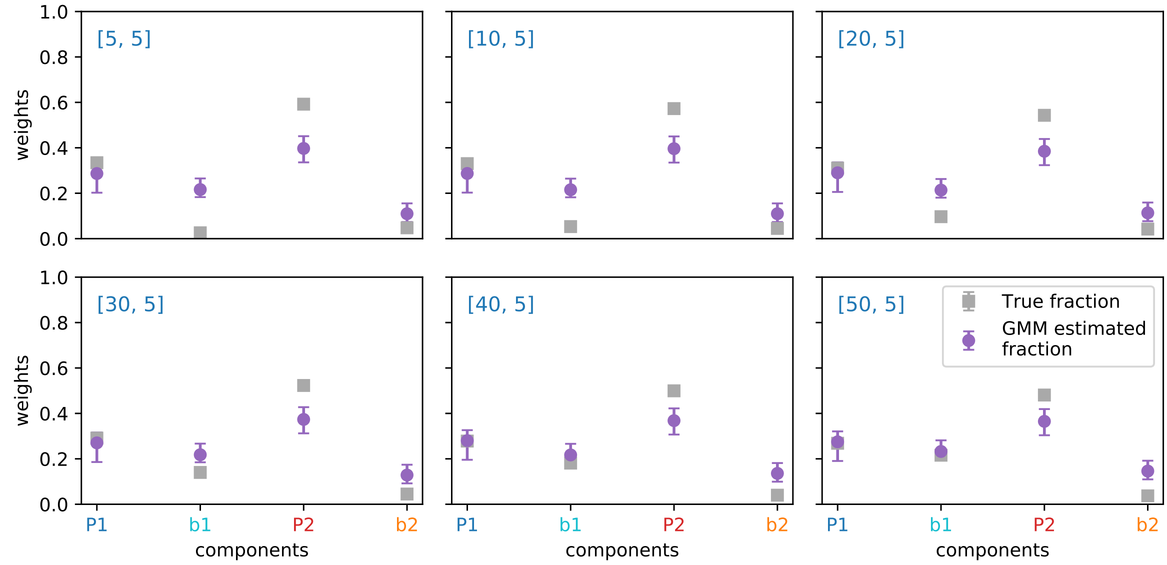

Figure 3.8: This figure is build similar to Figure 3.7 but now the contribution of the P1 binaries increases per panel from left to right and top to bottom. The increase in P1 binaries compared to other components manifests in an increased weight of all fitted Gaussians (the first, third and fourth which are P1, P2 and b2 respectively).

the third Gaussian fits too few P2 stars.

As the above figures only examine the standard cluster ([P1, P2] = [33, 67] and [b1, b2] = [30, 5]) I subsequently looked at the increase of P1 binaries. There are 50 repetitions for each b1 percentage. The result is presented in Figure 3.8. Here, the b1 percentage increases from left to right and top to bottom. The abscissa shows the 4 components and the symbols show true (grey squares) and estimated (purple dots) fractions as previously introduced. The figure shows again the surprisingly precise estimation of the P1 fraction over all six clusters. The second interesting find is that the b1 estimate is very constant over all clusters even though the true fraction increases. In the last panel with the highest b1 percentage (bottom right) it looks as if the fraction is estimated well. This is a illusion however, as the trend continues so that the true fraction quickly outgrows the estimate. It is by chance that the 50% b1 is fitted well. With a broader metallicity gap the estimate and true fraction cross earlier at ≈40% b1 stars.

What can be observed here in any case is that as the true value of b1 grows the third and fourth Gaussians (P2 and b2) include more stars and their weights increase compared to the second (b1) Gaussian. So as the b1 percentage increases it is distributed across the P2 and b2 sequences. Also, regarding the population estimation from Section 3.2 this figure again shows how the population estimation is not influenced by the increase of binaries because the fit is not detecting them.

It must not be forgotten, that by comparing the weights of a Gaussian, the shape and position is not included. So, even if the weights match as in the case of the last panel in Figure 3.8 the shape and position might not match. Figure 3.9 shows the qualitative visualisation of

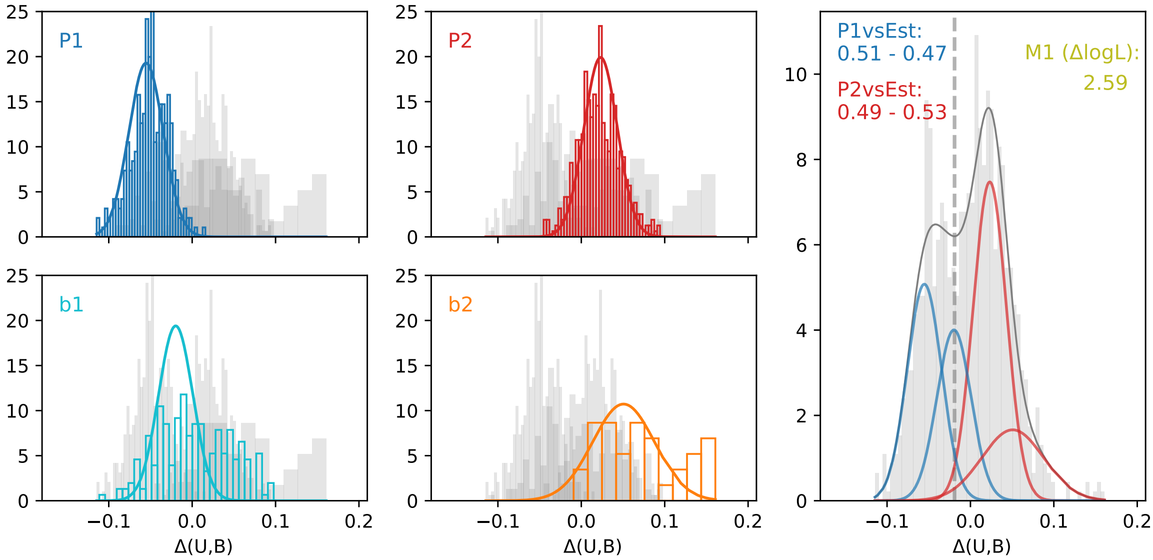

Figure 3.9: This is the same figure as Figure 3.6 only b1 is now 50% instead of the previous standard 30%. It shows each component (histograms) compared the corresponding fit (solid line) from the GMM. P1 in blue, P2 in red, b1 in cyan and b2 in orange. The original PDF and the correct ratios are depicted in the right panel. As the number of b1 stars increases, the stars are distributed over P2 and b2 sequences and fitted among these. Even though the weight of the second (cyan) Gaussian fits the true b1 (cyan histogram) fraction, the shape reveals that the b1 component is not actually fitted.

the cluster with 50% P1 binaries. The figure's format is the same as in Figure 3.6 above. It is apparent that even though the weight of the Gaussian and the fraction might match, the true distribution is not fitted at all. Again remembering the population estimation featured in Figure 3.5, the figure discussed here explains qualitatively why P2 and P1 are over- and underestimated, respectively. As the b1 percentage increases, many of these stars are included in the third (and fourth (with five GMM components)) Gaussian fit and thus regarded as P2 stars.

I conclude this section by mentioning that the method looks promising, however it needs improvement. While the main populations P1 and P2 (which harbour the most stars per data set) are reasonably well fitted the binary stars are not as easily recognised. The extraction of b1 stars is not possible with such a simple method. What would improve the fit is to use more prior information. As we know the binaries follow a flatter distribution, that is scattered normally it would help to define the standard deviation beforehand. Or even to find a consistent colour difference value of the b1 distribution's mean. Another idea that is investigated in Section 3.5 and further discussed in Chapter 4 Section 4.3 is to find a reliable gap size in colour difference for P1 and b1 and set a prior on the position of their colour separation.

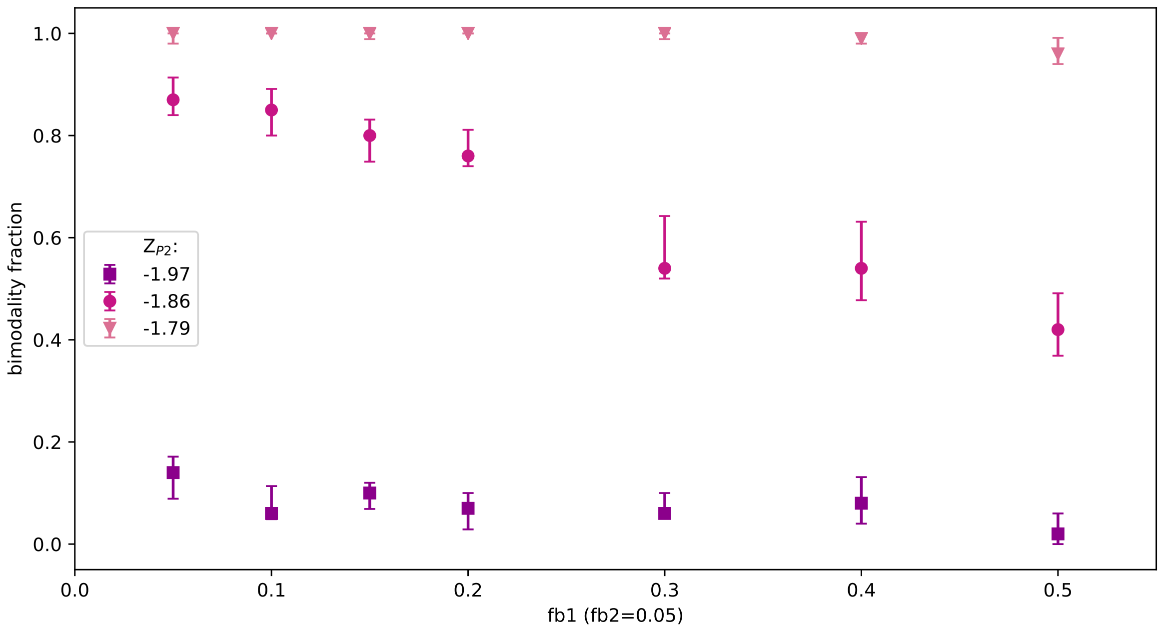

Figure 3.10: This figure sums up, how the metallicity difference changes the MSP detection rate. Z_{P1} stays the same, but Z_{P2} varies from big difference (light pink triangles) over intermediate difference (pink dots) to small gap (purple squares). As the gap size increases, more clusters are recognised as having MSPs even as the fraction of P1 binary stars increases.

3.4 Varying the metallicity difference of the two populations

Briefly summarised from Section 3.1, detection of bimodality strongly depends on the number of b1 stars. These partly inhabit the colour space between the two single star populations. For this reason it is interesting what happens when the split in the MS is bigger. I therefore downloaded two new SSPs with different metallicities representing alternative second populations. They consist of three sets of SSPs and were treated in the exact same way as described in Chapter 2 Sections 2.1 through 2.3. The new populations have lower and higher metallicity than the standard P2 being $[Fe/H]_{P2_{low}} = -1.97$ and $[Fe/H]_{P2_{high}} = -1.79$. For comparison, the standard metallicity P2 is $[Fe/H]_{P2} = -1.86$. I included colour-difference plots for all metallicity variations for comparison in the Appendix Section A.1.

The results of this investigation are demonstrated in Figure 3.10. Again, clusters are recognised as being bimodal, if they show $\Delta \log L \geq 7.0$. The plot shows clearly that when the metallicity gap is wider and thus the colour difference is larger, more clusters are detected as being bimodal. The clusters with the smallest colour difference (purple squares) show nearly no dependence on the increase of P1 binary stars. The pink dots represent the standard cluster and the trend is the same as in the previous two plots for 1000 data points and $M1 \geq 7.0$. With this colour difference it is never the case that all data sets are found to be bimodal beyond the M1 threshold. With the highest number of P1 binary stars, the detected fraction drops to $\approx 40\%$.

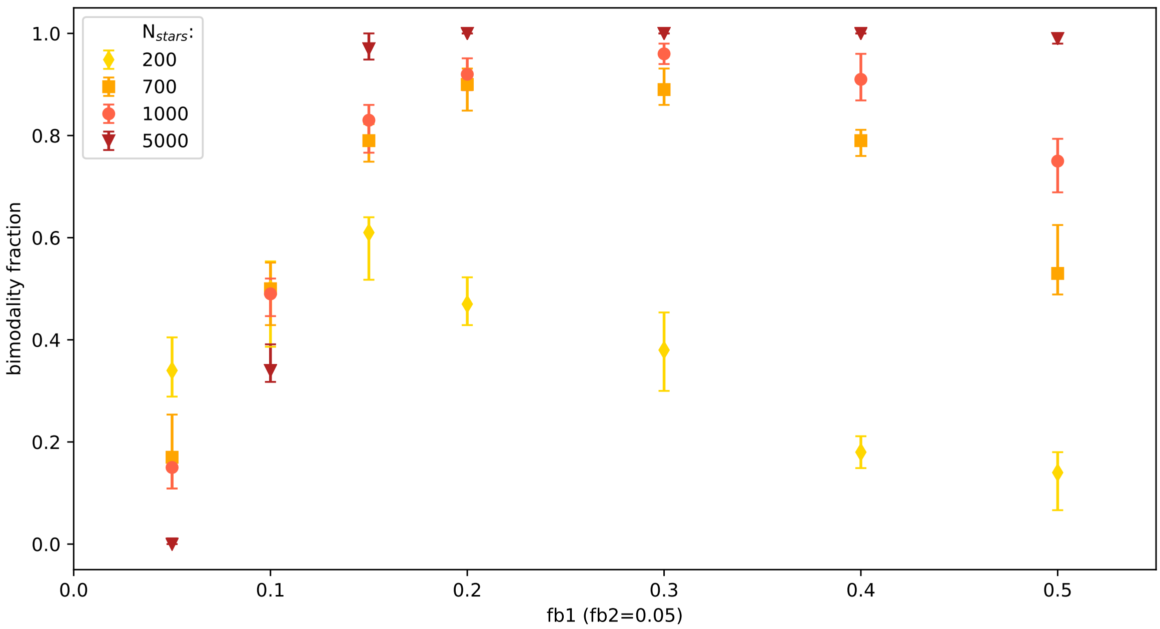

Figure 3.11: This figure intends to check if the code (using 3 Gaussians for the GMM fit) also classifies one population plus binaries as being bimodal. The abscissa increases with the fraction of b1 stars (fb1). Clearly, it does detect bimodality here which is strongly depending on the number of data points and the number of b1 stars as well.

For the cluster with the largest gap, 1000 stars is more than enough to detect bimodality independent on the number of b1 stars. Here, almost always a 100% of the MSPs in all data sets per cluster are detected.

Concerning the cluster with a very narrow colour difference, some of the data sets show bimodality (maximum ≈ 15%), but this might not detect he split between the populations. Specifically, some bimodality comes from separating the P2 binary stars from the rest. This possibility is looked into in the next section. Moreover, in Figure A.4 I varied the number of Gaussians used to fit the distribution and Figures A.6 to A.8 show the population fraction estimations for different abundance variations.

3.5 Check for false positive results

Until now, I only investigated the detection of MSPs and bimodality in colour-difference distributions. However, does the code also recognise one population plus binary stars, also referenced as single populations hereafter, as bimodal? For this, only the P1 and b1 stars were selected and the bimodality fraction calculated. The reason to use P1 and its binary stars is that they are the same for all clusters, independent of the metallicity. I used three Gaussian components to fit this distribution, as five would clearly over-fit the data that is now consisting only of two elements. Again the threshold of M1 ≥ 7.0 is used as detection limit.

Figure 3.11 shows the result. The detected bimodality fraction does not only increase with

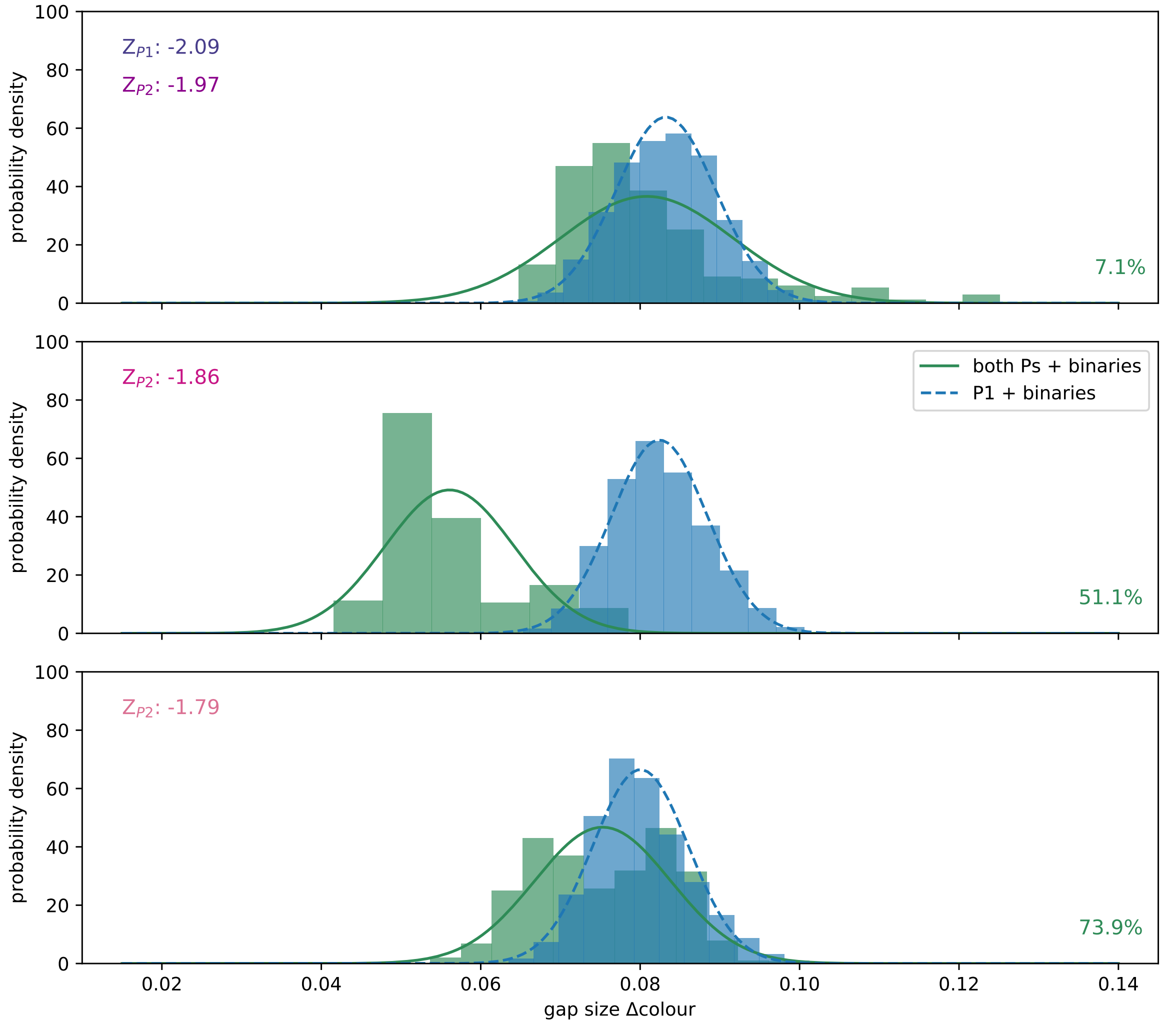

Figure 3.12: This figure shows the different gap widths (in colour difference on the abscissa) of one (blue dashed) and two populations (green solid) plus binaries for each metallicity gap. Metallicities of second populations (P2) increase from top to bottom and the percentage of clusters which show 2 peaks is printed in the bottom right corner in green. While the P1-b1 gap naturally does not vary in size or distribution for different P2 metallicities, the distributions vary strongly for the MSP clusters. It is confusing however that the cluster with the smallest metallicity difference (top row) shows such a large gap. For a correction of the confusion see Figure 3.15 on page 49.

the number of data points, but also with the increase of binary stars. For most single populations the bimodality fraction increases with the number of binaries, independent of the amount of data. Also, more bimodal colour-difference distributions are found for a smaller number of data points. Between a binary fraction of 0.1 and 0.15 the bimodality fraction per number of stars is inverted. Now a higher bimodality fraction is found in the data sets with more stars. Except for the data sets with 5000 stars, the bimodality detection drops at fb1 = 0.2 for 200 stars and at $0.3 < \mathrm{fb1} < 0.4$ for the other numbers of stars.

The reasons for the trends in Figure 3.11 can be explained as follows. As 5000 data points are very precise it shows that 5% of binary stars are not identified as a separate component, at least for this M1 threshold. Here, with 200 data points, the distribution is not as homogeneous which leads to a detection of bimodality. And thus, this is inverted when the number of binaries increase, as they create real bimodality with enough data point. Using less data, however, the increase in binaries create a more uniform distribution and also it is harder to get a good fit (see Figure 2.13 on page 29), thus leading to a decrease in the bimodality fraction.

It is now interesting, if the single population bimodality differs in some way from the MSPs bimodality. This would enable a differentiation between binary sequence and second stellar population, a subject that arises in Section 3.3.1. Since we work with the gap size as a means to distinguish populations this can be used here again. The idea is that the gap between recognised binary sequences and their corresponding populations differs in the size of colour difference from that of the MSPs. Also, if investigating multiple data sets the distribution of two MSPs might be flatter than the binary sequence gap as the latter should be a well defined and narrow Gaussian. As mentioned at the end of Section 3.3.1 this would help to establish a prior for fitting the GMM.

Therefore, I wrote an algorithm that calls 10 000 random data sets from the standard cluster model and only picks the bimodal distributions (2 peaks). Then it measures the size in colour difference between the two maxima for all bimodal data sets. The same is done with the data sets of only P1 (including b1). Finally, a Gaussian is fitted to the distribution of gap size in colour difference and the result plotted in Figure 3.12 (on page 45). Here, also the metallicity has been varied (top to bottom), so that the impact of different gap sizes due to variation in metallicity shows. It can be seen that whereas the distribution of the P1 (+ b1) data (blue with dashed fit) is quite narrow around 0.08 in colour difference and it naturally does not vary with metallicity. The MSPs bimodal distributions (green with solid fit) show an interesting development, however. In general the distribution is broader and it is not as defined (broader bars) because less data sets are only bimodal. The percentage of bimodal distributions from all 5000 sets is printed in the bottom right corner in green. Further, for the two higher metallicity differences there is an apparent trend with gap size in colour difference (from ≈ 0.055 to ≈ 0.075). But why is the trend not visible in the smallest metallicity difference (top panel).

To investigate this, I created Figure 3.13 which shows three randomly created bimodal data sets and their fitted PDFs in red on top to visualise the gap size. This is done for all metallicity differences again (top to bottom). The average size in colour difference between the maxima (black vertical solid lines) is printed in blue in the upper right corner. This figure reveals what I forgot to consider in Figure 3.12. For a detection threshold of M1 ≥ 7.0 the top panel is mostly considering the gap between both populations and the P2 binary stars. However, as it is of interest how the gap between the two populations P1 and P2 behaves the peak of b2 stars needs to be excluded. Thus, the gap in colour difference for the smallest metallicity difference (first rows) can not be larger than the clusters with other P2 metallicities.

In Figure 3.14 this method of excluding the b2 peak is visualised. In the left panel, there are no restrictions set. In the right panel is a distribution with a gap that is bimodal, has a

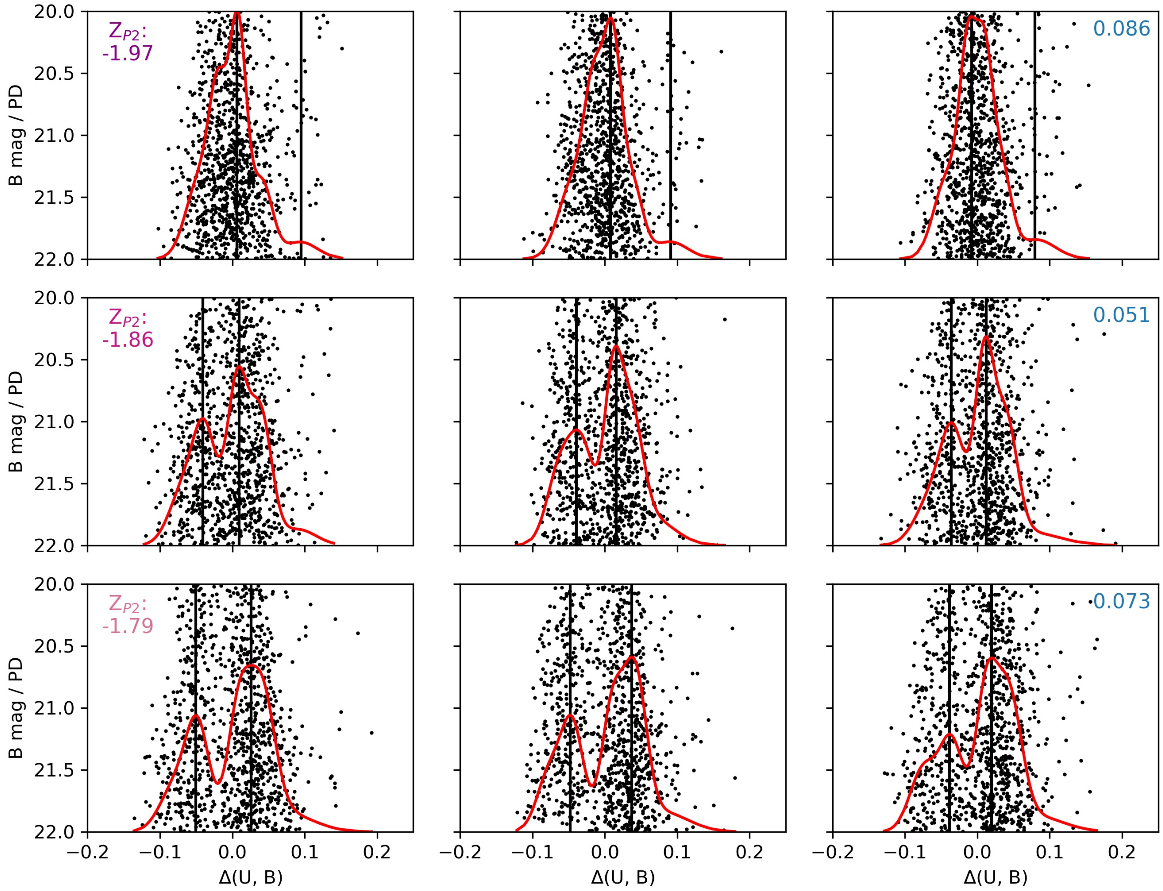

Figure 3.13: This figure visually compares the gap sizes between the two populations for the three different P2 metallicities increasing from top to bottom). There are three random cluster examples with a double peak for each P2 metallicity and the fitted Gaussians (red) are plotted on top of the verticalised colour distribution. To visualise the gap size the black vertical lines are plotted at the Δ(U,B) (ΔC) values of each peak. The blue number in the top right corner is the mean gap size of the three example clusters.

M1 value ≥ 7.0 and the second peak must be at $\Delta C < 0.5$. The value is chosen qualitatively. The format is similar to the previous figure where the black lines indicate the peaks, however here, the added red vertical line now shows the limit value at $\Delta C = 0.5$. In the left panel there is one below a colour difference of 0.0 and one small one beyond 0.1. The right panel with the restriction now provides the gap that I am looking for.

Finally, I redid Figure 3.12 and added a fourth version of P2 with an even higher metallicity. This is done in order to see if and how the trend in gap size that is seen in Figure 3.12 continues. This fourth P2 has a metallicity of $[Fe/H]_{P2_{highest}} = -1.71$. The result is seen in Figure 3.15 where format and colours are the same as in its predecessor. However, now it is apparent that the gap size distribution of the one population with binaries (P1 including b1) does not vary greatly, neither in position (as it is always the same population) nor in width. On the other hand the gap size distribution in colour difference varies greatly depending on the P2 metallicity. For one, the larger the metallicity gap between the two populations, the

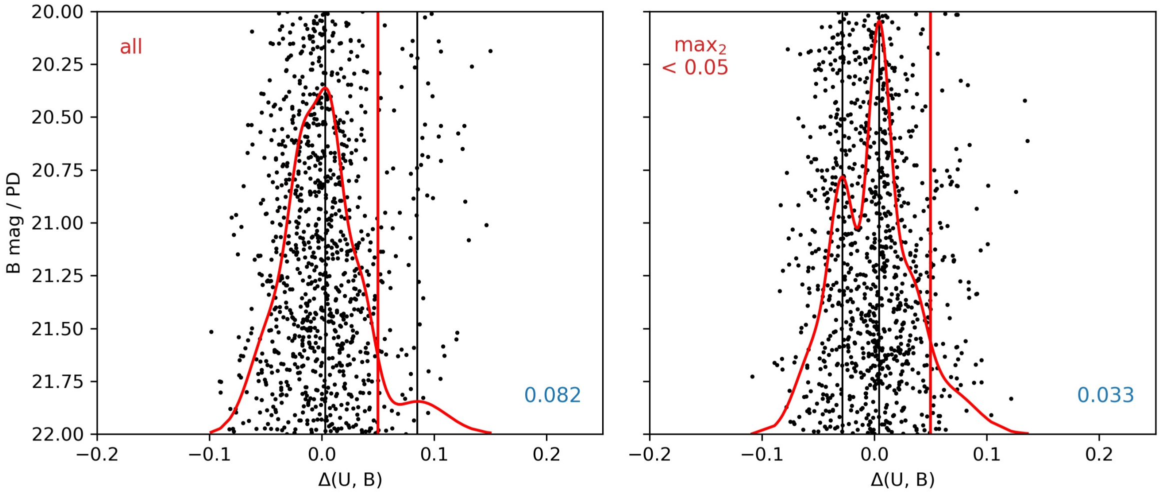

Figure 3.14: This figure again shows the verticalised CMD with its PDF plotted on top. **Left panel:** An example of a double peaked cluster with the lowest metallicity variation between P1 and P2. Here it is apparent that the P2 binary population (b2) is counted as the second peak which I want to exclude for the comparison in Figure 3.12. **Right panel:** An example where distributions with a second peak beyond the colour difference (ΔC or $\Delta(U,B)$) of 0.5 are not taken into account. This threshold is marked by the vertical red line in both panels.

more bimodal data sets are found and accordingly the distribution gets narrower and more Gaussian. Generally, the gap sizes of MSPs varies more than that of a single population and its binary stars.

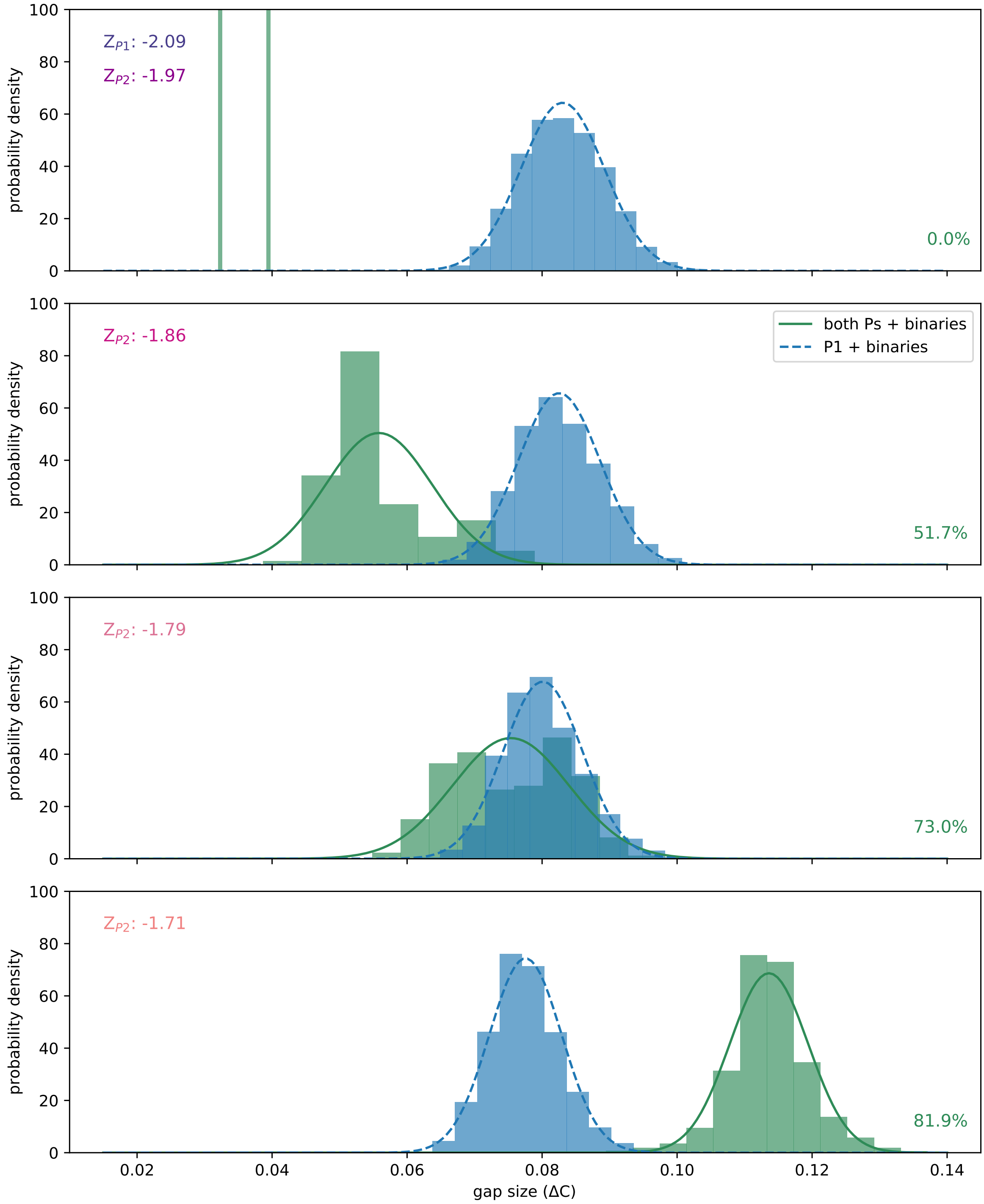

Figure 3.15: This figure is similar to Figure 3.12 but the first row now excludes gaps between the b2 component and the rest. In the bottom row, there is also the colour gap distribution (CGD) from clusters with an even wider metallicity difference. The mean value of the colour gap changes with the metallicity difference of the populations as expected. In the case were the CGD overlaps they can be distinguished by the distribution width (P1+b1 is narrower than the MSPs).

Chapter 4

Discussion

This thesis investigates the topic of MSPs and their interplay with binary stars in CMDs. This is accomplished by creating data sets of mock GCs containing MSPs and binary stars. I then create a method to measure the reliability of the bimodality. With this M1 value I investigate the effect b1 stars have on the photometric detection of MSPs, estimate the fraction of each population and look for a way to separate the binary stars from the rest of the cluster.

This chapter discusses each result and the methods that where used. I also reflect on the results in regard to current research and the bigger picture. I start with the creation of the clusters and the compromises and assumptions that were made in Section 4.1. Subsequently, the results (the dependence on b1 stars for the bimodality fraction in Section and the estimation of population fractions) are reviewed in Section 4.2 (page 55). Finally, I discuss the topic of separating these binaries from the distribution in a CMD in the Section 4.3 on page 59.

4.1 Qualification of the mock data

In the scope of this thesis a complete simulated model of a GC would exceed the time constraints. For this reason we decided on SSPs as mock cluster populations. Of course this comes short of the observed reality for many reasons that are discussed in the following. Even though the mock data that I created is not including all observed factor it is still a good method for this investigation. As already mentioned, the data in this thesis recreated observational CMDs from various observational papers (e.g. Milone et al. 2012 Nardiello et al. 2015) using simple techniques.

4.1.1 Several stellar populations

Observed CGs often host more than two MSPs (e.g. Milone et al. 2019, Milone et al. 2013). Also in respect of light element (LE) abundances they show a smooth transition between the stellar populations (Bastian and Lardo 2018 Section 2.2 shown in 'chromosome maps' from Milone et al. 2017b). This would also results in a smoothly colour-spread population in the CMD which is much more complex than a SSP that is smeared by a standard distributed error

Table 4.1: This table lists various versions of binary fractions for six different clusters. fb refers to the total binary fraction per cluster for 1000 data points. $fb1$ and $fb2$ are the blue and red binary fractions per cluster among 1000 stars. $fb1P1$ and $fb2P2$ are the fractions of binary stars per population (including binaries; blue and red, respectively). These are mean values that were calculated from 100 randomly created data sets per cluster. The standard deviation results in 0.0 for 16 to 19 digits for all and is thus not listed in the table.

P1, P2	25, 75	50, 50	67, 33		33, 67	
b1, b2		30, 5		5, 5	30, 5	50, 5
fb	0.140	0.186	0.210	0.070	0.156	0.204
fb1	0.097	0.162	0.195	0.025	0.120	0.173
fb2	0.043	0.024	0.014	0.045	0.036	0.031
fb1P1	0.325	0.326	0.325	0.074	0.326	0.446
fb2P2	0.076	0.076	0.077	0.077	0.077	0.076

as I implemented. Thus, these subpopulations effect the CMDs in such a way that the stars of each populations would have a broader distribution.

Concerning their influence on the algorithms I created, it could be more difficult to get a good fit on the population fractions as they rely on a distinct minimum in the fitted PDF. Furthermore, these subpopulations would not only soften the minimum in a PDF but also most likely each individual subpopulation would not be detected by 5 Gaussians. For the detection of subpopulations, for example when all components are to be found, the number of Gaussians for a GMM fit must increase. However, this is more a problem of sensitivity and if only the fitting of the parent population fractions for estimation is of interest, then the code is good enough. Here, the purpose of the fit needs to be specified since too many Gaussians often overfit the distributions if for example only the main populations are to be separated or the degree of bimodality is the subject of investigation.

Also, similar to many subpopulations, there can be more than two parent populations in a GC. It such a case the problem might become more complex as well. Since three MSPs (Milone et al. 2017a) (Milone et al. 2013) have been found more than once I take them as an example. Three MSPs surely bring three binary sequences with them as we do not have the optics to resolve all stars. This combined with the smooth LE abundance transition gives for a much smoother CMD than this thesis considers. Thus the algorithms must be evolved to recognise main and binary sequences so as not to confuse a weak population as another populations binary sequence for example.

4.1.2 Binary fractions

The binary fraction in this thesis listed in Table 4.1 do match observations nicely. In Milone et al. 2012 they provide comprehensive statistics from observations (Table 2 column 6 and Table 3 column 2) and my mock data compares successfully with those. This work does not separate between core and outer regions, however, the overall binary fractions (Table 4.1 row

1) match his range, from less than 0.1 to more than 0.3. They also match core fractions from Sollima et al. 2007 that range from 0.1 to 0.5. While these mock clusters are slightly above average regarding the total binary fractions, which in observations is roughly around 0.1, due to the variation in cluster parameters the full range from observations is covered in this work. Separating the binaries into enriched and primordial origin as a fraction of the total cluster (rows 2 and 3) my numbers are similar to what is found by Lucatello et al. 2015, who finds 0.05 primordial and 0.01 enriched binary fractions) and Dalessandro et al. 2018 (primordial 0.14 and enriched binary fraction 0.01). The last two rows (4 and 5) have the fraction of b1 stars among the first populations (P1 + b1) and the same for b2 stars.

4.1.3 Data manipulation

In order to simplify the GMM fitting process I reduced the CMD to one dimension by verticalising it (see Chapter 2 page 21). The method of rectifying the data uses the mean of a small number of stars (sorted by magnitude) in the CMD which is subtracted from its selection of stars. One aspect that needs to be kept in mind is that the new position of the star in the colour-difference diagram depends on the mean. If, for example, there is one star in this selection with an intermediate colour value and the rest has high colour values the one star is shifted more than expected. The stars will end up with a lower ΔC than it would if the colour values where more homogeneous. This case or a variation of it is likely to happen and even though it rarely happens it changes the data minimally. Further, as already mentioned on page 22 the final colour difference value of the stars beyond the plausible colour difference values (-1.0 and 1.5 ΔC) are either interpolated if in between the MS or extrapolated when at the top or bottom of the MS.

This interpolation of stars in the middle of the MS adds potentially wrong colour difference values to the MS by force and in the process falsifies the data. This manipulation moves some stars to another colour-difference which leads to over- or underestimation at that value. However, the interpolation concerns at most 100 stars in between all $\approx 4 \times 10^5$ stars of the MS of the created cluster. With randomly drawing 1000 stars for most of the analysis the chances are poor that one or more of them are included. Concluding, I would not correct these outliers but flag them as 'untrustworthy' and not include them in the analysis from thereon. The extrapolated stars that are outside the mentioned colour difference range (due to large errors) would be treated with the same procedure but given another flag to keep the two cases apart.

Observational rectification of CMDs is, for example as in Milone et al. 2012, accomplished similarly by fitting a spline to the median of the observed MS for small magnitude bins. This function is then subtracted from the colour values in the CMD. The median is not as influenced by these outlying stars that I interpolated. This is also something I would use instead of the mean, at least when using large enough magnitude bins. In general rectifying a CMD simplifies the problem but introduces some uncertainties due to data manipulation. Another perspective is to look at the problem in 2D – at the original CMD – and fit the GMM there.

4.1.4 Radial distributions and brightness

A further subject of this purely photometric creation of mock data is that radial cluster properties are completely ignored. As already known, the populations are spatially often not uniformly distributed. Enriched stars are often found closer to the centre of a GC even though the other extreme was observed as well (Bastian and Lardo 2018). There are biases in the detection of stars at both ends, towards the faint stars at the outskirts (Sollima 2020) and the very bright and crowded cluster centres (mentioned in Weigert 2012 and for GAIA in Pancino et al. 2017). And since the CMDs in this thesis are based on observations (Nardiello et al. 2015) they represent the current knowledge and thus distribution as well.

There is also an anticorrelation between binary fraction and radial distance from cluster centre that has been found for example by Milone et al. 2012, Hong et al. 2015 and Giesers et al. 2019. They find that the fraction of binary stars increases towards the cluster centre. As this varies binary fraction an analogue to different environments is also investigated. As the b1 fraction increases in the mock data we looked at what happened to clusters with higher binary fractions.

4.1.5 Mixed binaries

As simulated in Hong et al. 2015 and found by Milone et al. 2020 there is a significant percentage of mixed binaries in GCs. These binary stars consist of two stars where one comes from the primordial population and the other from enriched population. This observation is not included in my algorithm. However, mixed binaries would inhabit the CMD between the first and second binary sequence, depending on the dominant star from the binary mass ratio (Milone et al. 2020). If both stars are close to or equally bright, the binaries will inhabit the colour space of the P2 stars in my mock CMDs.

Thus, the mixed binary sequence biases the population fraction estimation towards higher fractions of P2 stars. It might also be very hard to detect the mixed binaries with a Gaussian among the other populations. However, if the distribution is similar to b1 and b2 than a prior could be set at the expected colour difference (see Section 4.3 for details).

4.1.6 Amount of available data

One of the greatest advantages of creating model data is that the number of stars is almost unlimited. This is of course not the case for observations. For this reason we investigated the influence on the number of stars on each method. Regarding Table 2 in Milone et al. 2017a their average number of analysed stars per cluster is about 700 which is used in this analysis but we also covered the much higher numbers as well.

Surprisingly, the estimation of the population fraction does not differ greatly depending on how many stars are in the data (see Figure 3.3 on page 36). With 100 stars the estimated fraction P1 is 44% and of P2 is 56%. With 400 data points P1 and P2 are estimated to be 37% and 63%, respectively. There is not such a large difference for the lowest number of data points as the true fraction values are 37% (P1) and 63% (P2). 400 stars even has a great median estimate already. Of course the estimates beyond 1000 data points have smaller errors, however, it is surprising that even for smaller data sets the results are reliable and good.

On the other hand, for the lost bimodality fraction the number of stars does play a significant role as expected (Figure 3.2 on page 35). The bimodality fraction shows in what fraction of data sets MSPs are detected, whereas the population estimation analyses the found clusters hosting MSPs. Even though all data sets have MSPs for 200 data points only 20% are recognised at most. With increasing binary fractions this percentage is reduced to about 10%. Of course this only holds for such a stellar population gap of the standard cluster (roughly 0.05 to 0.06 ΔC , see the second row of Figures 3.13 or 3.15 on pages 47 and 49, respectively). To increase the detection rate a larger data set is required since for observations the b1 fraction is not subject to modification. However, for 30% added b1 stars increasing the data to 5-times the size (200 to 1000 stars) the detected fraction only shows a 4-times increase ($\approx$ 15% to $\approx$ 60%).

It is not an unexpected argument to make, that increasing the available data size through observations is one of the main promises on shedding light into unsolved aspects concerning MSPs.

4.2 Bimodality fraction and population fraction estimation

4.2.1 Bimodality fraction

The result from my thesis concerning the detected bimodality fraction (Chapter 3 Section 3.1) is that not all MSPs are detected in the cluster even though they are there. There are multiple factors that influence the detected fraction. The largest influence comes from the number of data points available (see Section 4.1.6 for a discussion). Furthermore, the number of P1 binary stars and the gap size between the two main populations have an effect on the detection.

We detected that the binary stars of the first population plays a major role in the detection of binary stars. After recreating the CMDs of GCs from CMDs for example such as in Nardiello et al. 2015 the b1 fraction was varied to investigate its effect. The Figure 3.2 on page 35 shows that the more b1 stars there are the less CMDs are detected as hosting MSPs. Of course this is for a confident M1 threshold of greater than 7.0. But even with a low threshold (M1 $\geq$ 5.0) in Figure 3.1 (page 34) not all data sets having a split MS are detected for 1000 stars. So, first the detection depends on the amount of P1 binary stars as the bimodality fraction decreases for all thresholds with increasing fraction of b1 stars. Then the threshold also reduces the number of detected clusters. However, this is only a tool to gain certainty of the detected cluster hosting MSPs. The higher the threshold the more certain it is for the cluster to really host two populations.

Regarding the light element abundance variations, they also have an impact on the lost bimodality fraction. We mimicked them by choosing different metallicities for the second population and hence, having clusters with very narrow splits (small abundance variations) in the MS as well as some with very defined, wide splits (larger variations). In Figure 3.10 (page 43) the effect of different metallicity gaps on the detection is shown. The clusters with the narrowest sequences are not influenced by the b1 stars. They have a very high lost bimodality fraction since very few pass the threshold of $M1 \geq 7.0$ (Figure 2.15). The majority of the data sets that do pass, are most likely included because of the gap between the b2 stars and the rest of the cluster (see the left panel of Figure 3.14). This problem is faced later in Section 3.5 by excluding the peak for b2 stars. Else, the lost bimodality fraction is very likely close to 100%, especially for only 50 repetitions/ different data sets. For the wider gap between the populations, the P1 binary stars do not prevent the detection of MSPs. I already established that the standard metallicity gap with is affected by the b1 stars, as they apparently fill the gap between the P1 and P2 sequences and thus make the detection less clear.

50% added binary stars (30% of the first population are then b1 stars) already reduce the number of detected MSPs greatly (to less than a half). This is one of the reasons that binary stars are an important factor to consider in every investigation of MSPs in GCs.

4.2.2 Population fraction estimation

In Chapter 3 Section 3.2 I found that the fraction of the first and second populations including their binary sequences are well estimated by fitting a GMM to the colour-difference distribution. The Gaussian weights are added up depending on their separation by the minimum that divides the two population peaks. For the example in Figure 3.3 (page 36) I used the standard cluster as in previous examples and the estimation is extraordinarily good and almost independent on the number of available stars. When fitting different population fractions and binary percentages the estimation is not as accurate but the constancy of the estimation is still given. This is shown in Figure 4.1 for the first two subfigures (a) and (b) and the last (e). Both populations are over- and underestimated in all three variations. The first one (a) has a very small P1/P2 ratio and even though the estimation is fairly good for all versions of data points the Gaussians are fitted in such a way that more stars are attributed to the P1 than P2. It is the opposite for the subfigure (b) where the parts of the b1 sequence are assigned to P2. The bottom panel (e) is showing the b1: 50% cluster and again the estimates are constant towards higher numbers of data points but estimate the fractions wrongly.

What can be seen in Figure 3.5 on page 38 is also visible in the subfigures (c) and (d) of Figure 4.1. For the same number of single population stars but a higher b1 fraction, the estimation process fails the distribution. The distribution is split such that the fP1 is underestimated even though it is now larger than the fP2 because of the higher b1 percentage. The same happens for panel (d) where the method does not work as well. The problem is that the distributions are most of the times fitted with two Gaussians having means smaller than the (first) minimum and three larger. And even though the minimum is the correct one to separate the populations the b1 stars are distributed so widely that the latter three Gaussians still contain more stars.

Figure 4.2 shows the distribution of the b1 stars and the fit for the standard cluster and

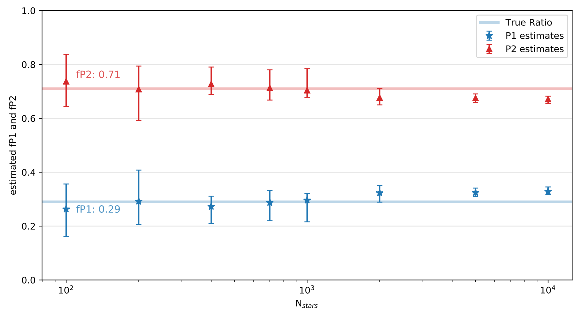

(a) The cluster properties are P1: 25%, P2: 75%, b1: 30% and b2: 5%.

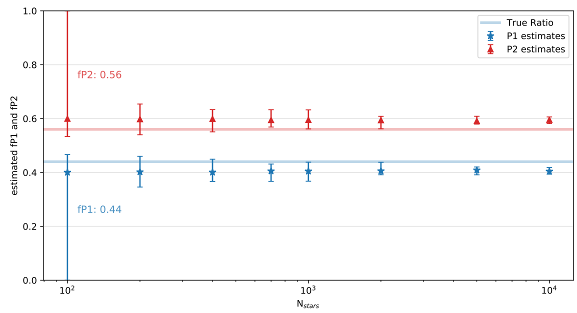

(b) The cluster properties are P1: 40%, P2: 60%, b1: 30% and b2: 5%.

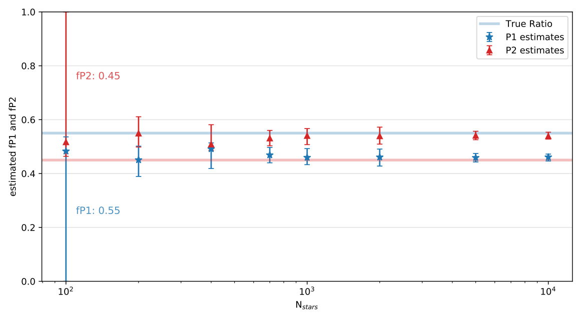

(c) The cluster properties are P1: 50%, P2: 50%, b1: 30% and b2: 5%.

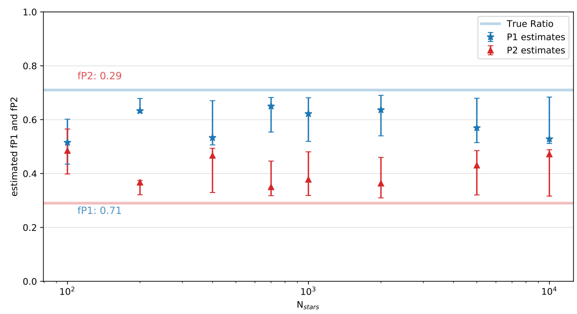

(d) The cluster properties are P1: 67%, P2: 33%, b1: 30% and b2: 5%.

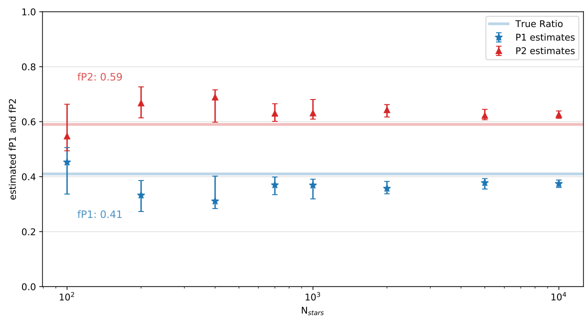

(e) The cluster properties are P1: 33%, P2: 67%, b1: 50% and b2: 5%.

Figure 4.1: This figure shows five different versions of population fraction estimation plots but not including the standard cluster. The horizontal lines are the true cluster fractions of P1 (blue) and P2 (red) including their binary stars. The median values of 50 estimates are plotted as red triangles and blue stars for P1 and P2, respectively. The errorbars show the 16th and 84th percentiles. The first four panels (a, b, c, d) show variations of population fraction where the b1, b2 ratio stays the same. The last one (e) at the bottom shows the estimates for a higher b1 percentage. The figure supports the fact that the b1 stars influence the distribution shape but the fits are not precise enough to take these stars into account. This, alongside the limitations of the algorithm, produces inconsistent results.

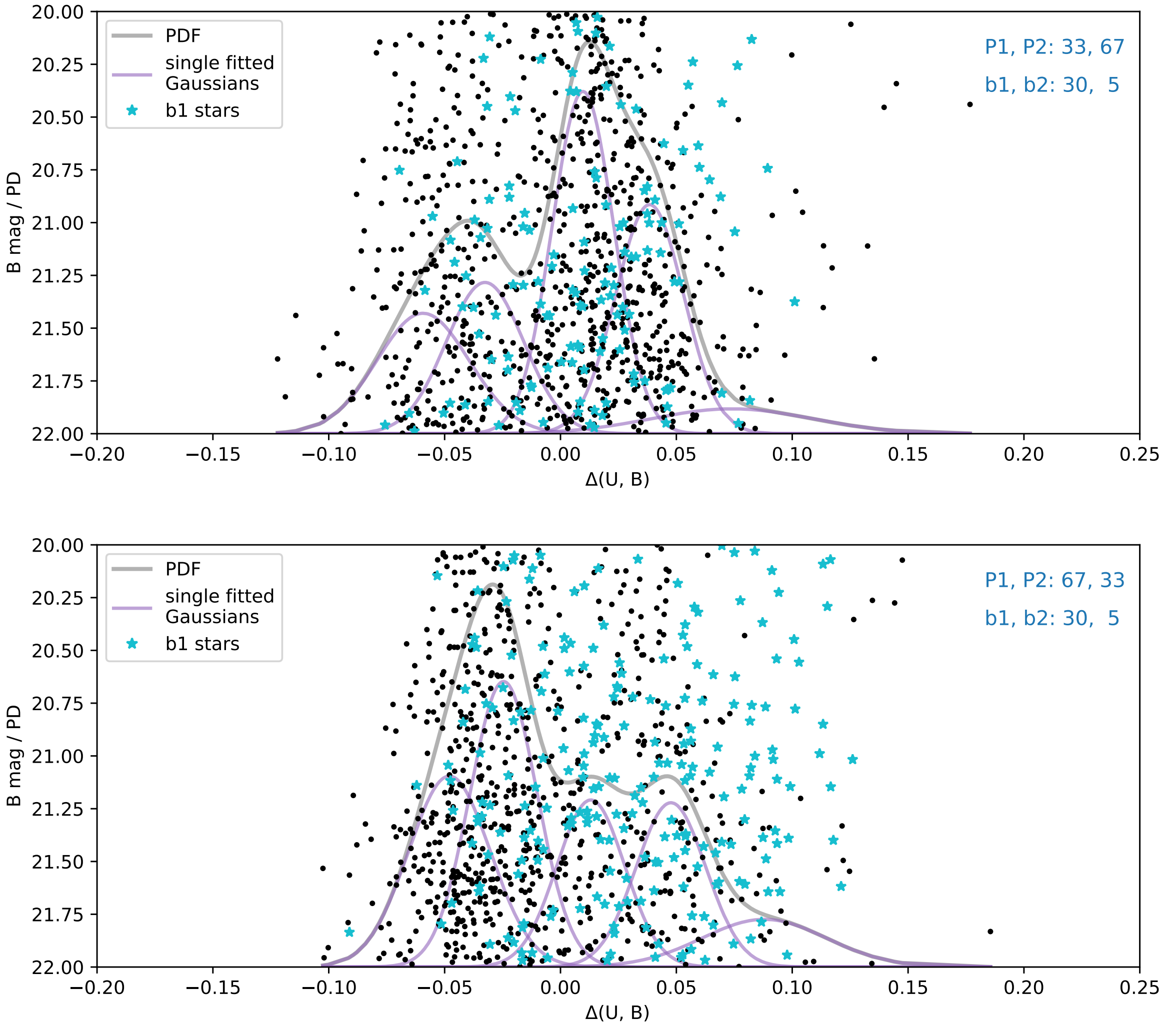

Figure 4.2: Here, the colour-difference distribution is plotted over the fitted PDF (grey) with the five individual Gaussians (purple) to visualise the discrepancy. The b1 stars are the cyan stars. It is obvious that the b1 stars are distributed all over the two populations and consequently the estimation of the population fractions is off.

subfigure (d). They are again with 1000 stars and the b1 stars are highlighted in cyan star-symbols. It becomes obvious why the estimation is inaccurate with the reversed standard cluster. In the top panel the standard cluster has less b1 stars but the distribution is the same. So there are many b1 stars in the P2 section. But here they are but a small fraction of the P2 estimate. For the reversed standard cluster there are more P1 binary stars and additionally less P2 and b2 stars. So the b1 stars that are in the section of the second population stars make a larger fraction and are missed in the estimate of P1 stars. That is why the fP1 is underestimated and the fP2 overestimated.

The b1 stars only allow a good population fraction estimation if their numbers are limited. The algorithm and method that I used does work well for a 'classic' GCs composition but fails for higher b1 numbers or b1/(P2+b2) ratios. For this reason and many others already mentioned it is of great interest to find the b1 positions.

4.3 Separating the binaries from the GC

As mentioned throughout the thesis there are several reasons to separate the binary stars (b1 in particular) from the GC's population. Binary stars not only influence the dynamical properties of clusters (e.g. Dalessandro et al. 2018) and affect cluster mass loss (Hong et al. 2015) but also their environmental information might help understanding the birth conditions of the MSPs they belong to. In regard to this thesis, knowledge of the position and distribution of binaries in CMDs supports improvement of the population fraction estimation and recognition of MSPs.

In an attempt to do this, I created Figure 3.15 on page 49. In theory the gap between the binary stars and their host population with single stars should have a consistent size. The binary stars are two unresolved stars seen as one, and follow a mass ratio distribution (Milone et al. 2012) and can only inhabit a defined sequence in the CMD (e.g. Milone et al. 2012, Milone et al. 2020). Essentially this is a result from Figure 3.15. The blue distribution is narrow and has quite constant mean values of about 0.075 to 0.08 defining the distance from P1 to b1 maximum. Knowing that the b1 sequence has a probability density peak ≈ 0.08 in colour difference apart from the P1 peak makes it possible to set prior constraints on the GMM fit.

First the distribution of the b1 stars has to be known, which does not necessarily have to be a Gaussian. And then the position of its most likely mean, relative to the P1 single stars, needs to be established. Subsequently, a prior can be used in GMM fits with the purpose of getting more accurate estimates. If the fit 'knows' the position of the b1 stars and has an idea of the distribution then b1 stars can statistically be selected. If the method was successful the problem mentioned in Section 4.2.2 would be solved and the estimates from Figure 3.5 (page 38) and 4.1 (c) and (d) (page 57) more accurate.

The algorithm to implement the prior could first run a GMM fit without constraints to locate the position and peal of P1 and then set a prior for the b1 stars. Finally the fit must be run again with the prior and the estimation process based on this result. Further, in case of success the same can be done for the b2 distribution and even for the mixed binaries if included and investigated.

Of course this does not return the exact binary stars but only the probability of their location and distribution in the CMD. However, through this the fractions of all components can be determined and thus the composition of the cluster unravelled. For one, subtraction of the distribution of binary stars leaves the single population stars for clear MSP detection and better evaluation of abundance variations. Secondly, the knowledge of (almost) exact binary fractions and their mass ratios would improve cluster mass estimates.

Chapter 5

Summary

This thesis delves into globular clusters (GCs) which host the oldest stars found in the galaxy and are discovered to host the phenomenon of multiple stellar populations (MSPs). These are seemingly two coeval populations having the same metallicity but show star-to-star variations in light element abundances. It is not yet understood how they formed and it is an intensely debated topic. It was already shown that binary stars do play an important role in the understanding of the formation and characteristics MSPs. MSPs are most commonly observed photometrically because it provides a large spatial area to observe which also improves statistics. MSPs are well detectable in colour-magnitude diagrams (CMDs) as the stellar abundance variations create a split in the main sequence (MS), one to the bluer and one to the redder side of the colour distribution.

To investigate the subject of binaries among MSPs, I first used simple stellar populations (SSPs) from PADOVA[15] to mimic CMDs of MSPs from a typical GC. I then created a metric in order to classify the extent of bimodality found in colour distribution of MSPs. This was achieved by using populated isochrones of the same age but different metallicties to mimic the light element abundance spread for the split MS. Finally, I added a realistic error based on previous observations and binary stars, made of the luminosity of two single stars, for each population an thus made the CMD complete.

Subsequently, I varied several parameters to find a dependency between them. The parameters are the fraction of blue binaries, the ratio between the two populations, the number of detected stars and the abundance spread (mimicked by the metallicity spread). I also implemented to algorithms to detect the existence of MSPs for one and estimate the population fraction from the colour-difference distribution. The algorithms are based on Gaussian mixture models (GMMs) that are fit to the colour-difference distributions. Also, I looked into the congruence between the actual colour distribution of each component and the single Gaussians that were fit to the global distribution.

The results of this investigation are as follows:

- I found that the blue binary stars (b1) have a large impact on the detection of MSPs as

[15] https://people.sissa.it/~sbressan/parsec.html

they fill up the gap between the parent stellar population for large b1 numbers. This does not hold for smaller and larger abundance spreads than the default but each for different reasons. In the clusters with a narrower gap the two populations are so close as not to be influenced by the number of the b1 stars. When having a wider gap on the other hand, the b1 stars are not able to obscure the split MS.

- Secondly, the population estimations does not depend on the b1 stars as the GMM fit is not sensitive enough to detect up to an intermediate increase of binary stars. If the bluer population (P1) stars increase by much and the binary fraction with it, then the estimation algorithm and method is insufficient to make a good estimate.

- Moreover, for an observational average of 700 stars (Milone et al. 2017b) the detection of MSPs and estimation of population fractions is very feasible although results majorly improve with an increasing amount of data. Binary fraction from observations are represented in the standard cluster (primordial 0.120 and enriched binary fraction 0.036) and result in solid distinction and estimation of population fractions throughout the the analysis.

- Concerning the topic of the overlap between the component distributions and the GMM fit it shows that with four Gaussians the prominent features of the two parent populations are well detected and fit closely. More often than not the red binary (b2) stars are so distinct as to be also fitted well. The b1 stars are scattered across both populations and even among the b2 stars and can not be detected by simply fitting a basic GMM. However, I found that the binary stars have a tight range of distance from the P1 stars in colour-difference. This would help to set a potential prior in order to separate the b1 stars from the rest.

Although the mock CMDs have some shortcomings compared to more sophisticated simulations that include the physical structures of a GC as well, this thesis illustrates well that it would be unreasonable for any observation of MSPs to ignore the aspect and presence of binaries.

Bibliography

Bastian, Nate and Carmela Lardo (Sept. 2018). "Multiple Stellar Populations in Globular Clusters". In: *Annual Review of Astronomy and Astrophysics* 56, pp. 83–136. DOI: 10.1146/annurev-astro-081817-051839. arXiv: 1712.01286 [astro-ph.SR].

Bressan, Alessandro et al. (Nov. 2012). "PARSEC: stellar tracks and isochrones with the PAdova and TRieste Stellar Evolution Code". In: *Monthly Notices of the Royal Astronomical Society* 427.1, pp. 127–145. DOI: 10.1111/j.1365-2966.2012.21948.x. arXiv: 1208.4498 [astro-ph.SR].

Cohen, Roger E., Aaron M. Geller, and Ted von Hippel (Jan. 2020). "Bayesian Characterization of Main-sequence Binaries in the Old Open Cluster NGC 188". In: *The Astronomical Journal* 159.1, 11, p. 11. DOI: 10.3847/1538-3881/ab59d7. arXiv: 1911.08390 [astro-ph.SR].

D'Ercole, Annibale et al. (Dec. 2008). "Formation and dynamical evolution of multiple stellar generations in globular clusters". In: *Monthly Notices of the Royal Astronomical Society* 391.2, pp. 825–843. DOI: 10.1111/j.1365-2966.2008.13915.x. arXiv: 0809.1438 [astro-ph].

Dalessandro, E. et al. (Sept. 2018). "The Unexpected Kinematics of Multiple Populations in NGC 6362: Do Binaries Play a Role?" In: *The Astrophysical Journal* 864.1, 33, p. 33. DOI: 10.3847/1538-4357/aad4b3. arXiv: 1807.07918 [astro-ph.GA].

de Boer, T. J. L. et al. (June 2019). "Globular cluster number density profiles using Gaia DR2". In: *Monthly Notices of the Royal Astronomical Society* 485.4, pp. 4906–4935. DOI: 10.1093/mnras/stz651. arXiv: 1901.08072 [astro-ph.GA].

Forbes, Duncan A. et al. (Dec. 2018). "Extending the globular cluster system-halo mass relation to the lowest galaxy masses". In: *Monthly Notices of the Royal Astronomical Society* 481.4, pp. 5592–5605. DOI: 10.1093/mnras/sty2584. arXiv: 1809.07831 [astro-ph.GA].

Giesers, Benjamin et al. (Dec. 2019). "A stellar census in globular clusters with MUSE: Binaries in NGC 3201". In: *Astronomy and Astrophysics* 632, A3, A3. DOI: 10.1051/0004-6361/201936203. arXiv: 1909.04050 [astro-ph.SR].

Hong, Jongsuk et al. (May 2015). "Evolution of binary stars in multiple-population globular clusters". In: *Monthly Notices of the Royal Astronomical Society* 449.1, pp. 629–638. DOI: 10.1093/mnras/stv306. arXiv: 1503.02087 [astro-ph.GA].

Hong, Jongsuk et al. (Feb. 2019). "Spatial mixing of binary stars in multiple-population globular clusters". In: *Monthly Notices of the Royal Astronomical Society* 483.2, pp. 2592–2599. DOI: 10.1093/mnras/sty3308. arXiv: 1812.01229 [astro-ph.GA].

Hunter, J. D. (2007). "Matplotlib: A 2D graphics environment". In: *Computing in Science & Engineering* 9.3, pp. 90–95. DOI: 10.1109/MCSE.2007.55.

Ibata, Rodrigo A. et al. (Apr. 2019). "Identification of the long stellar stream of the prototypical massive globular cluster ω Centauri". In: *Nature Astronomy* 3, pp. 667–672. DOI: 10.1038/s41550-019-0751-x. arXiv: 1902.09544 [astro-ph.GA].

Janes, K. (2000). "Star Clusters". In: *Encyclopedia of Astronomy and Astrophysics*. Ed. by P. Murdin, p. 1871. DOI: 10.1888/0333750888/1871.

Keller, Benjamin W. et al. (July 2020). "Where did the globular clusters of the Milky Way form? Insights from the E-MOSAICS simulations". In: *Monthly Notices of the Royal Astronomical Society* 495.4, pp. 4248–4267. DOI: 10.1093/mnras/staa1439. arXiv: 2005.05342 [astro-ph.GA].

Leaman, Ryan et al. (Mar. 2020). "Globular cluster ejection, infall, and the host dark matter halo of the Pegasus dwarf galaxy". In: *Monthly Notices of the Royal Astronomical Society* 492.4, pp. 5102–5120. DOI: 10.1093/mnras/staa004.

Lucatello, S. et al. (Dec. 2015). "The incidence of binaries in globular cluster stellar populations". In: *Astronomy and Astrophysics* 584, A52, A52. DOI: 10.1051/0004-6361/201526957. arXiv: 1509.05014 [astro-ph.SR].

Martocchia, S. et al. (July 2017). "The search for multiple populations in Magellanic Cloud Clusters - III. No evidence for multiple populations in the SMC cluster NGC 419". In: *Monthly Notices of the Royal Astronomical Society* 468.3, pp. 3150–3158. DOI: 10.1093/mnras/stx660. arXiv: 1703.04631 [astro-ph.GA].

Milone, A. P. et al. (Apr. 2012). "The ACS survey of Galactic globular clusters. XII. Photometric binaries along the main sequence". In: *Astronomy and Astrophysics* 540, A16, A16. DOI: 10.1051/0004-6361/201016384. arXiv: 1111.0552 [astro-ph.SR].

Milone, A. P. et al. (Apr. 2013). "A WFC3/HST View of the Three Stellar Populations in the Globular Cluster NGC 6752". In: *The Astrophysical Journal* 767.2, 120, p. 120. DOI: 10.1088/0004-637X/767/2/120. arXiv: 1301.7044 [astro-ph.SR].

Milone, A. P. et al. (Apr. 2014). "The M 4 Core Project with HST - II. Multiple stellar populations at the bottom of the main sequence". In: *Monthly Notices of the Royal Astronomical Society* 439.2, pp. 1588–1595. DOI: 10.1093/mnras/stu030. arXiv: 1401.1091 [astro-ph.SR].

Milone, A. P. et al. (Mar. 2017a). "Multiple stellar populations in Magellanic Cloud clusters - V. The split main sequence of the young cluster NGC 1866". In: *Monthly Notices of the Royal Astronomical Society* 465.4, pp. 4363–4374. DOI: 10.1093/mnras/stw2965. arXiv: 1611.06725 [astro-ph.SR].

Milone, A. P. et al. (Jan. 2017b). "The Hubble Space Telescope UV Legacy Survey of Galactic globular clusters - IX. The Atlas of multiple stellar populations". In: *Monthly Notices of the Royal Astronomical Society* 464.3, pp. 3636–3656. DOI: 10.1093/mnras/stw2531. arXiv: 1610.00451 [astro-ph.SR].

Milone, A. P. et al. (Apr. 2019). "The HST Large Programme on NGC 6752 - II. Multiple populations at the bottom of the main sequence probed in NIR". In: *Monthly Notices of the Royal

Astronomical Society 484.3, pp. 4046–4053. DOI: 10.1093/mnras/stz277. arXiv: 1901.07230 [astro-ph.SR].

Milone, A. P. et al. (Mar. 2020). "The Hubble Space Telescope UV Legacy Survey of Galactic globular clusters - XXI. Binaries among multiple stellar populations". In: *Monthly Notices of the Royal Astronomical Society* 492.4, pp. 5457–5469. DOI: 10.1093/mnras/stz3629. arXiv: 2002.06479 [astro-ph.SR].

Nardiello, D. et al. (Jan. 2015). "Observing multiple stellar populations with VLT/FORS2. Main sequence photometry in outer regions of NGC 6752, NGC 6397, and NGC 6121 (M 4)". In: *Astronomy and Astrophysics* 573, A70, A70. DOI: 10.1051/0004-6361/201424117. arXiv: 1410.7503 [astro-ph.SR].

Pancino, E. et al. (May 2017). "Globular clusters with Gaia". In: *Monthly Notices of the Royal Astronomical Society* 467.1, pp. 412–427. DOI: 10.1093/mnras/stx079. arXiv: 1701.03003 [astro-ph.GA].

Pedregosa, F. et al. (2011). "Scikit-learn: Machine Learning in Python". In: *Journal of Machine Learning Research* 12, pp. 2825–2830.

Sollima, A. (June 2020). "The eye of Gaia on globular clusters structure: tidal tails". In: *Monthly Notices of the Royal Astronomical Society* 495.2, pp. 2222–2233. DOI: 10.1093/mnras/staa1209. arXiv: 2004.13754 [astro-ph.GA].

Sollima, A. et al. (Sept. 2007). "The fraction of binary systems in the core of 13 low-density Galactic globular clusters". In: *Monthly Notices of the Royal Astronomical Society* 380.2, pp. 781–791. DOI: 10.1111/j.1365-2966.2007.12116.x. arXiv: 0706.2288 [astro-ph].

Stetson, P. B. et al. (June 2014). "Optical and Near-Infrared UBVRIJHK Photometry for the RR Lyrae Stars in the Nearby Globular Cluster M4 (NGC 6121)". In: *Publications of the Astronomical Society of the Pacific* 126.940, p. 521. DOI: 10.1086/677195. arXiv: 1406.7531 [astro-ph.SR].

Weigert, Alfred (2012). *Astronomie und Astrophysik: Ein Grundkurs*. Weinheim: Wiley. ISBN: 978-3-527-67095-6.

Variation of Gaussian components and metallicity difference

A.1 Colour-difference diagrams for different abundance variations

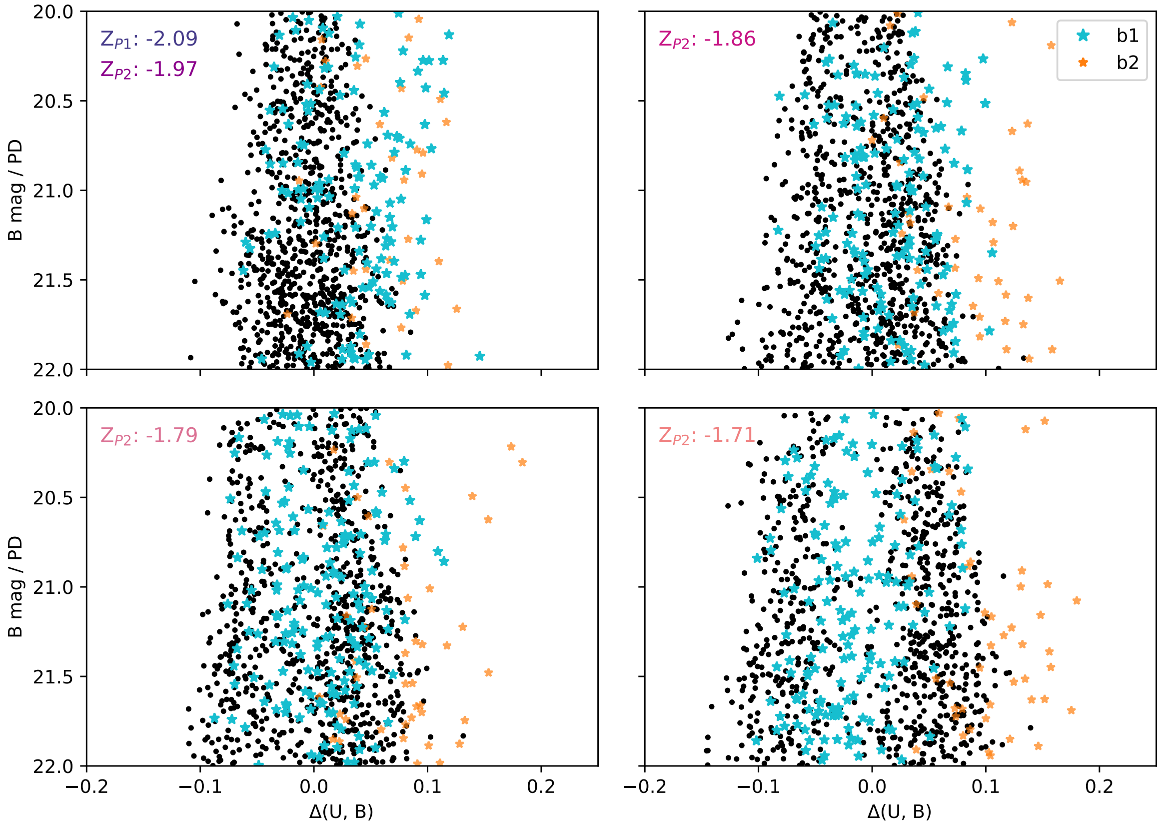

Figure A.1: The figure shows verticalised CMDs for all four metallicity differences created in this thesis. The metallicity is written in the upper left corners in their usual colours and the P1 metallicity is also noted in the first panel. The gap increases from top left to bottom right. P1 and P2 binary stars are plotted in cyan and orange, respectively, for an easy visualisation of their relative position to single stars in the colour-difference plots.

A.2 Bimodality fraction

⇒ for 7 clusters (c) increasing in b1 fraction (5, 10, 15, 20, 30, 40, 50):

↪ for each number (x) of 200, 700, 1000, 5000 stars:

↪ for **10** times:

↪ for **50** times:

- draw randomly **x** number of stars from cluster **c**
- fit GMM to distribution
- measure ΔlogL (**M1**) for PDF
- if **M1** ≥ 7.0:
save as 1
else:
save as 0

- calculate the mean for all 50 repetitions as the fraction of detected MSPs

- calculate the median and 16^{th} and 84^{th} percentiles of the 10 mean values

plot statistics in figure for different b1 fractions

Figure A.2: This figure visualises the algorithm in pseudo code that calculates the bimodality fraction from Chapter 3 Section 3.1. This is an example for the number of stars. For the dependency on detection thresholds (M1) switch the second row for the M1 values of 5.0, 7.0, 10.0, 15.0 and consistently draw 1000 stars.

Regarding the plot table of bimodality fraction measurements on the next page the top row shows the the narrower and broader abundance variation for 5 Gaussians each. The second row show the narrowest metallicity gap for 4 and 3 Gaussians each where the 3 Gaussians also have a lower detection threshold (M1 $\geq$ 5.0) to foster the recognition of small gaps between the two populations. Below is the standard metallicity gap for 4 and 6 Gaussians each and the last row shows the highest metallicity difference for 4 and 6 Gaussians each.

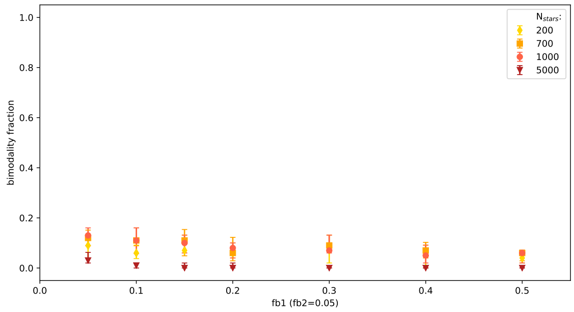

(a) $Z_{P2} = -1.97$ and 5 Gaussians.

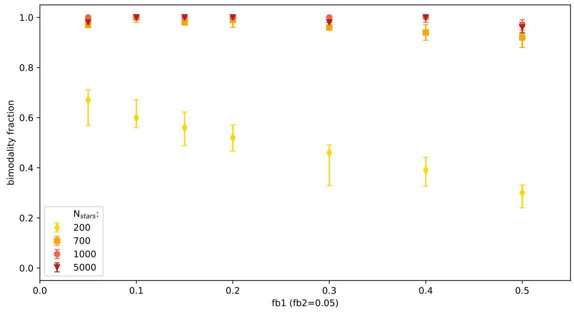

(b) $Z_{P2} = -1.79$ and 5 Gaussians.

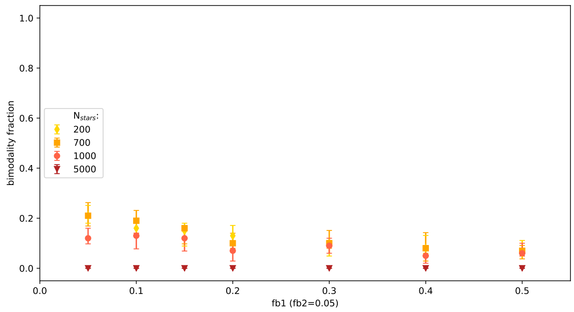

(c) $Z_{P2} = -1.97$ and 4 Gaussians.

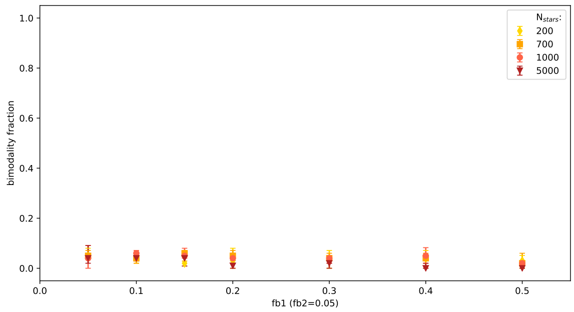

(d) $Z_{P2} = -1.97$ and 6 Gaussians.

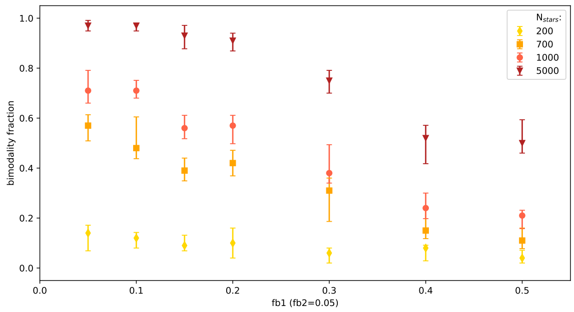

(e) $Z_{P2} = -1.86$ and 4 Gaussians.

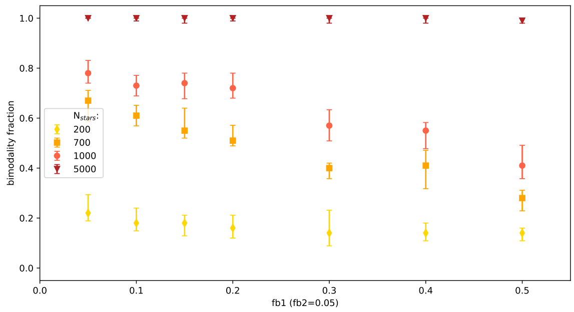

(f) $Z_{P2} = -1.86$ and 6 Gaussians.

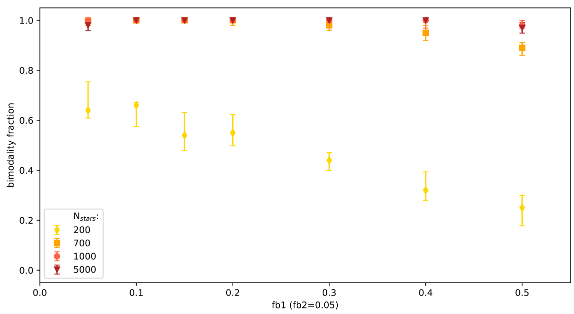

(g) $Z_{P2} = -1.79$ and 4 Gaussians.

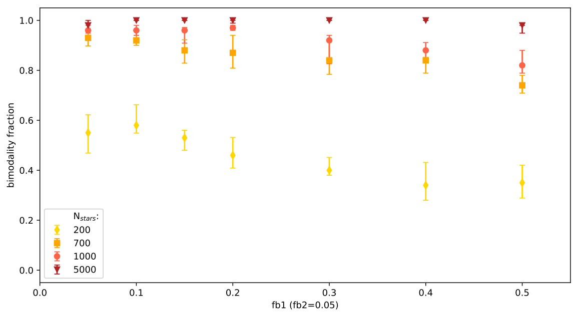

(h) $Z_{P2} = -1.79$ and 6 Gaussians.

Figure A.3: The bimodality fraction depending on the fraction of b1 stars and the number of data points varying in the abundance variation and number of Gaussians used for the GMM fit. The number of stars increases from yellow to dark red (from diamond, square, dot to reversed triangle) where the symbols represent the median values of 50 times 10 measurements; errorbars are the 16% and 84% percentiles.

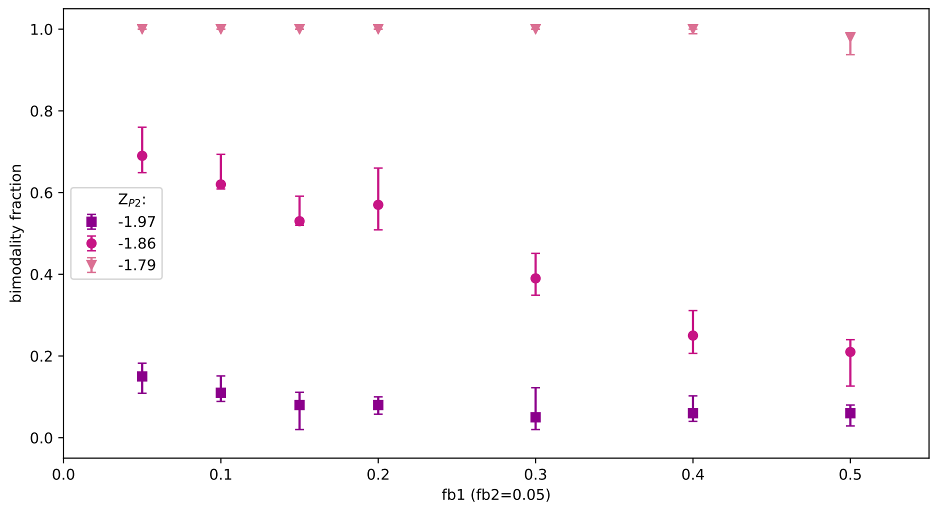

(a) Using 4 Gaussians to fit the colour-difference distribution.

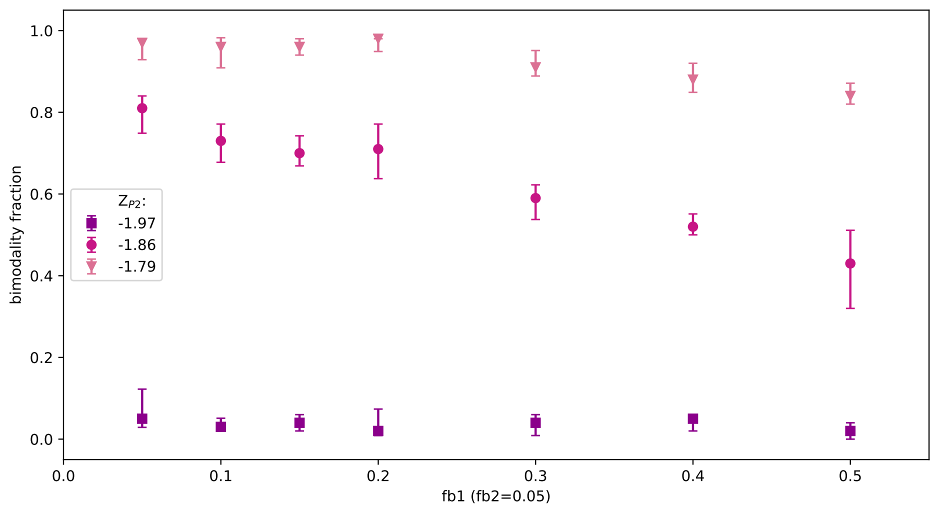

(b) Using 6 Gaussians to fit the colour-difference distribution.

Figure A.4: The bimodality fraction depending on the fraction of b1 stars and the extend of abundance variation for 4 and 6 Gaussians each. The metallicity difference increases from purple to light pink (squares, dots, reversed triangles) where the symbols represent the median values of 50 times 10 measurements; errorbars are the 16% and 84% percentiles.

A.3 Estimation of population fractions

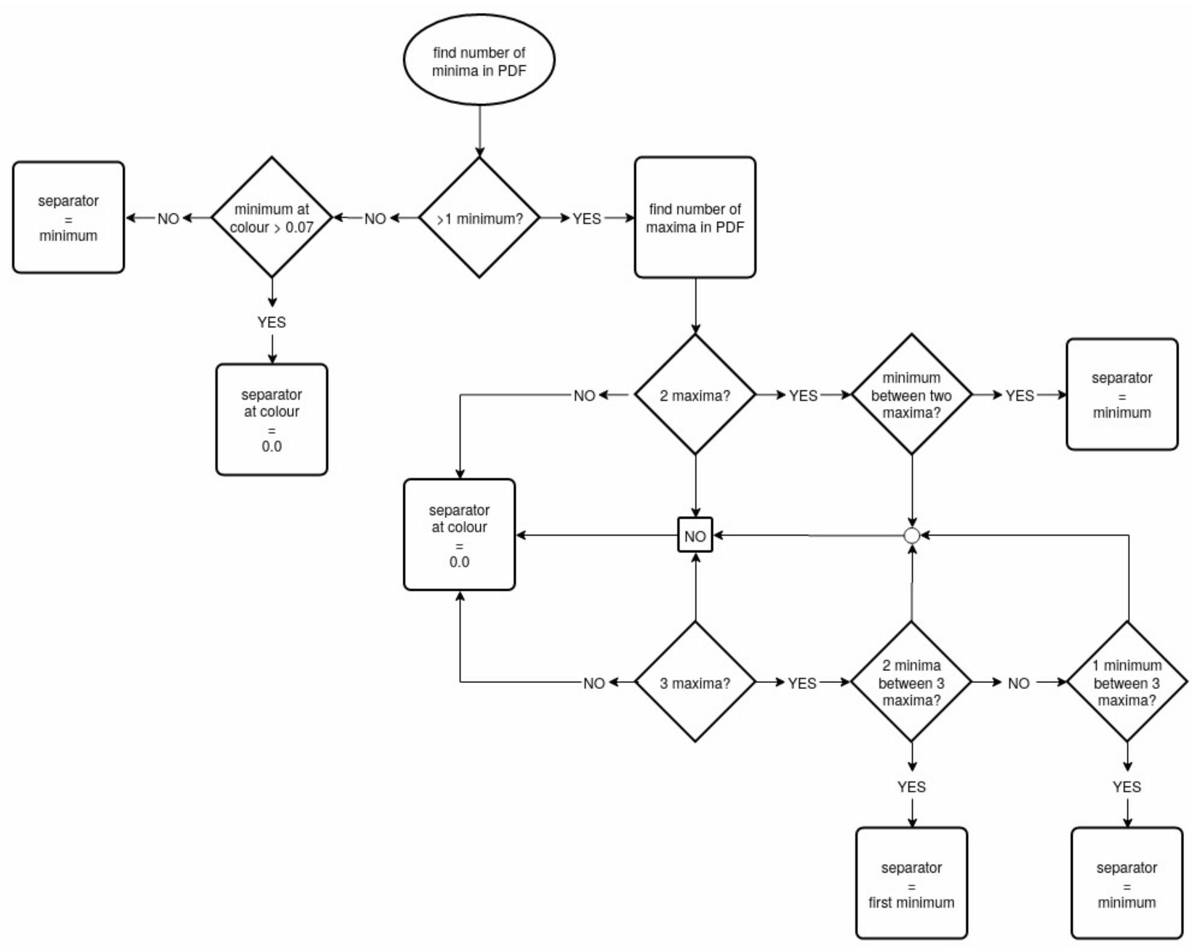

Figure A.5: This flowchart visualises the algorithm that determines the colour which separates Gaussian components belonging to P1 to components belonging to P2. The figure refers to Section 3.2 in Chapter 3.

Regarding the plot tables of estimates of the population fractions regardless of which dependency they are structured as follows: The first row are the estimates of different abundance variation (metallicity gap) for the usual 5 Gaussians. The second row shows the narrower metallicity difference with 4 and 3 Gaussians each, as 6 Gaussians are not effective at such a tight distribution. The second row is the standard metallicity difference for 4 and 6 Gaussians each and the last row shows the estimates for the bradest gap for 4 and 6 Gaussians each.

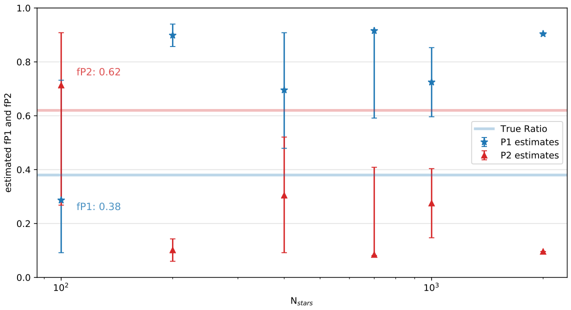

(a) $Z_{P2} = -1.97$ and 5 Gaussians.

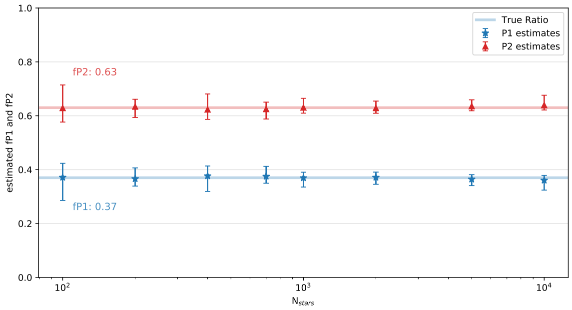

(b) $Z_{P2} = -1.79$ and 5 Gaussians.

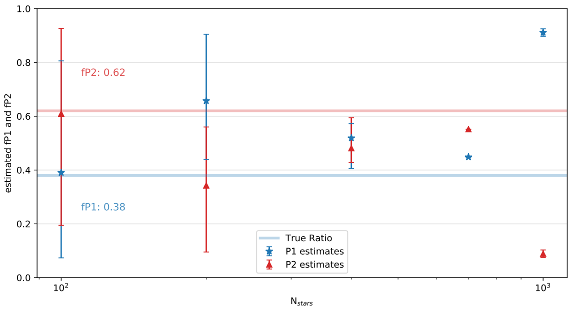

(c) $Z_{P2} = -1.97$ and 4 Gaussians.

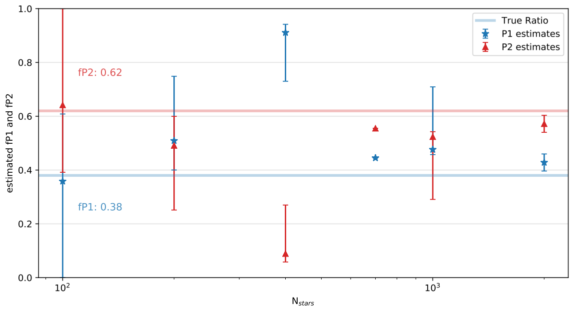

(d) $Z_{P2} = -1.97$ and 3 Gaussians.

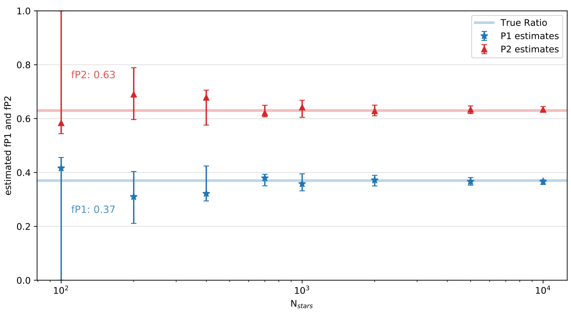

(e) $Z_{P2} = -1.86$ and 4 Gaussians.

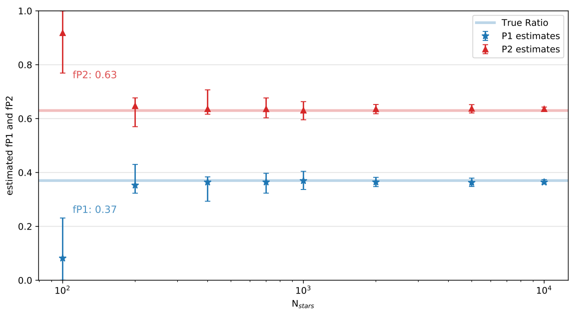

(f) $Z_{P2} = -1.86$ and 6 Gaussians.

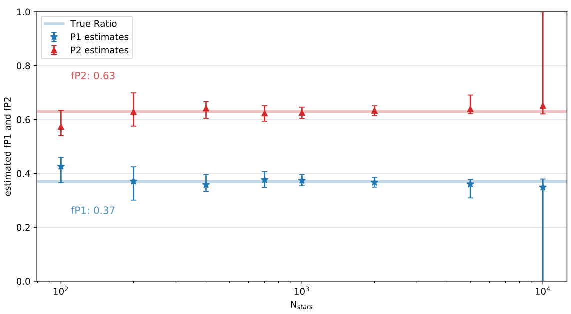

(g) $Z_{P2} = -1.79$ and 4 Gaussians.

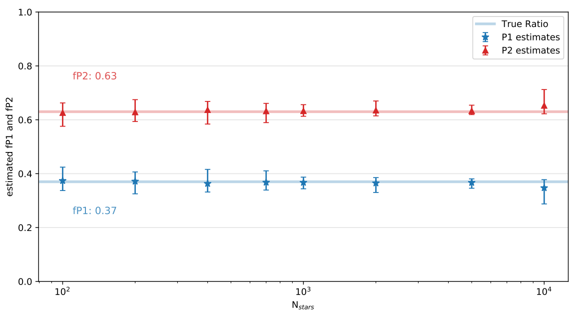

(h) $Z_{P2} = -1.79$ and 6 Gaussians.

Figure A.6: The estimation of the population fraction depending on the number of data points, varying for abundance variation (Z_{P2}) and number of fitted Gaussians. Blue and red lines are the actual fractions of P1 and P2, respectively, and blue stars and red triangles are the median values of 50 estimations and the error bars are the 16% and 84% percentiles.

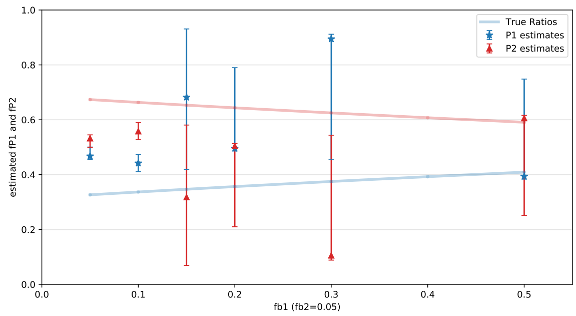

(a) $Z_{P2} = -1.97$ and 5 Gaussians.

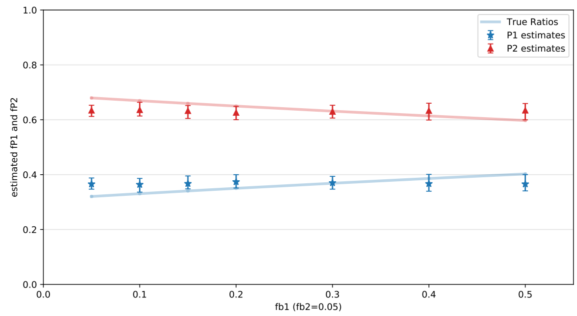

(b) $Z_{P2} = -1.79$ and 5 Gaussians.

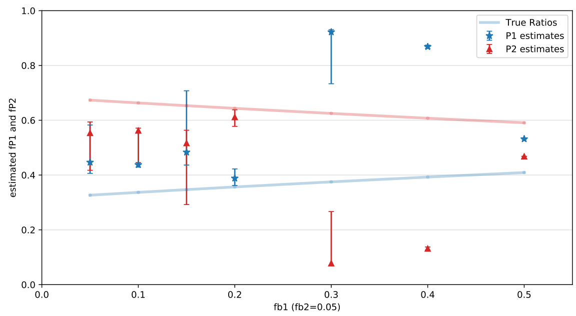

(c) $Z_{P2} = -1.97$ and 4 Gaussians.

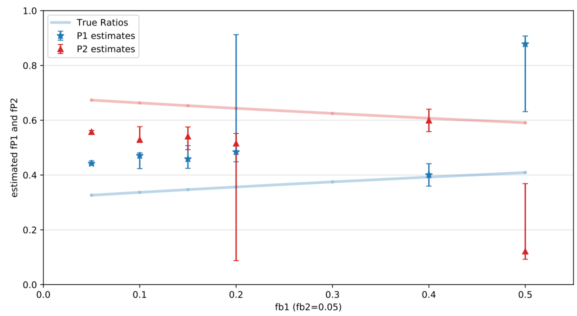

(d) $Z_{P2} = -1.97$ and 3 Gaussians.

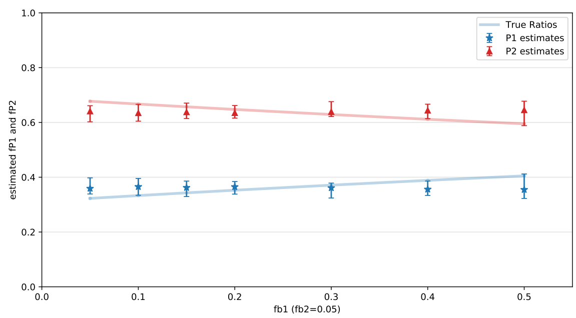

(e) $Z_{P2} = -1.86$ and 4 Gaussians.

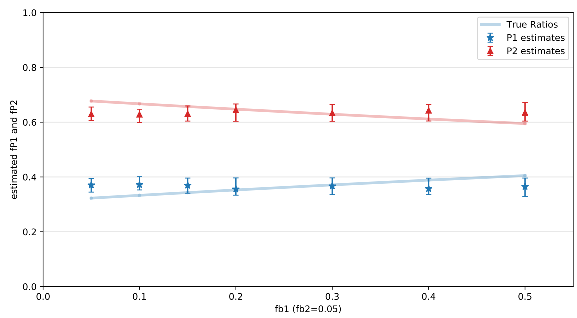

(f) $Z_{P2} = -1.86$ and 6 Gaussians.

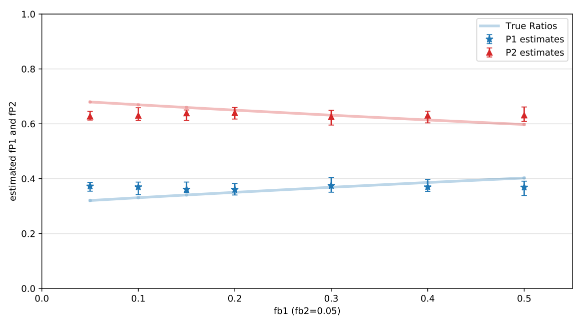

(g) $Z_{P2} = -1.79$ and 4 Gaussians.

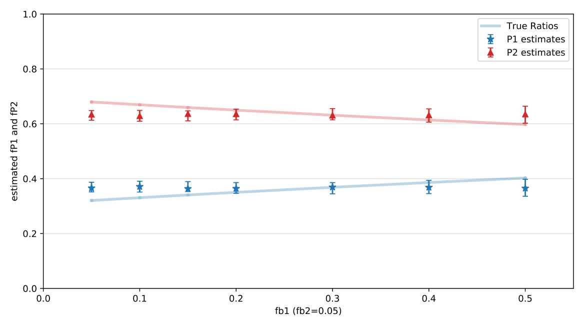

(h) $Z_{P2} = -1.79$ and 6 Gaussians.

Figure A.7: The estimation of the population fraction depending on the fraction of b1 stars, varying for abundance variation (Z_{P2}) and number of fitted Gaussians. Blue and red lines are the actual fractions of P1 and P2, respectively, and blue stars and red triangles are the median values of 50 estimations and the error bars are the 16% and 84% percentiles.

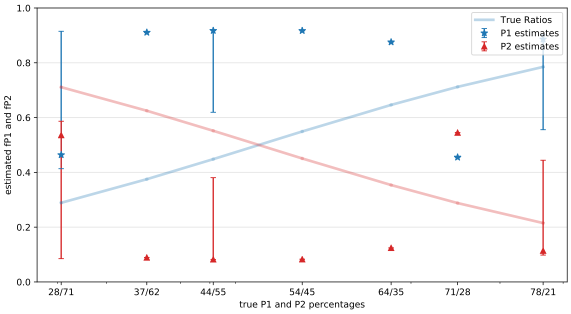

(a) $Z_{P2} = -1.97$ and 5 Gaussians.

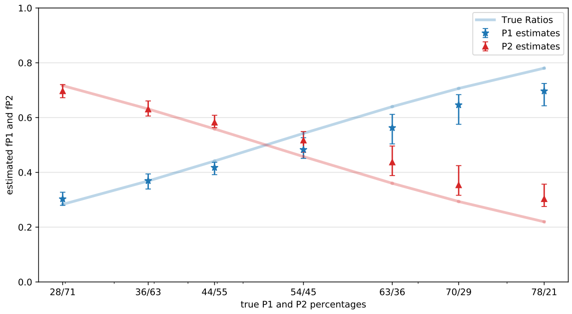

(b) $Z_{P2} = -1.79$ and 5 Gaussians.

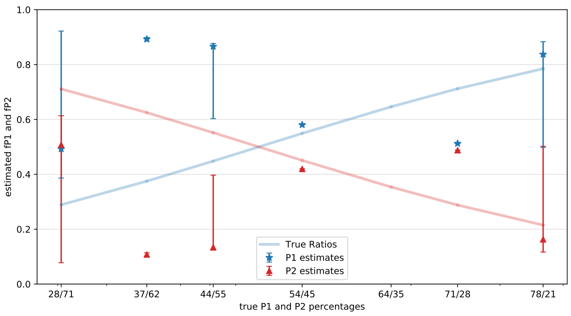

(c) $Z_{P2} = -1.97$ and 4 Gaussians.

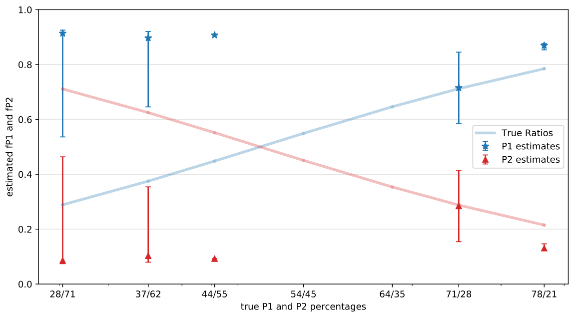

(d) $Z_{P2} = -1.97$ and 3 Gaussians.

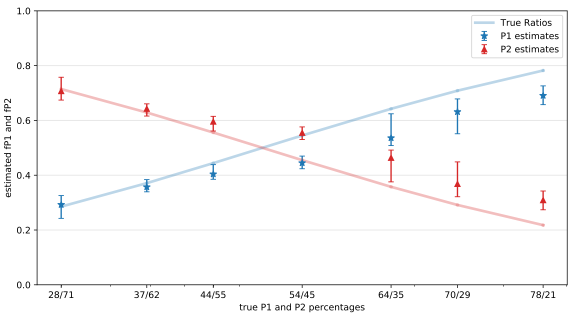

(e) $Z_{P2} = -1.86$ and 4 Gaussians.

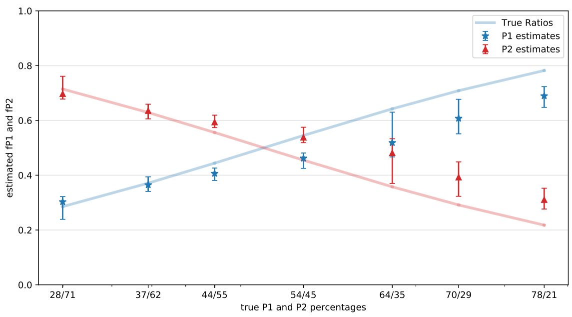

(f) $Z_{P2} = -1.86$ and 6 Gaussians.

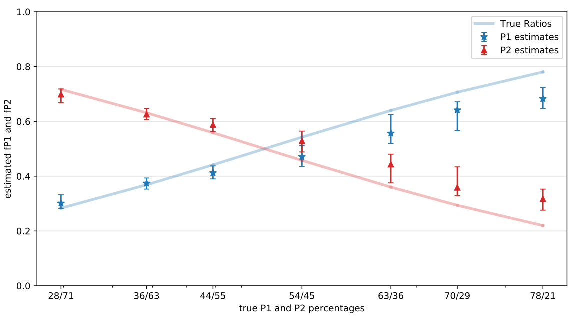

(g) $Z_{P2} = -1.79$ and 4 Gaussians.

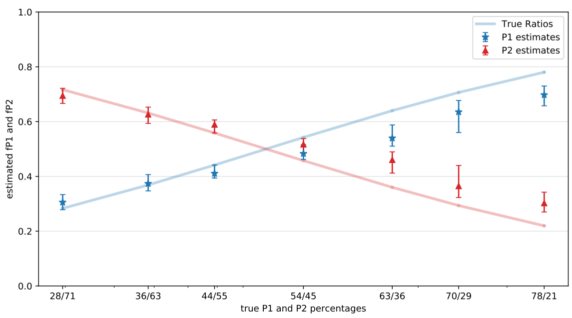

(h) $Z_{P2} = -1.79$ and 6 Gaussians.

Figure A.8: The estimation of the population fraction depending on the ratio of the populations, varying for abundance variation (Z_{P2}) and number of fitted Gaussians. Blue and red lines are the actual fractions of P1 and P2, respectively, and blue stars and red triangles are the median values of 50 estimations and the error bars are the 16% and 84% percentiles.